

---

# Absolute Calibration and image quality assessment of RISAT-1 FRS and MRS mode data

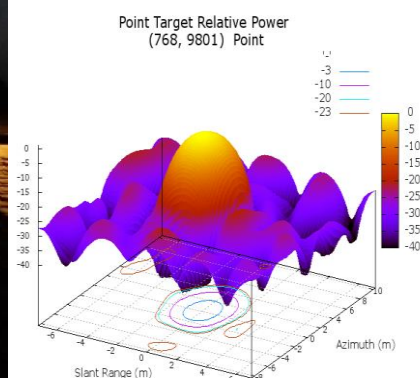
---

## Scientific Report

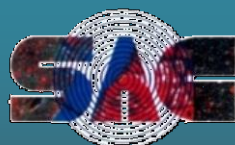
---

**CAL-VAL Team**

---



**March- 2016**



**Calibration and Validation Division**  
**Earth, Ocean, Atmosphere, Planetary Sciences & Applications Area**  
**Space Applications Centre (ISRO)**  
**Ahmedabad - 380 015**

## DOCUMENT CONTROL SHEET

1. Report No.	SAC/EPESA/ADVG/CVD/CAL-VAL/SR/01/03/2016
2. Publication date	March 2016
3. Title and subtitle	Absolute Calibration and image quality assessment of RISAT-1 FRS and MRS mode data
4. Type of report	Scientific
5. Number of pages	3+117
6. Number of references	36
7. Authors	CAL-VAL Team
8. Originating unit	CVD- EPESA
9. Abstract	<p>This report presents results obtained from absolute radiometric calibration of RISAT-1 MRS and FRS mode HH polarization data by utilizing the point target (corner reflectors) as well as distributed target. Amazon rainforest was used as the distributed target. The impulse response functions of the deployed corner reflectors were analysed and various calibration and image quality parameters have also been computed. Geometric calibration of RISAT-1 data was also attempted. Analysis of data corresponding to twelve campaigns synchronized with RISAT-1 overhead pass shows that calibration coefficient difference is <math>&lt; 1\text{dB}</math>(FRS-1 and MRS modes) meeting the mission requirement. Other results regarding suitability of sites are also discussed.</p>
10. Key words	Corner reflector, Corner reflector Deployment, Impulse Response Function, Calibration Constant, Backscattering Coefficient
11. Security classification	Unrestricted
12. Distribution statement	General

## CAL-VAL Team

### **1. Space Applications Centre (SAC-ISRO), Ahmedabad**

Mrs. Shweta Sharma- Principal Investigator

Mr. R.P. Prajapati- Co-Principal Investigator

Dr. A K Mathur- Coordinator

### **2. Nirma University, Ahmedabad**

Mr. Gautam Dadhich- Junior Research Fellow

Dr. P R Patel- Co-Principal Investigator

### **3. M.G. Science Institute, Ahmedabad**

Mr. Mihir Rambhia- Junior Research Fellow

Dr. Alpana Shukla- Co-Principal Investigator

## **TABLE OF CONTENTS**

TABLE OF CONTENTS .....	1
LIST OF FIGURES .....	4
LIST OF TABLES .....	9
ACRONYMS .....	11
SUMMARY .....	12
1 INTRODUCTION .....	13
1.1 Background .....	13
1.2.1 RISAT-1 SAR Sensor .....	14
1.2.2 External Calibration .....	16
1.2.2.1 Point Target Analysis .....	17
1.2.2.2 Distributed target .....	19
1.2.3 Geometric Calibration .....	21
1.3 SAR Image Quality Assessment .....	21
1.3.1 Spatial resolution .....	22
1.3.2 Peak side lobe ratio .....	23
1.3.3 Integrated side lobe ratio .....	23
1.3.4 Signal to Clutter Ratio .....	24
2 CAL VAL SITE .....	25
2.1 Site selection .....	25
2.2 Description of sites .....	25
2.2.1 SAC-Bopal site, Ahmedabad .....	26
2.2.2 Desalpar site, Rann of Kutch .....	26
2.2.3 Grounds at M.G. Sci. Institute and L.D. Arts College, Ahmedabad .....	27
2.2.4 Nirma University Ground, Ahmedabad .....	28
3 MATERIALS AND DATA USED .....	30

3.1	Corner Reflectors.....	30
3.2	General Criteria for Designing a Corner Reflector .....	30
3.2.1	The Material of Corner Reflector .....	30
3.2.2	The Shape of Corner Reflector .....	31
3.2.3	The Installation of Corner Reflector .....	33
3.2.4	The Bending of Corner's Plate.....	33
3.3	Data Used.....	33
4	METHODOLOGY.....	35
4.1	General .....	35
4.2	Approach for Radiometric calibration using Point targets.....	35
4.3	Determination of Signal to clutter ratio (SCR).....	38
4.4	Radiometric calibration using distributed target.....	41
4.5	Approach for Geometric Calibration.....	42
4.6	Mobilization and deployment of Corner Reflectors .....	43
5	RESULTS AND DISCUSSION .....	45
5.1	General .....	45
5.2	Results of absolute radiometric calibration using point targets.....	46
5.2.1	Results for Ahmedabad site.....	46
5.2.1.1	21 April 2015: FRS-HH Polarization .....	47
5.2.1.2	25 April 2015: FRS-HH Polarization .....	49
5.2.1.3	5th July 2015: MRS-HH Polarization.....	51
5.2.1.4	30th July 2015: MRS-HH Polarization .....	54
5.2.1.5	24th August 2015: MRS-HH Polarization .....	57
5.2.1.6	18 <sup>th</sup> September 2015: MRS-HH Polarization.....	60
5.2.1.7	13th October 2015: MRS-HH Polarization .....	63
5.2.1.8	7th November 2015: MRS-HH Polarization .....	66

5.2.1.9	2nd December 2015: MRS-HH Polarization .....	69
5.2.1.10	27th December 2015: MRS-HH Polarization .....	72
	Summary of the results for Ahmedabad sites and discussion .....	75
5.2.2	Results for Desalpar, Rann of Kutch site .....	77
5.2.2.1	22nd January 2016, FRS-1 (RH).....	77
5.2.2.2	14th February 2016, MRS (HH) .....	80
5.2.2.3	15th February 2016, FRS-1 (RH) .....	90
5.3	Results of radiometric calibration using distributed targets .....	95
5.4	Results of geometric calibration using point targets .....	97
5.5	Effect of Clutter window on ISLR .....	102
6	CONCLUSIONS .....	107
7	FUTURE SCOPE .....	109
	Acknowledgements .....	110
	Important Web resources and Reference .....	111
	Visual Walkthrough of Deployed Corner reflector .....	115

## LIST OF FIGURES

Figure 1-1 Schematic Diagram showing different beam modes of RISAT-1 SAR .....	14
Figure 1-2 Imaging Geometry of RISAT-1 .....	15
Figure 1-3 Graphical representation of a SAR point target response showing several quality parameters [16]. .....	22
Figure 2-1 Study area map of Cal Val Site .....	25
Figure 2-2 Calibration site near SAC, Bopal Campus [ <i>courtesy: Google earth</i> ] .....	26
Figure 2-3 Calibration site at Desalpar, Rann of Kutch [ <i>courtesy: Google earth</i> ] .....	27
Figure 2-4 Calibration grounds at MG Science Institute and L.D. Arts College, Ahmedabad [ <i>courtesy: Google earth</i> ] .....	28
Figure 2-5 Calibration site at Nirma University, Ahmadabad [ <i>courtesy: Google earth</i> ] .....	28
Figure 3-1 Triangular Trihedral Corner Reflector (size 0.90m) .....	32
Figure 3-2 Square Trihedral Corner Reflector (size 0.60m) .....	32
Figure 3-3 Dihedral Corner Reflector (size 1.5m) .....	33
Figure 4-1 RISAT-1 FRS-1 image of 22nd January 2016 .....	36
Figure 4-2 Schematics showing the subset of the data containing CR .....	37
Figure 4-3 Subset of the image containing corner reflector .....	37
Figure 4-4 Selection of the clutter windows around CR .....	37
Figure 4-5 Schematics showing the area containing clutter and point target .....	39
Figure 4-6 Flowchart of the methodology adopted in the study .....	40
Figure 4-7 (a-e) Mobilization and deployment of Corner reflectors .....	44
Figure 5-1 Location of CR at Ahmedabad site on Google earth image .....	46
Figure 5-2 Response of CR at SAC, Bopal, Ahmedabad site of FRS-1 SAR intensity data on 21/04/15 .....	47
Figure 5-3 Impulse response function of the CR for 21 <sup>st</sup> April 2015 FRS-1 image for different target and clutter window sizes .....	48

Figure 5-4 Response of CR at SAC, Bopal, Ahmedabad site of FRS-1 SAR intensity data on 25/04/15.....	49
Figure 5-5 Impulse response function of the CR for 25 <sup>th</sup> April 2015 FRS-1 image for different target and clutter window sizes.....	50
Figure 5-6 Response of CR at SAC, Bopal, Ahmedabad site of MRS SAR intensity data on 05/07/15.....	51
Figure 5-7 Impulse response function of the CR for 5 <sup>th</sup> July 2015 MRS image for different target and clutter window sizes.....	52
Figure 5-8 Calculated SCR for different target and clutter window sizes .....	53
Figure 5-9 Range and azimuth spatial resolution estimated from IRF.....	53
Figure 5-10 Response of CR at SAC, Bopal, Ahmedabad site of MRS SAR intensity data on 30/07/15.....	54
Figure 5-11 Impulse response function of the CR for 30 <sup>th</sup> July 2015 MRS image for different target and clutter window sizes.....	55
Figure 5-12 Calculated SCR for different target and clutter window sizes .....	56
Figure 5-13 Azimuth spatial resolution estimated from IRF .....	56
Figure 5-14 Response of CR at SAC, Bopal, Ahmedabad site of MRS SAR intensity data on 24/08/2015.....	57
Figure 5-15 Impulse response function of the CR for 24 <sup>th</sup> August 2015 MRS image for different target and clutter window size .....	58
Figure 5-16 Calculated SCR for different target and clutter window sizes .....	59
Figure 5-17 Azimuth spatial resolution estimated from IRF.....	59
Figure 5-18 Response of CR at SAC, Bopal, Ahmedabad site of MRS SAR intensity data on 18/09/2015.....	60
Figure 5-19 Impulse response function of the CR for 18 <sup>th</sup> September 2015 MRS image for different target and clutter window size .....	61
Figure 5-20 Calculated SCR for different target and clutter window sizes .....	62
Figure 5-21 Azimuth spatial resolution estimated from IRF .....	62

Figure 5-22 Response of CR at SAC, Bopal, Ahmedabad site of MRS SAR intensity data on 13/10/2015..... 63

Figure 5-23 Impulse response function of the CR for 13<sup>th</sup> October 2015 MRS image for different target and clutter window sizes ..... 64

Figure 5-24 Calculated SCR for different target and clutter window sizes ..... 65

Figure 5-25 Azimuth spatial resolution estimated from IRF ..... 65

Figure 5-26 Response of CR at SAC, Bopal, Ahmedabad site of MRS SAR intensity data on 07/11/2015..... 66

Figure 5-27 Impulse response function of the CR for 7<sup>th</sup> November 2015 MRS image for different target and clutter window sizes ..... 67

Figure 5-28 Calculated SCR for Bopal site and for different target and clutter window sizes 68

Figure 5-29 Azimuth spatial resolution estimated from IRF ..... 68

Figure 5-30 Response of CR at SAC, Bopal, Ahmedabad site of MRS SAR intensity data on 02/12/2015..... 69

Figure 5-31 Impulse response function of the CR for 2<sup>nd</sup> December 2015 MRS image for different target and clutter window sizes ..... 70

Figure 5-32 Calculated SCR for Bopal and Nirma University sites and for different target and clutter window sizes ..... 71

Figure 5-33 Azimuth spatial resolution estimated from IRF ..... 71

Figure 5-34 Response of CR at SAC, Bopal, Ahmedabad site of MRS SAR intensity data on 27/12/2015..... 72

Figure 5-35 Impulse response function of the CR for 27<sup>th</sup> December 2015 MRS image for different target and clutter window sizes ..... 73

Figure 5-36 Calculated SCR for Bopal and Nirma University sites and for different target and clutter window sizes ..... 74

Figure 5-37 Azimuth spatial resolution estimated from IRF ..... 74

Figure 5-38 Time series variation of average estimated and provided calibration constant along with SCR ..... 76

Figure 5-39 Locations of deployed CRs on Google Earth Image (common for 21<sup>st</sup> January 2016 FRS-1 pass and 22<sup>nd</sup> January 2016 FRS-1 pass)..... 78

Figure 5-40 Response of deployed CRs as seen on 22<sup>nd</sup> January 2016 FRS-1 image) ..... 78

Figure 5-41 Impulse response function of the CR (2 & 7) for 22<sup>nd</sup> January 2016 MRS ..... 79

Figure 5-42 Snap showing the distance between deployed CRs ..... 81

Figure 5-43 Locations of deployed CRs on Google Earth Image (common for 14<sup>th</sup> February MRS pass and 15<sup>th</sup> February 2016 FRS-1 pass) ..... 81

Figure 5-44 Locations of deployed CRs at Rann of Kutch (with field photographs) on Google Earth Image (common for 14<sup>th</sup> February MRS pass and 15<sup>th</sup> February 2016 FRS-1 pass) ..... 82

Figure 5-45 Locations of deployed CRs at the fields in front of ISR cabin (with field photographs) on Google Earth Image (common for 14<sup>th</sup> February MRS pass and 15<sup>th</sup> February 2016 FRS-1 pass)..... 82

Figure 5-46 CR deployed on black cloth background..... 83

Figure 5-47 Response of CRs (1-7) as seen in RISAT-1 MRS image of 14<sup>th</sup> Feb 2016..... 83

Figure 5-48 Response of CRs (8-10) as seen in RISAT-1 MRS image of 14<sup>th</sup> Feb 2016 ..... 84

Figure 5-49 Impulse response function of the CR (7 & 9) for 14<sup>th</sup> February 2016 MRS ..... 87

Figure 5-50 Calculated SCR for different CRs and for different target and clutter window sizes ..... 88

Figure 5-51 Azimuth spatial resolution estimated from IRF for different target and clutter window sizes ..... 89

Figure 5-52 PSLR in azimuth estimated from IRF for different target and clutter window sizes ..... 89

Figure 5-53 PSLR in azimuth estimated from IRF for different target and clutter window sizes ..... 90

Figure 5-54 Response of CRs (8-12) as seen in RISAT-1 FRS-1 image of 15<sup>th</sup> Feb 2016 ..... 90

Figure 5-55 Response of CRs (1-7) as seen in RISAT-1 FRS-1 image of 15<sup>th</sup> Feb 2016 ..... 91

Figure 5-56 Impulse response function of the CR (5 & 1) for 15<sup>th</sup> February 2016 FRS-1 ..... 92

Figure 5-57 Study Area map for distributed target analysis ..... 96

Figure 5-58 Amazon Forest in Google Earth Image and Response of Amazon Forest in FRS Mode SAR Image .....	96
Figure 5-59 ISLR Variation for 12Sep13_RH_Beam no.74.....	103
Figure 5-60 ISLR Variation for 16June13_HH_Beam no.74 .....	103
Figure 5-61 ISLR Variation for 11sep13_RH_Beam no.95 .....	104
Figure 5-62 ISLR Variation for 11Sep13_RV_Beam no.95.....	104
Figure 5-63 ISLR Variation for 28June13_RH_Beam no.95 .....	105
Figure 5-64 ISLR Variation for 28June13_RV_Beam no.95 .....	105
Figure 5-65 Variation of ISLR for different date of pass for RH polarization .....	106
Figure 5-66 Variation of ISLR for different date of pass for RV polarization .....	106

## **LIST OF TABLES**

Table 1-1 RISAT-1 Image quality parameters.....	15
Table 2-1 center latitude and longitudes of cal val sites .....	29
Table 3-1 Theoretical maximum RCS for different types of Corner reflectors [17].....	31
Table 3-2 Details of the RISAT-1 data used in the study .....	34
Table 5-1 Number of CRs deployed for FRS-1 for different dates .....	45
Table 5-2 Number of CRs deployed for MRS for different dates .....	45
Table 5-3 Estimated calibration constant for 21 <sup>st</sup> April FRS-1 .....	48
Table 5-4 Estimated calibration constant for 25 <sup>th</sup> April FRS-1 .....	50
Table 5-5 Estimated calibration constant for 5 <sup>th</sup> July 2015 .....	52
Table 5-6 Estimated calibration constant for 30 <sup>th</sup> July 2015 .....	55
Table 5-7 Estimated calibration constant for 24 <sup>th</sup> August 2015 .....	58
Table 5-8 Estimated calibration constant for 18 <sup>th</sup> September 2015.....	61
Table 5-9 Estimated calibration constant for 13 <sup>th</sup> October 2015.....	64
Table 5-10 Estimated calibration constant for 7 <sup>th</sup> November 2015.....	67
Table 5-11 Estimated calibration constant for 2 <sup>nd</sup> December 2015.....	70
Table 5-12 Estimated calibration constant for 27 <sup>th</sup> December 2015 .....	73
Table 5-13 Difference between average estimated CC and provided CC along with the calculated value of SCR for MRS .....	75
Table 5-14 Calculated value of SCR for FRS-1 .....	76
Table 5-15 Estimated Calibration Constant for different CRs.....	80
Table 5-16 Estimated Calibration Constant for different CRs.....	87
Table 5-17 Estimated Calibration Constant for different CRs.....	92
Table 5-18 Estimated Average Calibration Constant for FRS-1 .....	93
Table 5-19 Estimated Average Calibration Constant for MRS .....	94
Table 5-20 Estimated Calibration constant (CC) using distributed target method.....	97

Table 5-21 Coordinates of deployed CRs .....	98
Table 5-22 Estimated Geometric error for FRS-1, RH .....	98
Table 5-23 Estimated Geometric error for FRS-1, RV .....	99
Table 5-24 Coordinates of deployed CRs for 14 <sup>th</sup> February 2016 MRS pass .....	100
Table 5-25 Estimated Geometric error for MRS, HH .....	100
Table 5-26 Design Specifications of RISAT-1 satellite.....	101
Table 5-27 Estimated RMSE for FRS-1 and MRS.....	101

## **ACRONYMS**

CR: Corner Reflector

CC: Calibration Constant

FFT: Fast Fourier Transform

FRS: Fine resolution stripmap

GRD: Ground Range data

IRF: Impulse Response Function

ISLR: Integrated Side Lobe Ratio

MRS: Medium Resolution ScanSAR

NISAR: NASA-ISRO Synthetic Aperture Radar

PSLR: Peak Side Lobe Ratio

PTs: Point Targets

SAR: Synthetic Aperture Radar

SCR: Signal to Clutter Ratio

SLC Single Look Complex

## **SUMMARY**

This report brings out the results of independent calibration exercise carried out by the team for RISAT-1 FRS-1 and MRS data. In all, twelve calibration campaigns data (4 for FRS-1 and 8 for MRS HH mode) synchronized to RISAT-1 pass of different beams and polarizations, covering the span of eleven months from April 2015 to February 2016, have been analysed. Point target as well as the distributed target data were used for the absolute radiometric calibration of RISAT-1 data. In order to study the response sensitivity, Corner reflectors (CR) of different shapes and sizes (dihedral, square trihedral and triangular trihedral having 1.5m, 0.60m and 0.90m leg length respectively) were utilized. Ahmedabad Sites (SAC-Bopal site and grounds of M.G. Science Institute and Nirma University) with near homogeneous background bare soil and a desert environment site in Desalpar, Rann of Kutchh(Gujarat) were used for the deployment of point targets, whereas, Amazon Rainforest was used as the distributed target for estimating the calibration constant. Geometric calibration of Geo-Tiff data for both the modes was also attempted. In view of high sensitivity of signal to clutter ratio(SCR) for the precise calibration results, an experiment was also conducted using black cloth (5 X 5 m) as a background for deployment of CR.

Initial calibration analysis revealed that the SAC-Bopal cal-val site is suitable for the absolute radiometric calibration of RISAT-1 FRS mode data. Whereas, Rann of Kutch site was found to be suitable for C-band FRS as well as MRS mode data. The difference between the average estimated calibration constants and the constants provided with the data was found to be within 1dB for both MRS and FRS mode data with the exception of FRS-1, beam 66, for which the difference was found to be ~ 2dB. For MRS mode data, it was observed that the difference was found to be within 1dB when the SCR value exceeds 20dB, whereas for the SCR values between 15 to 20 dB, the difference was ~ 2dB. The results for which SCR was found to be  $\leq$  20dB are considered to be precise and reported here. Radiometric calibration using distributed target yielded the average difference of 0.32 dB for HH Polarization and 0.87 dB for HV polarization meeting the satellite mission specifications. Geometric calibration results for MRS showed the RMSE to be ~43 m in latitude and ~15m for longitude. Future work will include the site suitability test of Rann of Kutch site for L-band data, geometric calibration using Differential GPS measurements and to explore the facility for RCS characterization of the CRs currently being used for the calibration exercise.

## 1 INTRODUCTION

---

### 1.1 Background

Calibration is the act or process of comparing certain specific measurements in an instrument with a standard. The major goal in utilizing imaging radar data is to infer some bio- or geophysical parameter about target areas within the scene via analysis of the recorded radar signal. For coherent radar systems such as a synthetic aperture radar (SAR), the recorded signal consists of both phase and amplitude information. Although many applications like InSAR, PolInSAR require extraction of phase information from SAR data, a majority of applications utilize the amplitude information recorded in the SAR signal history. To utilize this amplitude information requires a normalization process to remove radar system effects. This normalization process usually results in an estimate of the radar cross section ( $\sigma$ ) or scattering coefficient ( $\sigma_0$ ) on a pixel-by-pixel basis for the various targets being imaged by the radar and is referred to as radiometric calibration.

SAR data used for quantitative temporal and/or spatial analysis requires calibration to ensure that observed pixel values of amplitude and phase can be related to the geophysical parameters of interest. Furthermore, if SAR images from different sensors are absolutely calibrated they can (in principle) be directly compared. The process of radiometric calibration of SAR images involves comparison of the backscattered radar reflectivity signal from a ground resolution element containing a calibration target of known signal response, such as a Corner reflector (CR) [7]. CR are considered to be reliable targets for SAR calibration because the magnitude of the returned signal is large relative to the size of the target, their signal response is insensitive to errors in alignment (unlike dihedral reflectors), and they are relatively cheap to manufacture and maintain (unlike transponders). If the geodetic location of a deployed CR is accurately known, then it can be used for geometrical calibration of SAR products as long as it is visible above the background signal level in the SAR imagery. Over a period of time, need of radiometric calibration has become absolutely necessary in view of availability of SAR data from various spaceborne sensors like ERS-1/2, ENIVISAT, RADARSAT-1/2, ALOS PALSAR-1/2, COSMO SkyMed, TerraSAR-X and RISAT-1. To compare data from different sensors, extract geophysical parameters from backscatter measurements using models, carrying out multi-temporal studies over large areas, build up a database of backscatter measurements for different types of terrain/incidence angle, etc., requires calibrated SAR data products. Thus

the present study focuses on the radiometric calibration of RISAT-1 SAR sensor for passive standard target.

### 1.2.1 RISAT-1 SAR Sensor

RISAT-1 is India's first space borne SAR sensor operating at C band. RISAT-1 is not only capable of acquiring data in multi polarisation mode, including quad linear polarisation, but it is also first of its kind to operate in hybrid circular polarimetric mode for earth observation [29]. It operates at various beam modes having a number of combinations of linear polarisation modes as well as circular polarisation modes, incidence angle, swath and resolution. Fig. 1-1 shows schematic diagram of RISAT-1 SAR beam modes [6]. Detailed specifications of RISAT-1 SAR beam modes are given in Table 1-1.

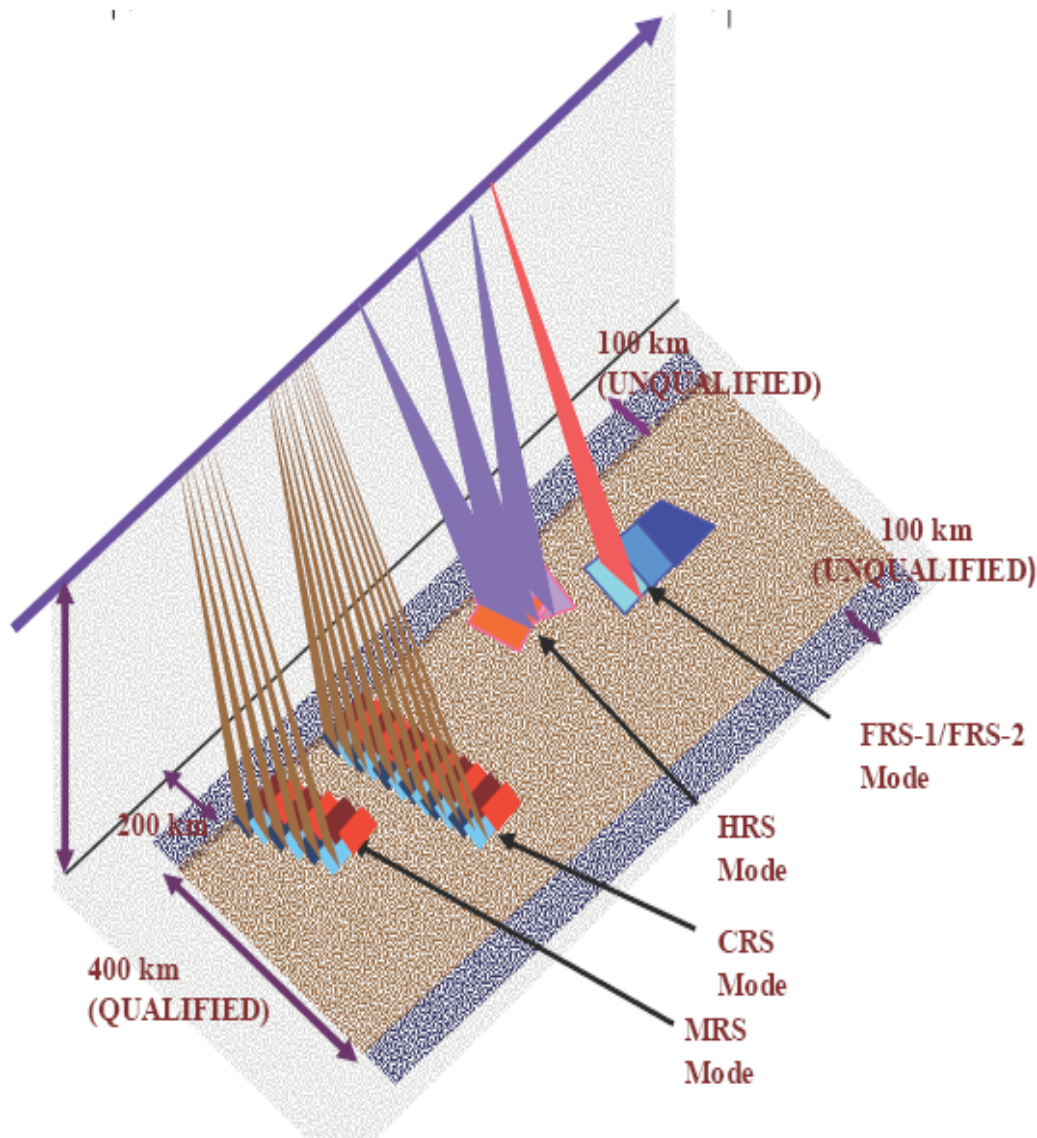
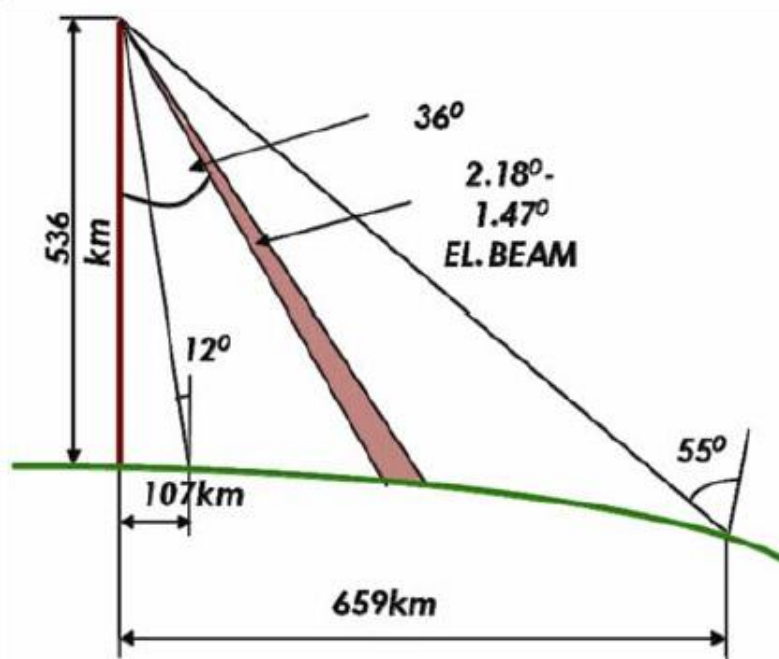


Figure 1-1 Schematic Diagram showing different beam modes of RISAT-1 SAR

**Table 1-1 RISAT-1 Image quality parameters**

Swath coverage	Selectable within 107–659 km off-nadir distance on either side			
Incidence angle coverage	12°–55°			
Image quality Mode	Single pol HH/HV/VV/VH	Polarization Dual pol HH + HV/VV + VH	Circular (hybrid) polarimetry TX: CP Rx: V and H (experimental)	Quad pol HH + HV + VV + VH
HRS	1 m (azimuth) × 0.67 m (range) resolution, 10 × 10 km (10 × 100 km experimental) spot, Min $\sigma_0 = -16$ dB			
FRS-1	3 m (azimuth) × 2 m (range) resolution, 25 km swath, Min $\sigma_0 = -17$ dB			
FRS-2			3 m (azimuth) × 4 m (range) resolution, 25 km swath, Min $\sigma_0 = -19$ dB	9 m (azimuth) × 4 m (range) resolution, 25 km swath, $\sigma_0 = -20$ dB
MRS	21–23 m (azimuth) × 8 m (range) resolution, 115 km swath, Min $\sigma_0 = -17$ dB			
CRS	41–55 m (azimuth) × 8 m (range) resolution, 223 km swath, Min $\sigma_0 = -17$ dB			

HRS: High resolution stripmap, FRS: Fine resolution stripmap, MRS: Medium Resolution ScanSAR, CRS: Coarse resolution ScanSAR, C-HRS, C-FRS, C-MRS and C-CRS refers to circular polarization in respective modes.



**Figure 1-2 Imaging Geometry of RISAT-1**

This C-band active antenna based, multi-mode SAR payload was launched on 26th April 2012 by PSLV-C19 flight. After positioning at 536 km sun-synchronous dawn-dusk circular orbit it was operated on May 1, 2012.

To achieve calibration accuracies required for most scientific analysis, a complex process utilizing **Internal** (built-in device) measurements and **External** (ground deployed device) measurements is needed. In general, any scientific application which involves the comparative study of radar reflectivity requires some level of radiometric calibration. A synthetic aperture radar (SAR) instrument maps the radar reflectivity of the earth's surface for a variety of remote sensing tasks. Depending on the application, a different degree of radiometric calibration is required. In the order of increasing complexity, this can be either

- a) Relative radiometric calibration within one scene,
- b) Relative radiometric calibration within all scenes of one mission, or
- c) Absolute radiometric calibration.

A physical unit can only be attached to the measured reflectivity map after radiometric calibration. The first case (a) is sufficient, for instance, for visual feature extraction. Exemplary, the second type (b) is a prerequisite for multi-temporal coverage, the derivation of repeat-pass interferometric images, or relatively calibrated polarimetric channels. On the other hand, absolute radiometric calibration (c) is beneficial or required for

- Derivation of physical parameters like soil moisture from reflectivity measurements
- Automatic feature extraction and classification for instance for land usage maps
- Comparability and cross-calibration between different SAR instruments

It has to be noted that absolutely calibrated images are the most versatile, as they inherently include relative calibration. This is the reason why SAR image products are usually delivered absolutely calibrated.

### **1.2.2 External Calibration**

The use of ground targets with known scattering properties to derive the radar system transfer function is referred to as external calibration. The advantage of external calibration over internal calibration is that the end-to-end system performance can be directly measured. Therefore, system parameters, which are difficult to measure, such as antenna pattern, the bore sight gain and angle and also signal propagation effects, can be determined from the external

calibration. All data products generated by SAR correlator are absolutely calibrated such that image pixel intensity is directly expressed in terms of the mean surface back scatter coefficient. External calibration allows absolute determination of the scattering coefficient ( $\sigma_0$ ). It is desirable to calibrate a radar image by measuring the return power from a target of known radar cross section [8, 9]. The external calibration technique generally involves two type of targets:

**Point Targets** e.g. Active target – Active Radar Calibrator (Transponder), Passive Targets – Corner reflector (Dihedral or Trihedral), Flat rectangular Plate, Sphere (Metal), Luneberg – Lens reflector etc.

**Distributed Targets** e.g. Forest, Desert, Run way, rough sea, large towns etc. [10]

Amazon Rainforest is an established distributed target for SAR data calibration as announced by SAR subgroup of Working Group on Calibration and Validation (WGCV) of Committee on Earth Observation Satellite (CEOS). Canadian Boreal forest is also being used by researchers as distributed target for SAR calibration [22, 23]. There are various standard point targets for SAR data calibration which can be classified based on their nature of functionality viz. active and passive standard targets. In active domain, active radar calibrator (ARC) and polarimetric active radar calibrator (PARC) are used whereas in passive domain dihedral corner reflector (DHCR), triangular trihedral corner reflector (TTCR), square trihedral corner reflector (STCR), luneburg lens are used. In this study, passive standard target (DHCR, TTCR and STCR) has been utilized for RISAT-1 SAR calibration. For absolute calibration, point target RCS is computed and compared with the theoretical RCS of CR.

### **1.2.2.1 Point Target Analysis**

Point targets are typically manmade devices such as, corner reflectors (Passive devices), transponders or Active Radar Calibrators - ARCs, tone generators and receivers (Active devices). The advantage of using ARC is that it has larger radar cross-section, the size is small and can be tuned as per one's requirement as compared to corner reflectors. Now-a-days, it is very difficult to find an area free from bright man-made targets for use of corner reflectors whereas, ARC can be used anywhere because it has high radar cross section value. Each of these device spans a geometric area much less than a resolution cell but exhibits a radar cross section that is bright with respect to the total backscattered power from the surrounding target area within the resolution cell. The strength of the radar signal reflected from an object is conventionally represented by the radar cross-section (RCS)  $\sigma$ . It is expressed in terms of the

physical size of an isotropic radiator that would give rise to the same level of reflection as that observed from the sample target. The RCS,  $\sigma$  is essentially a measure of target's ability to reflect radar signals in the direction of the radar receiver and has units of area ( $m^2$ ), or when expressed in decibels as  $dBm^2$ . RCS is usually used for point targets or targets comparable to the resolution cell. To minimize the calibration errors from the background area, point target RCS should be at least 20 dB larger than the total power scattered from the SAR image resolution cell. The pointing angle of the device relative to the radar must be precisely measured (an uncertainty  $< 1\sigma$ ), since generally the radar cross section is highly dependent on orientation. An additional consideration is the contribution from multipath [11]. This occurs when either the transmitted or reflected signal scatters off the local terrain or nearby structures and is received by the SAR antenna simultaneously with the calibration target return. The device RCS should be characterized by measuring its scattering properties in a controlled environment over a range of temperatures and viewing angles. There are basically two methods available for determination of  $\sigma_0$  by using point targets

- Integral Method
- Peak Estimation Method

In integral method, the value of calibration constant is derived by integrating the power from all the pixel values of point target whereas for peak estimation method estimated peak value of a reflector is used [13, 30, 31].

Gray et al. (1990) [13] showed that integral method for SAR image calibration is better than the peak estimation method. SAR image calibration where the peak pixel value of the impulse response of a known radar reflector is used to derive the backscatter coefficient of adjacent clutter areas may be affected from the problems arising from coherent and non-coherent radar or processor phase errors with associated focus problems, look registration, and underestimation of the peak value of the reflector. It was shown by them [13] that the integral method is independent of the radar system focus or partial coherence and thereby possesses an important advantage over the usual technique which relies on an estimate of the peak of the reflector impulse response. The impulse response function (IRF) is the point target return which measures the focusing and energy distribution in SAR image in both elevation and azimuth direction. As it has already been proven that integral method is better than peak estimation method, hence, in this work, integral method has been used for deriving the calibration constant.

There are other variations which also affect the value of back scattering coefficient, they are:

- Range and Incidence Angle Variation
- Multilooking
- Slant Range to Ground Range Conversion
- Fading Considerations

### **1.2.2.2 Distributed target**

Distributed targets are an extension of point targets; due to terrain irregularities, most natural targets do not have well-defined reflection geometry, but rather they tend to have many scattered reflection points. Distributed targets are comprised of many elementary point scatterers, where each scatterer has random reflection amplitude, but the superposition of these random amplitudes will result in the total RCS for that distributed target.

Followings assumptions are taken in to consideration while selecting distributed target

- A flat terrain is considered, i.e. there is no slope.
- Any change in incidence angle across a distributed target is neglected, i.e. a distributed target corresponds to one average value of the incidence angle.
- The pixel value in the image is proportional to square root of intensity,
- The intensity value is proportional to the radar brightness  $\beta^0$

The two derivation methods of the backscattering coefficient  $\sigma^0$  are:

- The simplified derivation method allows a rough estimate of the backscattering coefficient
- The comprehensive derivation method includes a set of equations for accurate derivation of the backscattering coefficient to remove the sources of radiometric errors (e.g. ADC nonlinearities or replica pulse power variations, the elevation antenna pattern)

The radar brightness  $\beta^0$  is proportional to the backscattering coefficient  $\sigma^0$  divided by the Sine of the pixel incidence angle,

$$\beta^0 = \frac{\sigma^0}{\sin\alpha}$$
$$\sigma^0 = \beta^0 \times \sin\alpha \quad (1)$$

where,  $\alpha$  is local incidence angle

The digital number giving the value of a pixel in PRI products say DN is directly related to  $\beta^0$  and to  $\sigma^0$  by the relation

$$\begin{aligned} [DN]^2 &= constant \times \beta^0 \\ &= constant \times \frac{\sigma^0}{\sin\alpha} \\ &= constant(\alpha) \times \sigma^0 \end{aligned} \quad (2)$$

where, the constant ( $\alpha$ ) is a function depending on the local incidence angle and can be written as:

$$constant(\alpha) = K \times \frac{\sin\alpha_{ref}}{\sin\alpha} \quad (3)$$

where, K is the calibration constant and  $\alpha_{ref}$  is the reference incidence angle (mid range incidence angle). K is specific to the type of data product and to the processing centre.

The back scattering coefficient is usually expressed in decibels,

$$\sigma^0 (dB) = 10 \times \log_{10} \sigma^0 \quad (4)$$

The back scattering coefficient of a distributed target by simplified method is given by:

$$\sigma^0 = \left( \frac{1}{N} \times \sum_{i,j=1}^N DN_{i,j}^2 \right) \times \frac{1}{K} \times \frac{\sin\alpha}{\sin\alpha_{ref}} \quad (5)$$

where, N is the number of pixels within the Area of Interest (AOI),

i and j are the range and azimuth locations of the pixel within the distributed target containing N pixels,

$DN_{ij}$  is the digital number corresponding to the pixel at location (i,j),

$\alpha$  is the average incidence angle within the distributed target,

$\alpha_{ref}$  is the reference incidence angle

Second method for the derivation of backscattering coefficient is Comprehensive method, which gives the absolute value of  $\sigma^0$ . But for this method we have absolute values of other parameters also. These parameters are sensor dependent and derived only by using internal calibration method. If these parameters are not known, we can't determine absolute value of  $\sigma^0$ .

Both of the above described methods give the value of back scattering coefficient for distributed target. Simplified method gives the rough estimate of back scattering coefficient whereas, comprehensive method gives the absolute value of back scattering coefficient. Comprehensive method gives good result as compared to simplified method because in that method, all the loss factors are calculated and added to the final calculation. If the point targets are not available in that case, we can calculate the back scattering coefficient by taking distributed target as a reference.

### **1.2.3 Geometric Calibration**

The Geometric Calibration of an image refers to the accuracy with which an image pixel can be registered to an earth-fixed grid. Geometric distortion arising from variation in the terrain elevation is especially severe for a side-looking, ranging instrument such as a SAR.

To check the geometric calibration of a SAR image, the image co-ordinate system is compared with a reference, usually some ground map projection. In this study, it is done by comparing the known locations of corner reflectors whose positions have been adequately surveyed with the location estimated from Geo-tiff image of RISAT-1 MRS/FRS.

### **1.3 SAR Image Quality Assessment**

Image quality refers both to the impulse response properties of a radar/processor combination, and to the response of the system to distributed scatterers. The SAR response to a point target, assuming negligible background reflectivity and thermal noise, is commonly referred to Impulse Response Function (IRF). Calibration and monitoring of SAR instruments parameters with respect to different beams and polarizations is required to ensure the consistency in the derived backscattered values. Use of passive corner reflectors as point targets is one of the fundamental approaches for SAR calibration. To evaluate the image quality parameters, impulse response of these reflectors in both elevation and azimuth directions is measured. The analysis of the signature of a point target in a SAR image allows the determination of several parameters that are related to the SAR side lobe peaks [16]. The image quality parameters evaluated are background to peak ratio (BP) ratio, peak side lobe ratio (PSLR), spatial resolution, radiometric resolution and integrated side lobe ratio (ISLR) for each of the corner reflectors. Figure 1-3 shows the IRF of an isolated point target. The Impulse Response Function is a *sinc* function with a mainlobe and many secondary lobes. The figure shows a one dimensional cut of the IRF in the azimuth direction (spacecraft velocity direction) and two quality parameters measured from it (spatial resolution and PSLR). A SAR image is the result

of coherently processing returned echo signals; thus, the pixel values are complex quantities. The peak intensity is the maximum pixel value in the main lobe of the impulse response function.

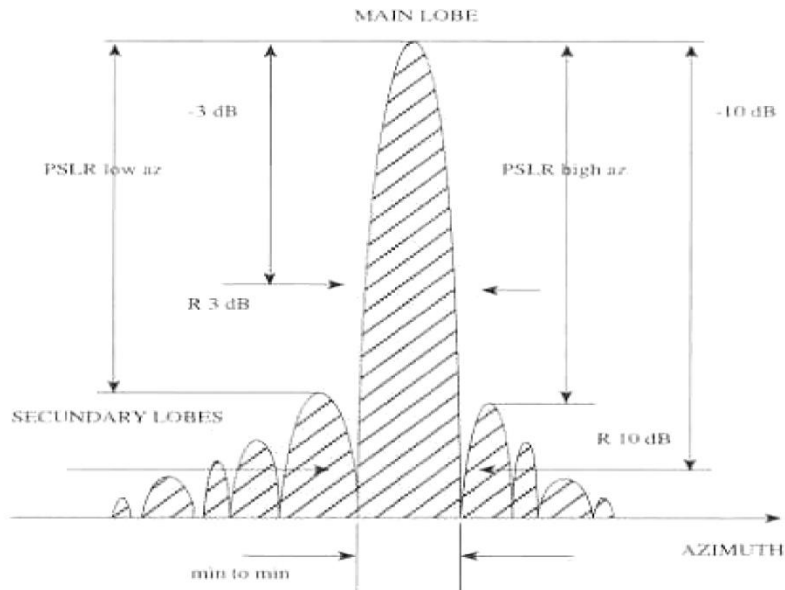


**Figure 1-3 Graphical representation of a SAR point target response showing several quality parameters [16].**

### 1.3.1 Spatial resolution

The spatial resolution is the distance between two objects on the ground at which the images of the objects appear distinct and separate [16]. From the impulse response function, it is calculated as the distance between the points with intensities 3dB below the maximum intensity of the main lobe peak in the azimuth and range directions. The definition of the 3dB points is equivalent to the points with half the intensity of the maximum. The ideal spatial resolution of a SAR system can be computed from theory and then compared with that obtained from the IRF analysis.

The spatial resolutions in range and azimuth are obtained from theory:

$$\text{Slant range resolution: } \rho_{rs} = \frac{c}{2B}$$

where  $c$  the speed of the light and  $B$  the chirp bandwidth.

$$\text{Ground range resolution: } \rho_{rg} = \frac{\rho_{rs}}{\sin\phi}$$

where  $\phi$  is the local incidence angle.

$$\text{Azimuth resolution: } \rho_{az} = \frac{L}{2}$$

where  $L$  is the antenna length in azimuth direction.

IRF of a point target and the points 3dB below the maximum intensity are shown in Figure 3. To determine these resolution it is necessary to calculate the pixel and line spacings (range and azimuth spacing, respectively). These values are calculated as:

$$S_{Pr} = \frac{c}{2F_s}$$

where  $S_{Pr}$  is the pixel spacing (i.e. the range spacing) and  $F_s$  is the sampling frequency.

$$S_{Pa} = \frac{V_{st}}{PRF}$$

where  $S_{Pa}$  is the line spacing (i.e. the azimuth spacing),  $V_{st}$  is the sensor-target mutual velocity and  $PRF$  is the pulse repetition frequency. These values are very close to those of the range and azimuth resolutions. It means that the main lobe of the IRF is contained just in one pixel and it becomes impossible to determine the distance between the -3dB points. So, an interpolation is needed by a factor of at least 8 to make the measurement possible.

### **1.3.2 Peak side lobe ratio**

The peak side lobe ratio, PSLR, is defined as the ratio of the peak intensity of the most prominent side lobe to the peak intensity of the main lobe. There are two measures of the PSLR, corresponding to the two sides of the main lobe both in azimuth and range directions. This parameter is expressed in decibels. [16]. It represents the ability of the SAR to identify a weak target from a nearby strong one.

The PSLR is calculated as

$$PSLR = 10 \log_{10} \frac{I_s}{I_m} \quad (6)$$

where  $I_s$  stands for the peak intensity of the most intense side lobe and  $I_m$  stands for the peak intensity of the main lobe. The PSLR may be improved by means of a side lobe clutter and noise minimization with multiple-aperture SAR, which considerably improves the quality of SAR image.

### **1.3.3 Integrated side lobe ratio**

The integrated side lobe ratio (ISLR) is the ratio of the power (energy) in the main lobe to the total power in all the side lobes. It characterizes the ability to detect weak targets in the neighborhood of bright targets and is a measurement of the relative importance of the side lobes with respect to the main lobe [16].

The European Space Agency (ESA) established the ISLR as the ratio of the power within a square centered on the maximum and ten resolution cells side, without considering an inner window of two resolution cells side and the power in the second window.

$$ISLR = 10 \log_{10} \frac{\int_{10 \times 10} I dx dy - \int_{2 \times 2} I dx dy}{\int_{2 \times 2} I dx dy} \quad (7)$$

### **1.3.4 Signal to Clutter Ratio**

The large RCS is required to ensure adequate visibility above the surrounding background scatterers, often termed clutter. Due to the clutter and noisy environment on the ground, the clutter contribution adjacent to ground-fixed reference target should be taken into account for the performance estimation. One measure of visibility is the target signal-to-clutter ratio (SCR) and is estimated as follows:

$$SCR = \frac{\sigma_P}{\sigma_{0A_{res}}} \quad (8)$$

where  $\sigma_P$  is the backscattered energy of a reference point target and  $\sigma_{0A_{res}}$  represents the mean backscattered energy of the clutter within a resolution cell [16]. To measure the target signal-to-clutter ratio from an actual SAR image, the ratio of the peak power in the target impulse response to the mean background clutter power, estimated from an area located close to the target, is often used.

## 2 CAL VAL SITE

### 2.1 Site selection

For the proper calibration of the data, suitable site selection for the point target deployment is the prime requirement. Following factors are taken into account when choosing sites for point target deployment:

1. The flatness and homogeneity of the surrounding land.
2. Perceived sources of radar clutter in the vicinity.
3. Distance from metallic boundary fences.
4. Overlap of adjacent point target (CR) responses.

### 2.2 Description of sites

Four sites were selected in and around Ahmedabad and Rann of Kutch, Gujarat based on the above mentioned factors for the present study. Study area map selected sites is presented in Figure 2-1. These selected sites are comprised of homogenous areas with uniform soil. The point targets were deployed at particular locations within these sites where background reflection is less as compared to point target return.

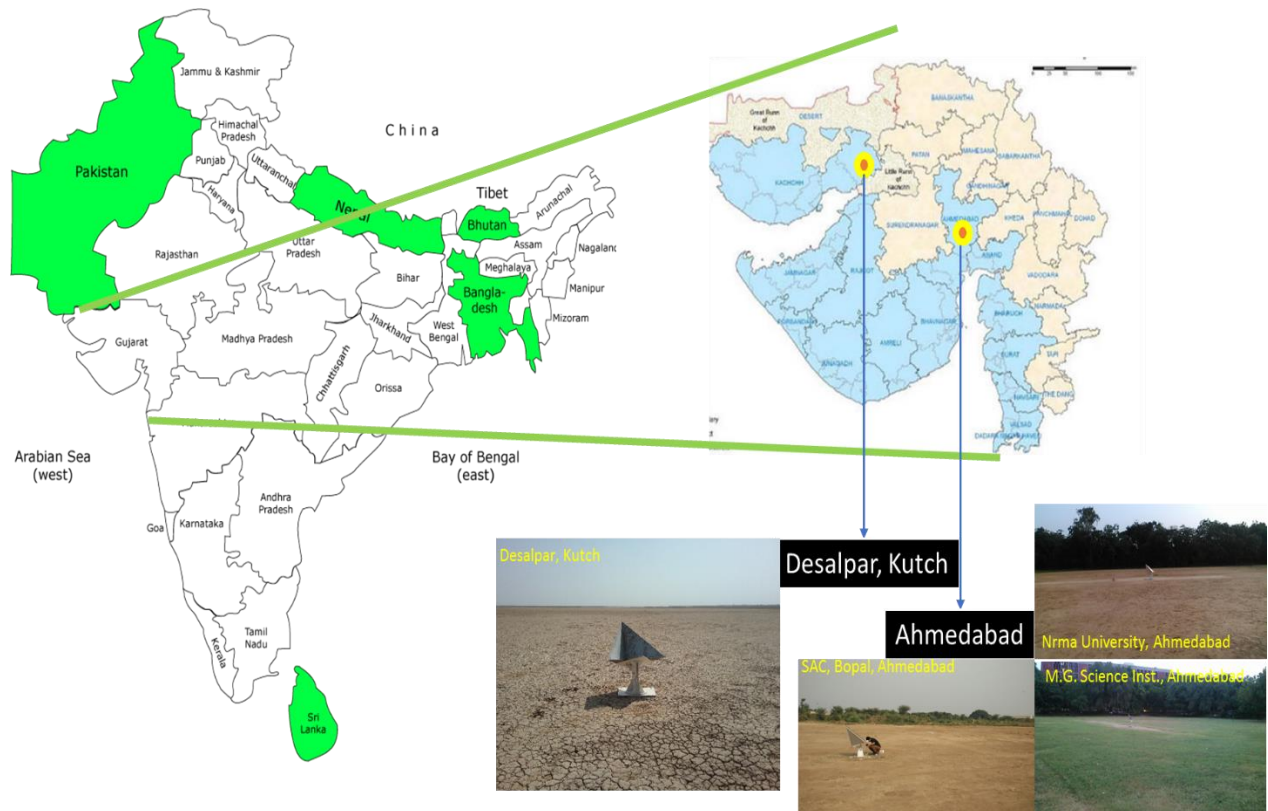


Figure 2-1 Study area map of Cal Val Site

### 2.2.1 SAC-Bopal site, Ahmedabad

The SAC-Bopal site in Ahmedabad has been developed for vicarious calibration of high resolution optical as well as SAR sensors. This site has been artificially created by SAC adjacent to Bopal campus. The site consists of a very uniform leveled bare land (yellow in color) of 115m x 115m with very clear brick boundary constructed on all four sides and 4m x 4m concrete white squares on the four corners of the site.



**Figure 2-2 Calibration site near SAC, Bopal Campus [courtesy: Google earth]**

Figure 2-2 shows its location (marked by yellow circle) on the google earth image. Due to its comparatively small size, this site is suitable for high resolution mode RISAT-1 data (FRS-1/2).

### 2.2.2 Desalpar site, Rann of Kutch

The Rann of Kutch site is an extensive mudflat which gets inundated during monsoon and flooding from fresh inland and saline water from the Gulf of Kutch during June-August. During summer months (March– July), the Rann becomes dry and barren with high temperatures (>40 deg C), resulting in creation of salt encrusted flat wasteland, totally devoid of vegetation. The fact that the site is devoid of any buildings and vegetation and its large uniform area, makes this site a potential site for the calibration of high and medium resolution SAR sensors.

In the winter season (November – February), the minimum temperature can go below 10 deg C. The average annual rainfall is less than 25mm and the area is situated about 7-10 m above sea level. The size of this site is nearly 3×7 sq km and Figure 2-3 shows its location on google earth image. Because of large size and uniform background, this site is suitable for calibration of both medium resolution (MRS) and high resolution (FRS-1/2) RISAT-1 data.



**Figure 2-3 Calibration site at Desalpar, Rann of Kutch [courtesy: Google earth]**

### **2.2.3 Grounds at M.G. Sci. Institute and L.D. Arts College, Ahmedabad**

This site is situated at the center of Ahmedabad city, which resolve lots of logistic issues. Two grounds at M.G. Science Institute and L.D. Arts college are being utilized for corner reflector deployment during satellite pass. These grounds have approximate area of 5600 sq. m. (80m X 70m) and 13225 (115m X 115m) respectively. These both sites are quite suitable for radiometric calibration of FRS-1 RISAT data but not suitable for MRS data due to small size, vicinity of buildings and high extent of vegetation around it. Figure 2-4 shows the location of two grounds on google earth image.

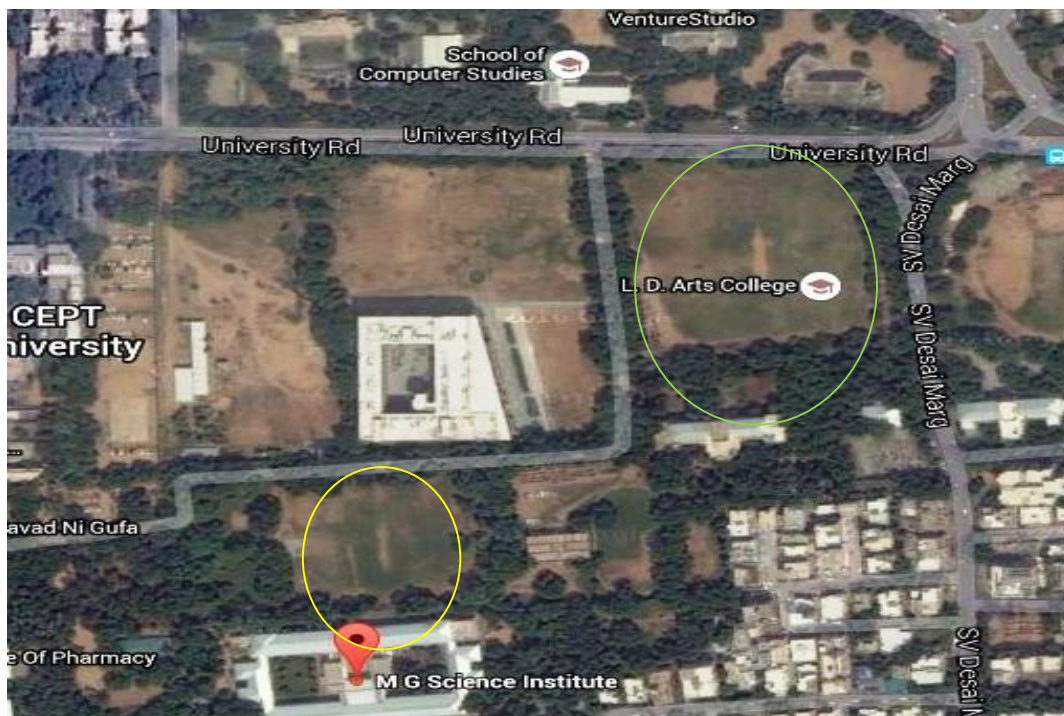


Figure 2-4 Calibration grounds at MG Science Institute and L.D. Arts College, Ahmedabad [courtesy: Google earth]

### 2.2.4 Nirma University Ground, Ahmedabad

Nirma University Football ground is used as suitable site for corner reflector deployment due to wide area, flat terrain, dry soil and homogenous soil texture. The shape of this site is rectangle covering 160 m in length and 80 m in width. The total area of this site is approximately 12800 sq. m. and this site is quite suitable for radiometric calibration of FRS-1 RISAT-1 data. The synoptic view of Nirma University ground is shown in Figure 2-5.

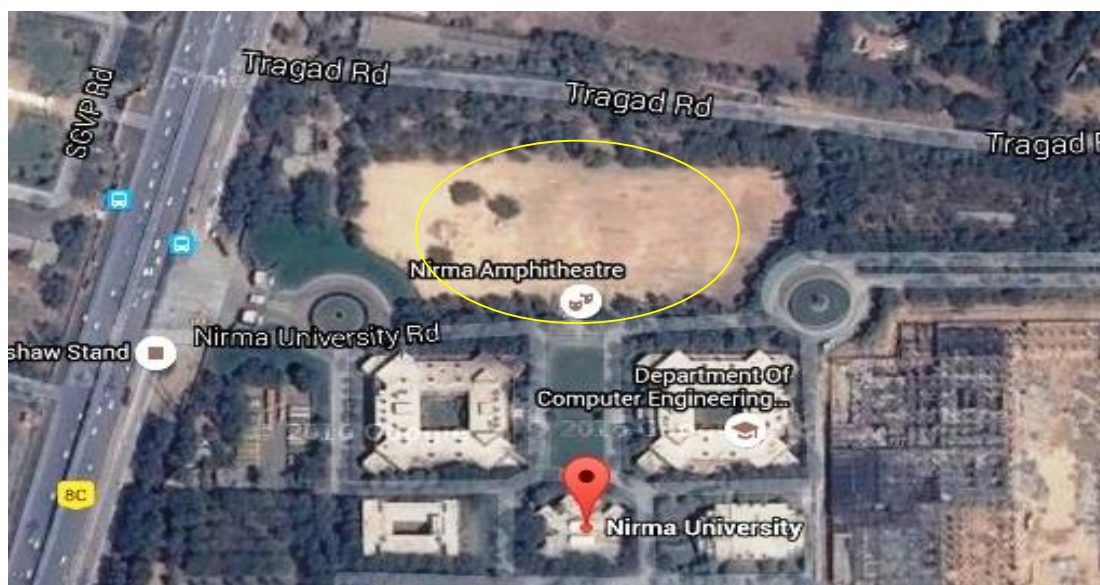


Figure 2-5 Calibration site at Nirma University, Ahmadabad [courtesy: Google earth]

**Table 2-1 center latitude and longitudes of cal val sites**

<b>Sr. No.</b>	<b>Location Name</b>	<b>Latitude N(deg.)</b>	<b>Longitude E(deg.)</b>
1	SAC, Bopal, Ahmedabad	23 <sup>0</sup> 02'43.06"	72 <sup>0</sup> 27'07.54"
2	MG Science Institute, Ahmedabad	23 <sup>0</sup> 02'10.15"	72 <sup>0</sup> 32'35.85"
3	Nirma University, Ahmedabad	23 <sup>0</sup> 07'47.97"	72 <sup>0</sup> 27'07.54"
4	Desalpar, Rann of Kutch	23 <sup>0</sup> 46'14.10"	70 <sup>0</sup> 43'19.30"

## **3 MATERIALS AND DATA USED**

---

---

### **3.1 Corner Reflectors**

In the present study, point targets (corner reflectors) have been used for the radiometric and geometric calibration of RISAT-1 data. The advantages of using passive calibration point targets over active transponders are that they can be built with high radiometric accuracies, do not delay the reflected signal (a desired property for geometric calibration), and are relatively robust for field-use during the calibration campaign. Their limitations being their bulky size because of which it cannot be moved easily to a new location and data recording cannot be done.

Trihedral corner reflectors are relatively insensitive to misalignments which is a main reason for their use. Utilizing precise levels and compasses (taking the local declination into account), an alignment accuracy of  $0.5^\circ$  for both azimuth and elevation can be achieved. This results in a misalignment uncertainty of below 0.1 dB. The theoretical values of the radar cross section of corner reflectors can be easily computed. However, mechanical imperfections will lead to a reduction of the theoretical value.

### **3.2 General Criteria for Designing a Corner Reflector**

In general, a corner reflector should be built regarding the following principles: it should be of light weight, easy to mount, difficult to be reached by unauthorized people, well fixed, and resistant to all weather conditions. The triangular trihedral corner reflectors used in this study are in cubic shape and made up of aluminum having wooden mount.

#### **3.2.1 The Material of Corner Reflector**

For the reason of keeping the mechanical stability and accuracy of artificial shifts to a millimetric level, both the size and the weight of the structure should be kept limited. In this regard, the most suitable material for corner reflector is aluminum, which is remarkable for its low density and ability to resist corrosion due to the phenomenon of passivation. The density of common aluminum alloy varies from 2.6 g/cm<sup>3</sup> to 2.9 g/cm<sup>3</sup>, while the density of common iron and steel can vary from 7.75 to 8.05 g/cm<sup>3</sup>. For example, a small trihedral corner reflector made of aluminum with a size of 50 cm x 50 cm x 75 cm and 2mm width weighs approximately 5.6 kg (take density as 2.8 g/cm<sup>3</sup>), but if the same corner is made of steel, it will weigh 16 kg (8 g/cm<sup>3</sup>) in total, which is a remarkable increase in weight.

### 3.2.2 The Shape of Corner Reflector

In principle, the reflector should be characterized by a reflectivity much higher than that of the surrounding scatterers, the reflector should have a high RCS for a relative small size. Some of the most common corner reflectors being used are flat plate, dihedral, triangular trihedral, and cubic trihedral. The theoretical maximum RCS for different types of corner reflectors is shown in Table 3-1[17].

**Table 3-1 Theoretical maximum RCS for different types of Corner reflectors [17]**

Target	Example	Maximum Theoretical RCS (dBm <sup>2</sup> )
Triangular Trihedral	 <p>Image credit: Geoscience Australia</p>	$\sigma_T = \frac{4\pi a^4}{3\lambda^2}$
Flat square plate	 <p>Image credit: Drake and Hatty [2013]</p>	$\sigma_T = \frac{4\pi a^4}{\lambda^2}$
Circular Trihedral	 <p>Image credit: www.radartutorial.eu</p>	$\sigma_T = \frac{0.507\pi^3 a^4}{\lambda^2}$
Dihedral	 <p>Image credit: Ferretti et al. [2007]</p>	$\sigma_T = \frac{8\pi a^4}{\lambda^2}$
Square Trihedral	 <p>Image credit: Qin et al. [2013]</p>	$\sigma_T = \frac{12\pi a^4}{\lambda^2}$

Considering the fact that the making of triangular trihedral is easier, it is considered better to use triangular trihedral. However, for the experimenting purpose, square trihedrals and a dihedral having leg length 0.60m, 1.5m were also used along with the triangular trihedrals (leg length 0.90m) in the present study. An assembly of two flat metal plates placed at right angles

to each other is called a dihedral corner reflector. If the line of intersection between the plates is perpendicular to the radar line of sight, the specular reflection from one plate will rebound from the other and return in the direction of the radar. Thus dihedral corner reflector presents a large radar cross section. The addition of third plate orthogonal to both the others will form a trihedral corner reflector, which will allow triple reflection in both elevation and azimuth relative to the trihedral symmetry axis. Figure 3-1, Figure 3-2 and Figure 3-3 show the triangular trihedral, square trihedral and dihedral used in this study for the radiometric calibration of RISAT-1 data.



**Figure 3-1 Triangular Trihedral Corner Reflector (size 0.90m)**



**Figure 3-2 Square Trihedral Corner Reflector (size 0.60m)**

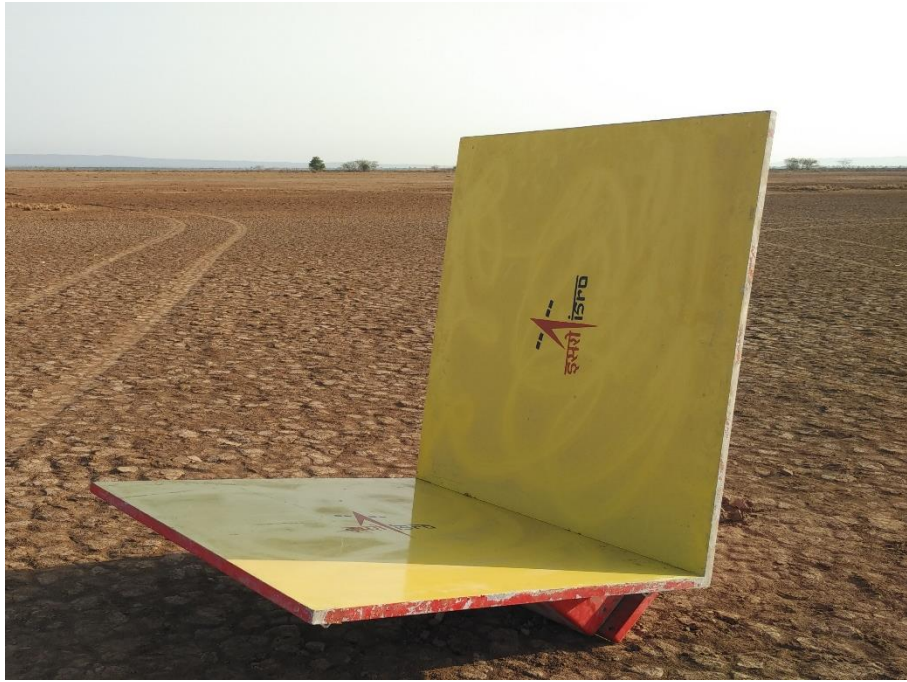


**Figure 3-3 Dihedral Corner Reflector (size 1.5m)**

### **3.2.3 The Installation of Corner Reflector**

In order to gain a maximum RCS, the corner reflector should be installed on a horizontal plate and the direction of the reflectors should be set along LOS in order to gain the maximum RCS. If the direction deviates from the LOS direction or tilts slightly, the RCS value would decrease considering the different shape and size of the corners.

### **3.2.4 The Bending of Corner's Plate.**

The most possible influencing factors that could bias the result are precipitation and bending plates. A possible phenomenon that may bend metallic plates is the thermal expansion. For a given leg length of the corner reflector, it should be calculated.

## **3.3 Data Used**

RISAT-1 Images of FRS-1 and MRS mode with various types of polarization were acquired over the area of interest. RISAT-1 operating in C-band, has capabilities in terms of coverage, polarization, range of incidence angles and contains scan SAR mode of operation. Total 13 (thirteen) SAR Image was acquired consisting 4 (four) FRS-1 image and 9 (Nine) MRS Image in CEOS format. For the data used in the present analysis, the incidence angle varies from  $14.25^\circ$  to  $44.78^\circ$ . Details of the data used is shown in Table-3-2.

**Table 3-2 Details of the RISAT-1 data used in the study**

<b>Mode</b>	<b>Date</b>	<b>Polarization</b>	<b>Beam No</b>	<b>Incidence Angle</b>	<b>Node</b>	<b>Orientation</b>
FRS - 1	21. Apr. 2015	HH, HV	104	44.78032	Ascending	Left
FRS - 1	25. Apr. 2015	HH, HV	21	31.20945	Ascending	Right
FRS - 1	22. Jan. 2016	RH, RV	66	14.24753	Ascending	Left
FRS - 1	15. Feb. 2016	RH, RV	87	32.98252	Ascending	Right
MRS	5. Jul. 2015	HH, HV	87-97	36.79629	Descending	Left
MRS	30. Jul. 2015	HH, HV	87-97	36.79907	Descending	Left
MRS	24. Aug. 2015	HH, HV	87-97	36.77593	Descending	Left
MRS	18. Sep. 2015	HH, HV	87-97	36.79698	Descending	Left
MRS	13. Oct. 2015	HH, HV	87-97	36.81646	Descending	Left
MRS	7. Nov. 2015	HH, HV	87-97	36.78942	Descending	Left
MRS	2. Dec. 2015	HH, HV	87-97	36.76666	Descending	Left
MRS	27. Dec. 2015	HH, HV	87-97	36.76462	Descending	Left
MRS	14. Feb. 2016	HH, HV	87-97	36.80517	Descending	Left

## 4.1 General

The most common image quality parameters measured from SAR images are derived from and describe the shape of the impulse response function. The impulse response function (IRF) of a SAR image is the response to a point target assuming negligible reflectivity and thermal noise. The IRF is also sometimes referred to as a point spread function. For absolute calibration, RCS of corner reflector is computed and compared with the theoretical RCS.

For point target analysis, passive corner reflectors of known radar cross-section were deployed considering three important points [33].

- (i) Orientation of corner reflector with respect to SAR antenna
- (ii) The deployment site characteristics and
- (iii) Size and material of the CR i.e. it should have sufficient energy for scattering.

Precise deployment of CR is the primary requirement and for the best results, CR should be pointed directly along the bore sight of the SAR antenna [34]. Secondly, deployment site should be free from the multi-path contributions and should be located distant from the power lines and housing colonies [35].

## 4.2 Approach for Radiometric calibration using Point targets

After deploying the series of standard angle reflectors with known scattering cross section on the ground calibration field, the theoretical scattering cross-section of the standard angle reflectors ( $\sigma_{ref}$ ) to the corresponding image power ( $\epsilon_p$ ) through the RISAT-1 image of the calibration field can be related to the calibration constant as [32]:

$$K_i = \frac{\epsilon_{pi}}{\sigma_{ref} \sin\theta_i} \quad (9)$$

where,  $\epsilon_{pi}$  is the energy associated with the point target  $i$ ;  $\sigma_{ref}$  is the theoretical radar cross-section of the corner reflector;  $\theta_i$  is the incidence angle of the target  $i$ .

In order to improve the precision, the number of samples should be as much as possible. Using the average of the measured values corresponding to the point targets as the final measurement result of the calibration, i.e. calibration constants were determined as follows:

$$K = \frac{1}{N} \sum_{i=1}^N K_i \quad (10)$$

The typical response of point target image as seen in the RISAT-1 FRS-1 image of 22<sup>nd</sup> January 2016 is shown in Figure 4-1 below:

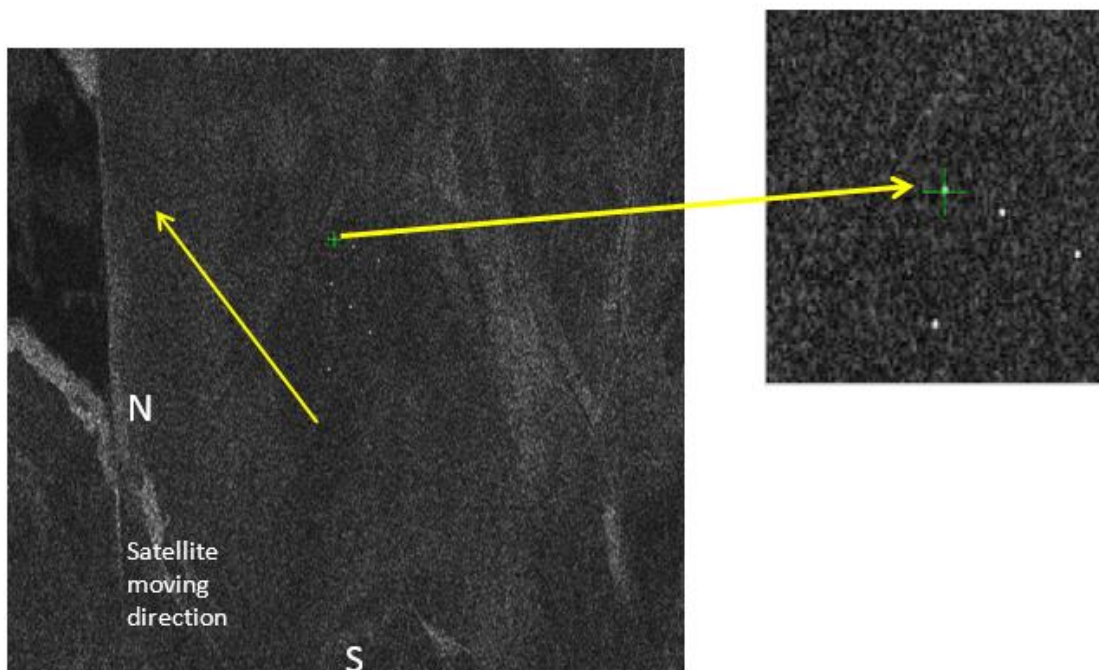


**Figure 4-1 RISAT-1 FRS-1 image of 22nd January 2016**

The key step in measuring the calibration constant is point target pulse response energy measurement. As already described in the previous sections that there are two types that are commonly used (i) peak estimation method and (ii) integral power method. In the present study, Integral Power method has been used. In integral method [13], power from a standard point target is taken by integrating the power from all pixel values corresponding to the point target, to arrive at the calibration constant. After receiving single look complex (SLC) data of FRS and ground range detected product (GRD) of MRS, reflectors were located in the image and Integral power method was applied to derive calibration constant.

The steps followed for the calculation of the energy associated with point target, following steps were used:

1. Firstly, the background corrected integrated power of point targets using corresponding RISAT-1 image has been calculated using the below mentioned approach [36]:
  - i. Extraction of a sub image of  $M \times M$  pixels (here  $M=32$  for FRS mode data) around the point target from image (Figure 4-2 & 4-3) converting the pixel values into intensity by squaring pixel DN values and calculation of the integrated power (PI) ( $PI = \sum (DN^2)$ ).

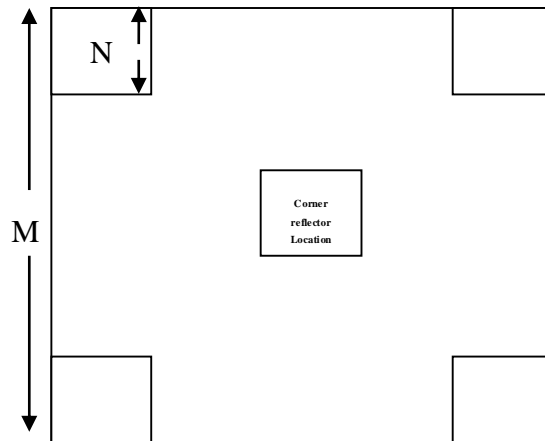


Figure 4-2 Schematics showing the subset of the data containing CR

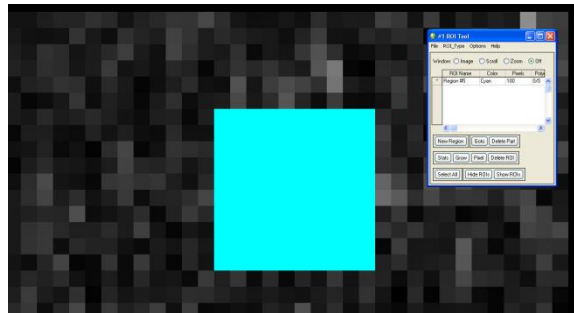


Figure 4-3 Subset of the image containing corner reflector

- ii. Selection of four corner areas around the point target in sub image with  $N \times N$  (here  $N=8$  for FRS mode data) pixels (as shown in Figure 4-4) and derivation of the mean background intensity and calculation of the mean background power ( $\langle B \rangle$ ).

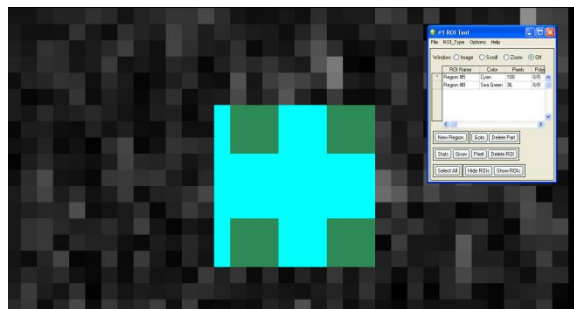


Figure 4-4 Selection of the clutter windows around CR

- iii. Subtraction of the mean background power from the integrated corner reflector power value to obtain background corrected integrated power (PT).

$$PT = PI - \frac{M}{N} \langle B \rangle \quad (11)$$

2. Using the background corrected integrated power, energy associated with point target is estimated using the following equation:

$$\varepsilon_{pi} = (PT) \times \text{pixel area} \quad (12)$$

Ground area of the pixel at point target can be calculated as,

$$A_i = (\text{Line spacing} \times \text{Pixel spacing}) / \sin \theta_{pt}$$

where, value of line spacing and pixel spacing can be obtained from *Output Line Spacing* and *Output Pixel Spacing* tags respectively of header file provided with the data and  $\sin \theta_{pt}$  can be manually calculated.

3. Using the energy estimated in step 2, and using following equation [38],

$$K_{dB} = 10 * \log_{10}(\sum DN^2) - \sigma_{dB} + 10 * \log_{10} \left( \frac{\sin i_p}{\sin i_{center}} \right) + 10 * \log_{10} (\text{scattering area}) \quad (13)$$

where,  $i_p$  = incidence angle at position of point target and

$$\text{scattering area} = (\text{azimuth resolution} * \text{slant range resolution}) / \sin i_p \quad (14)$$

calibration constant is determined for each corner reflector and then average value of the calibration constant is calculated and reported for that particular mode and beam.

Using the above steps, calibration constants was determined for each date data. The point target analysis was also carried out in Gamma software [Wegmüller and Werner, 1997] and the same results were compared by results obtained by manual calculations.

It should be noted that while calculating the calibration constant for MRS,  $\sin i_p$  term was not considered while calculating the scattering area (Eq. 14), as it was assumed that GRD product of MRS data, already takes into account this factor while converting from SLC to ground range. Also, output pixel spacing and output range spacing was used for the calculation.

### 4.3 Determination of Signal to clutter ratio (SCR)

For the determination of signal to clutter ratio, the methodology adopted in [13] has been used and is described below:

Consider the calibration of a uniform region of an actual SAR image as shown in Figure 8 of ground area  $A_{nu}$ , having  $N_{nu}$  pixels which has an unknown back scattering coefficient  $\sigma^o$ . The subscript nu denotes that the area in question contains receiver noise as well as uniform clutter signal. The known reference reflector is within ground area  $A_{pnu}$ , having  $N_{pnu}$  pixels and cross section  $\sigma$ . The subscript pnu denotes that the area in question contains the reflector, the receiver

noise and uniform clutter signal. Data is collected with the transmitter turned “Off” for the ground area  $A_n$ , having  $N_n$  pixels and being at the same incidence angle as other two areas. The integrated powers over these three specified areas are defined as  $\epsilon_{nu}$ ,  $\epsilon_{pnu}$  and  $\epsilon_n$  respectively.

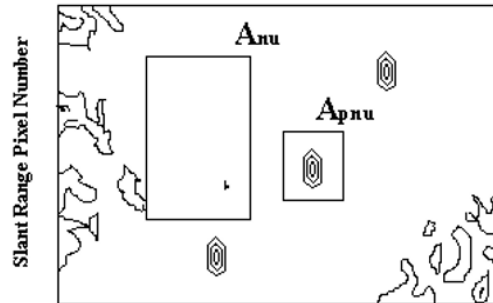


**Figure 4-5 Schematics showing the area containing clutter and point target**

$$\epsilon_u = \epsilon_{nu} - \epsilon_n (A_{nu} / A_n) \quad (13)$$

$$\epsilon_p = \epsilon_{pnu} - \epsilon_{nu} (A_{pnu} / A_{nu}) \quad (14)$$

$$\sigma_0 = (\sigma / A_{nu}) [\epsilon_{nu} - \epsilon_n (A_{nu} / A_n)] \quad (15)$$

where, each ground area  $A$  may be related to the number of pixels  $N$  by using

$$A = N \delta_r \delta_a / \sin \theta \quad (16)$$

where,  $\delta_r$  and  $\delta_a$  are the image slant range and azimuth sampling distances, and  $\theta$  is the local incidence angle. By restricting the range extent of the two areas,  $\theta$  may be invariant over each of the regions considered. If we don't have the values of slant range and azimuth sampling distances, we can determine so by converting it into ground range. Then, the equation (15) can be adjusted for a ground range image using:

$$\delta_r = \delta_g \sin \theta \quad (17)$$

where  $\delta_g$  is the ground range pixel separation. This assumes that the incidence angle of the distributed target and point target are same.

A sub image of  $M \times M$  pixels centered on the point target is extracted from the image. Next, the background intensity is determined. The size and position of the pixel regions used may be varied. This ensures that nearby bright points can be avoided, thus allowing accurate determination of the mean background from uniform areas located within the same field as the point target. The mean background is subtracted from the sub-image to leave an image containing only the point target. Return from point as well as distributed target are calculated using equations (18) and (19):

$$\epsilon_p = \left( \frac{\text{area} A_{pnu}}{N_{pnu}} \sum a_{ij}^2 - \frac{N_{pnu}}{N_{nu}} \frac{\text{area} A_{nu}}{N_{nu}} \sum a_{ij}^2 \right) A_{pnu} \quad (18)$$

where,  $a_{ij}$  is the image power associated with pixel  $ij$ . The normalized integrated uniform scatterer power in the area  $A_{nu}$  is:

$$\overline{\epsilon_u} = \frac{\epsilon_u}{N_{nu}} = \left( \frac{\text{area} A_{nu}}{N_{nu}} \sum a_{ij}^2 - \frac{N_{nu}}{N_n} \frac{\text{area} A_n}{N_n} \sum a_{ij}^2 \right) \frac{\delta r \delta a}{\sin \theta} \quad (19)$$

Then, the signal to clutter ratio is calculated as:

$$SCR = \frac{\epsilon_p}{\overline{\epsilon_u}} \quad (20)$$

The summary of the steps adopted for the absolute radiometric calibration of FRS-1 and MRS intensity data is shown in Figure 4-6.

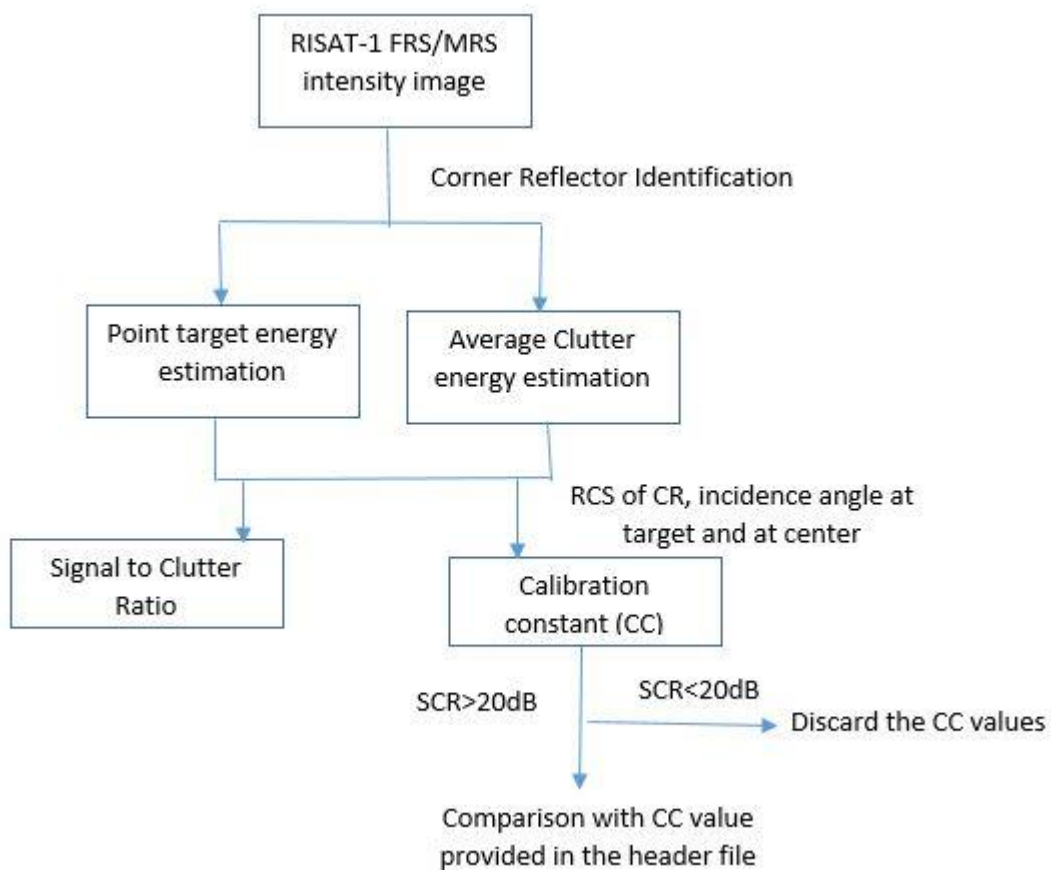


**Figure 4-6** Flowchart of the methodology adopted in the study

#### **4.4 Radiometric calibration using distributed target**

To perform a precise absolute image calibration, we can use distributed targets for deriving the radar backscattering coefficient. Distributed targets are the targets which are large and uniform in nature. Forest, Desert, run way, rough sea, large towns, etc. are some examples of distributed targets.

Distributed targets can be viewed as extension of point targets. Due to terrain irregularities, most natural targets do not have well-defined reflection geometry, but rather they tend to have many scattered reflection points. Distributed targets are comprised of many elementary point scatterers, where each scatterer has random reflection amplitude, but the superposition of these random amplitudes will result in the total RCS for that distributed target. They are constant over the time and shows very little variation in the back scattering coefficient. This property of the distributed targets is used to calibrate the SAR image.

Following assumptions are taken in to consideration while selecting distributed target:

1. A flat terrain is considered, i.e. there is no slope.
2. Any change in incidence angle across a distributed target is neglected, i.e. a distributed target corresponds to one average value of the incidence angle.
3. The pixel value in the image is proportional to square root of intensity.
4. The intensity value is proportional to the radar brightness  $\beta_0$ .

Here, we have taken Amazon Rainforest as a distributed target, due to its well defined nature in the literature. Its total area is approximately 5.5 Million km<sup>2</sup>.

For carrying out radiometric calibration using Amazon as the distributed target, following steps were carried out:

- 1) Amazon is selected as the area for performing calibration using distributed target method.
- 2) FRS mode image of the area is obtained in SLC format.
- 3) This image is then converted to amplitude image with the help of ENVI Software.
- 4) Further the image is opened in ENVI software for viewing and analyzing.
- 5) Region of Interest tool provided in the tools menu is used for selecting a region in the image. As the area is uniform in nature, so the region can be selected anywhere in the image.

- 6) Statistics of this area was obtained using the stats tool of ROI. It is obtained in the terms of Digital number for each pixel present in the region.
- 7) Further, total intensity of the selected area is calculated as:  $I = \sum DN^2$
- 8) Average Intensity of the area can be found out by dividing, the total intensity by the number of pixels ( $I_{avg} = I / N$ , where,  $N$  = number of pixels in the region).
- 9) Standard value of Gamma Naught is found to be constant for the Amazon Rainforest due to its uniform nature. This value is taken to be equal to -6.5 dB for HH and -12.5 for HV in performing calculations.
- 10) Calibration constant (K) is calculated using following relationship:

$$K = 10 * \log_{10} (I_{avg}) - \sigma_0 \quad (21)$$

where,  $\sigma_0 = \gamma_0 * \cos \theta$

Here,  $\theta$  is the average incidence angle of the region selected.

#### **4.5 Approach for Geometric Calibration**

Geometric calibration was attempted for Geo-Tiff images of the RISAT-1 data. Following are the steps adopted for the same:

- 1) Point targets are used as a point with known locations. Corner Reflector's were deployed at different locations in the field.
- 2) Geographic location of each corner reflector was taken with the help of hand held GPS device at the time of deployment.
- 3) Co-ordinates obtained through GPS device are recorded for each corner reflector.
- 4) Geo-Tiff data product is obtained for RISAT-1 FRS and MRS mode.
- 5) This Tiff format is opened using Image processing software ENVI.
- 6) Now, Corner Reflector's are identified in the image.
- 7) Using 'Cursor/Location value' tool provided in tools menu, the co-ordinates of each corner reflector is noted down.
- 8) Difference in co-ordinates is calculated in both latitude and longitude direction to find the actual geometric error.

9) Geo-location accuracy is checked by comparing the RMSE error with the actual specifications.

#### 4.6 Mobilization and deployment of Corner Reflectors

For the CRs deployment in Desalpar, Rann of Kutch, the cabin at Institute of Seismological Research (ISR) laboratory in Desalpar was used to store the corner reflectors and then the corner reflectors were transported to the sites (site at Runn and fields in front of ISR cabin) using tractor. Figure 4-7 shows the mobilization and deployment of corner reflectors at various sites.



(a): Truck carrying CRs at ISR Laboratory at Desalpar      (b): CRs being loaded into the truck



(c): Transportation of CRs to the site



(d): Setting of CRs in progress



(e): Deployed Corner Reflectors

**Figure 4-7 (a-e)** Mobilization and deployment of Corner reflectors

## 5 RESULTS AND DISCUSSION

### 5.1 General

The point target and distributed target analysis has been carried out for the radiometric calibration of RISAT-1 intensity data of FRS and MRS mode of different date of pass. In order to carry out absolute radiometric calibration of SAR, standard point targets with known Radar Cross Section (RCS) are deployed accurately pointing towards the SAR sensor over a low clutter region. Once the point targets are imaged, integrated power from two dimensional IRF of deployed standard target is analyzed after removing clutter noise. From the IRF, quality parameters like ISLR, PSLR and spatial resolution in the range and azimuth are also calculated. Signal to clutter ratio and calibration constant were calculated using the estimated point target and average clutter energy. Study of the effect of clutter window size on ISLR by keeping the point target window size constant was also attempted and the results are reported. Table 5-1 and 5-2 show the number of corner reflectors deployed at various sites for different dates for FRS-1 and MRS respectively.

**Table 5-1 Number of CRs deployed for FRS-1 for different dates**

Sr. No	Location	Date	Beam and Polarization	Number of CRs deployed
1	Ahmedabad	21st April 2015	Beam No. 104, HH	1 Triangular Trihedral
2	Ahmedabad	25th April 2015	Beam No. 21, HH	1 Triangular Trihedral
3	Desalpar, Rann of Kutch	22nd January 2016	Beam No. 66 , RH, RV	8 Triangular Trihedral
4	Desalpar, Rann of Kutch	15th February 2016	Beam No. 87 RH, RV	8 Triangular Trihedral, 3 Square Trihedral & 1 dihedral

**Table 5-2 Number of CRs deployed for MRS for different dates**

Sr. No	Location	Date	Number of CRs deployed
1.	Ahmedabad	5th July 2015, Beam 87-97, HH	1 Triangular trihedral
2.	Ahmedabad	30th July 2015, Beam 87-97, HH	1 Triangular trihedral
3.	Ahmedabad	24th August 2015, Beam 87-97, HH	2 Triangular trihedrals
4.	Ahmedabad	13th October 2015, Beam 87-97, HH	4 Triangular trihedrals
5.	Ahmedabad	7th November 2015, Beam 87-97, HH	4 Triangular trihedrals

6.	Ahmedabad	2nd December 2015, Beam 87-97, HH	4 Triangular trihedrals
7.	Ahmedabad	27th December 2015, Beam 87-97, HH	4 Triangular trihedrals
8.	Desalpar, Rann of Kutch	14th February 2016, Beam 87-97, HH	8 Triangular Trihedral, 3 Square Trihedral & 1 dihedral

## 5.2 Results of absolute radiometric calibration using point targets

The deployed reflector responses in RISAT-1 SAR images were analyzed to derive radiometric parameters of the data and computing the necessary calibration parameters.

### 5.2.1 Results for Ahmedabad site

The location and response of CR deployed at SAC Bopal, Ahmedabad site and its response in FRS-1/MRS image for different dates is shown in Figure 5-1 and 5-2 respectively. The building located at the south of CR can be clearly seen in the MRS image with very bright response.



**Figure 5-1 Location of CR at Ahmedabad site on Google earth image**

RISAT-1 SLC for FRS-1 and GRD for MRS data were taken to frequency domain using FFT and were interpolated in frequency domain with an interpolation factor of 16 in range and 16 in azimuth direction. An inverse FFT resulted in 16x interpolated IRF for point targets. Thus, for all the reflectors, interpolated Impulse Response Function (IRF) was derived. Using the

steps already explained in the methodology section, the calibration constant was derived and the results thus estimated for each date are as follows:

### 5.2.1.1 21 April 2015: FRS-HH Polarization

Beam no - 104

Incidence angle at scene center – 44.78032

Calibration Constant\_Band Meta – 79.699

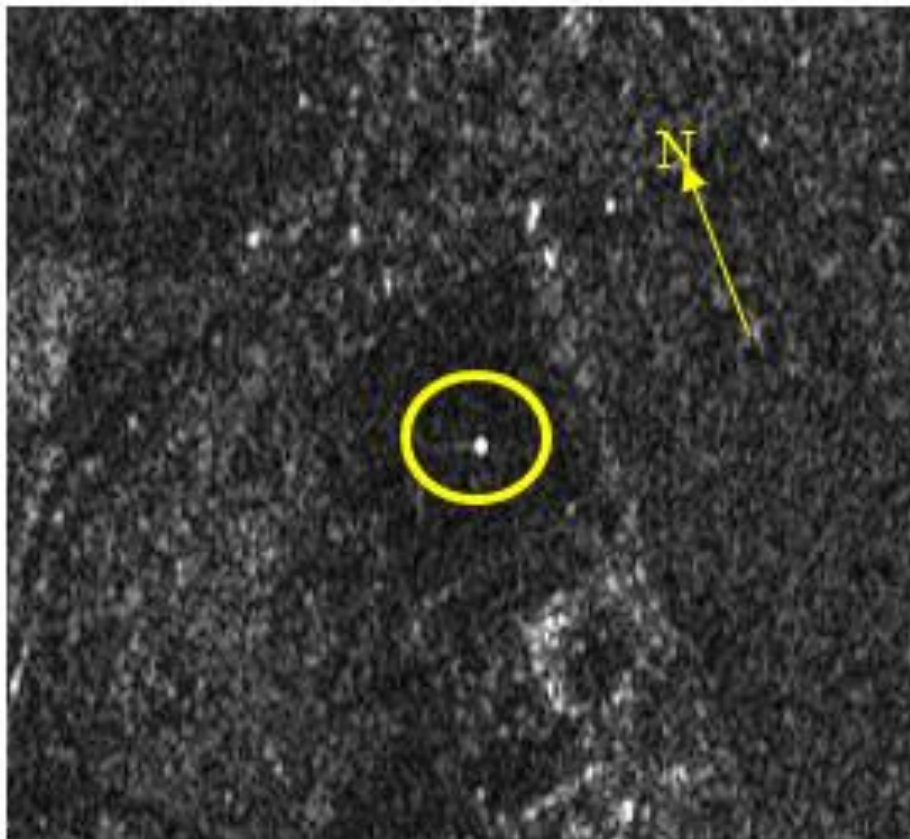
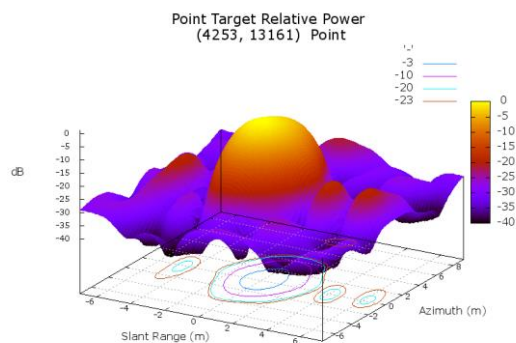


Figure 5-2 Response of CR at SAC, Bopal, Ahmedabad site of FRS-1 SAR intensity data on 21/04/15



CR\_Bopal\_8x8\_8x8

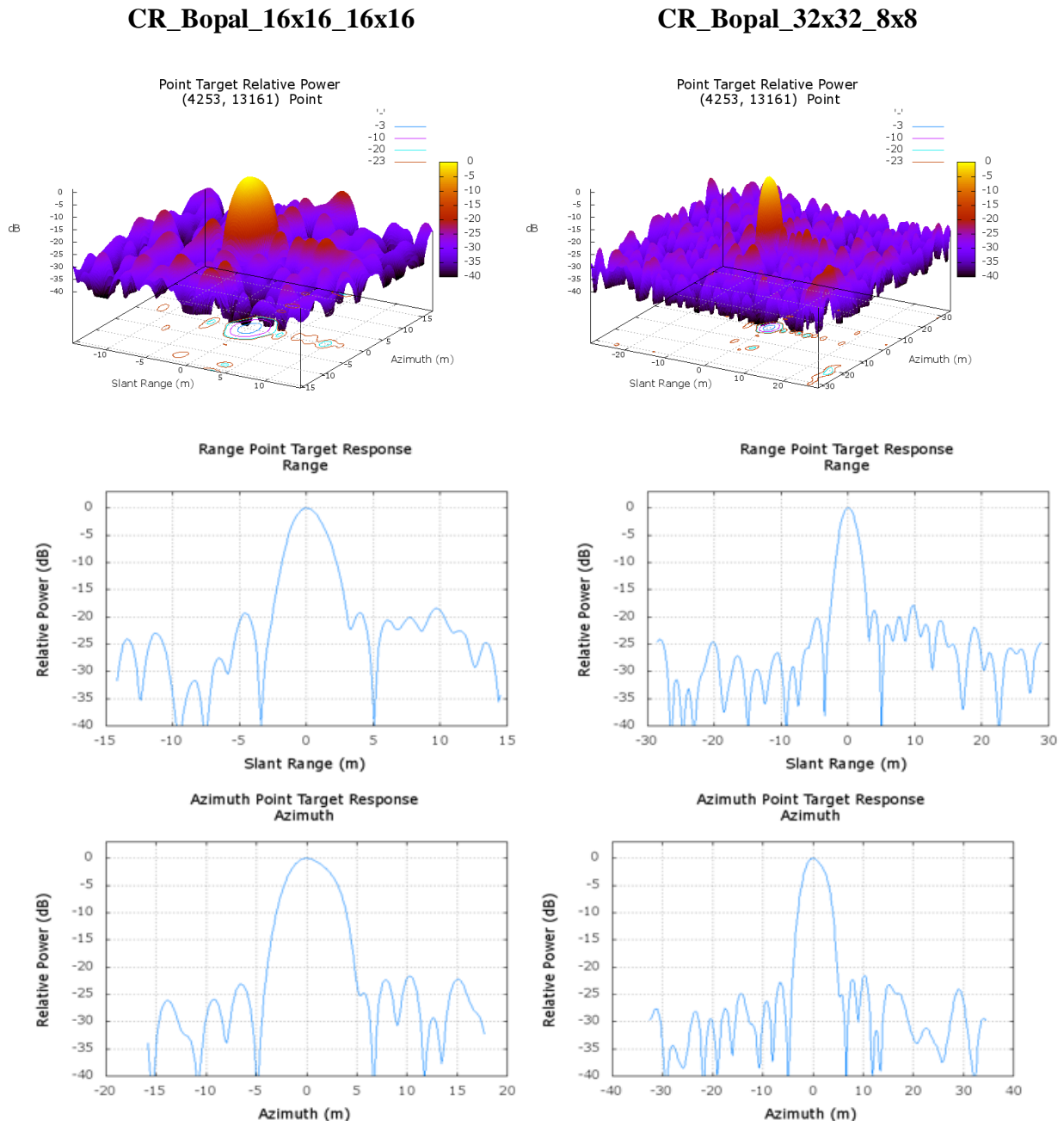


Figure 5-3 Impulse response function of the CR for 21<sup>st</sup> April 2015 FRS-1 image for different target and clutter window sizes

Table 5-3 Estimated calibration constant for 21<sup>st</sup> April FRS-1

CR No	Location	Point window size	Clutter window size	Calibration Constant	Difference (dB)
1	Bopal	8x8	4x4	79.1211	<b>0.5779</b>
1	Bopal	8x8	6x6	79.1139	<b>0.5851</b>
1	Bopal	10x10	8x8	79.1170	<b>0.5820</b>
				<b>Average</b>	<b>0.5817</b>

The difference between estimated calibration constant (CC) and provided CC for FRS-1 beam 104 having HH polarization was found to be within the specification of satellite (within 1dB) as can be seen from Table-5-3. It is also observed from the table that the variation of target and clutter window size have almost no impact on the estimated CC which is ideal and shows that the background is uniform.

### 5.2.1.2 25 April 2015: FRS-HH Polarization

Beam no - 21

Incidence angle at scene center – 31.20945

Calibration Constant\_Band Meta – 76.053

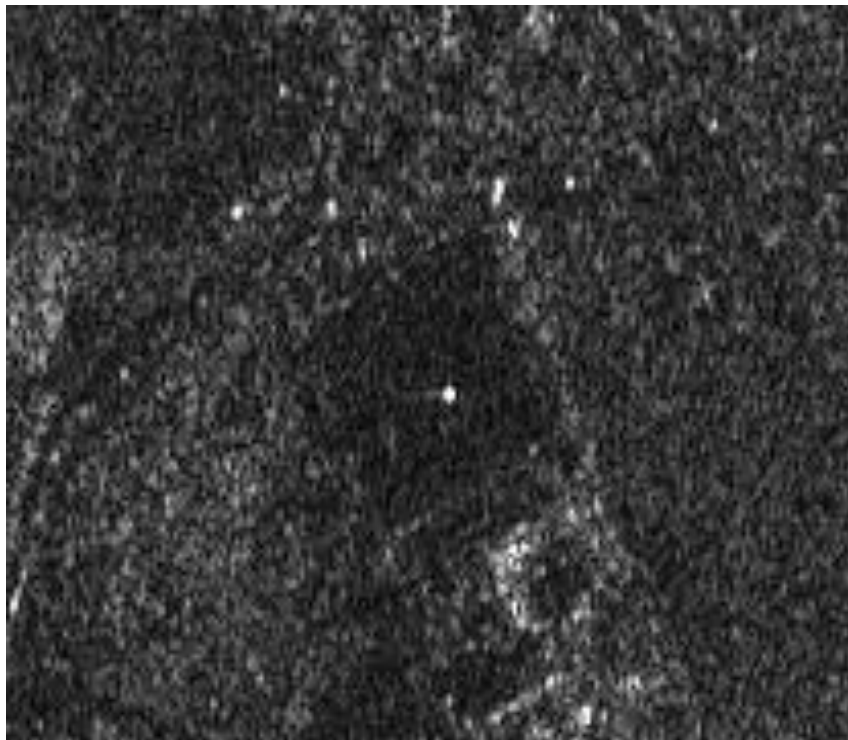
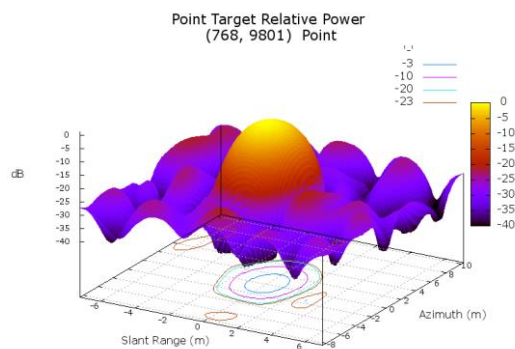


Figure 5-4 Response of CR at SAC, Bopal, Ahmedabad site of FRS-1 SAR intensity data on 25/04/15



CR\_Bopal\_8x8\_8x8

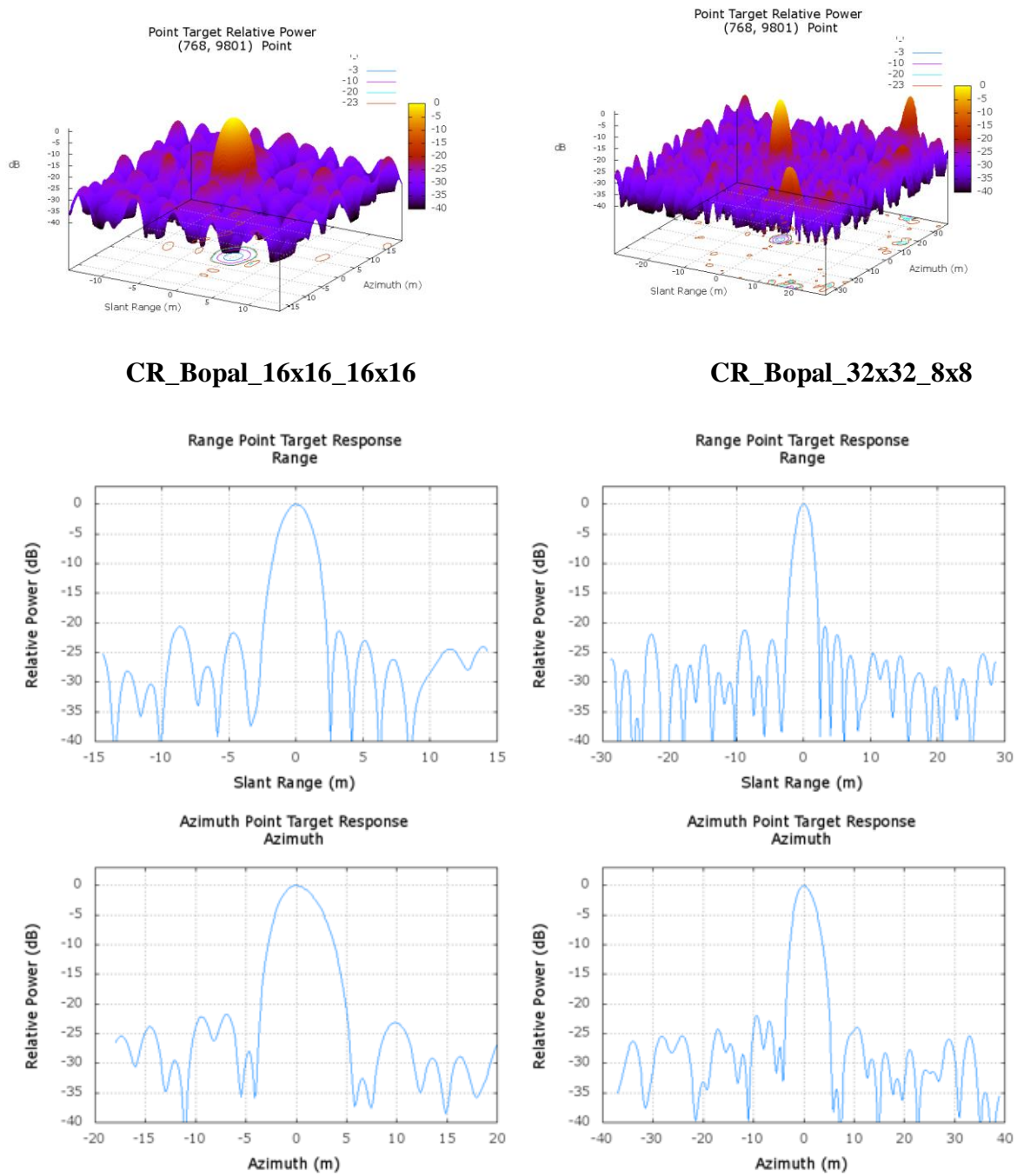


Figure 5-5 Impulse response function of the CR for 25<sup>th</sup> April 2015 FRS-1 image for different target and clutter window sizes

Table 5-4 Estimated calibration constant for 25<sup>th</sup> April FRS-1

CR No	Location	Point window size	Clutter window size	Calibration Constant	Difference (dB)
1	Bopal	8x8	8x8	74.7147	1.3383
1	Bopal	16x16	16x16	74.7545	1.2985
1	Bopal	16x16	8x8	74.7671	1.2859

1	Bopal	32x32	8x8	75.5823	<b>0.4707</b>
1	Bopal	32x32	16x16	75.5407	<b>0.5123</b>
				<b>Average</b>	<b>0.9811</b>

The difference between average estimated calibration constant (CC) and provided CC for FRS-1 beam 21 having HH polarization was found to be within the specification of satellite (within 1dB) as can be seen from Table-5-4. However, it is observed from the table that with the increase in the target and clutter window size, the estimated CC increases and the difference decreases.

### 5.2.1.3 5th July 2015: MRS-HH Polarization

Beam no - 87-89-91-93-95-97  
 Incidence angle at scene center – 36.79629  
 Calibration Constant\_Band Meta – 74.455

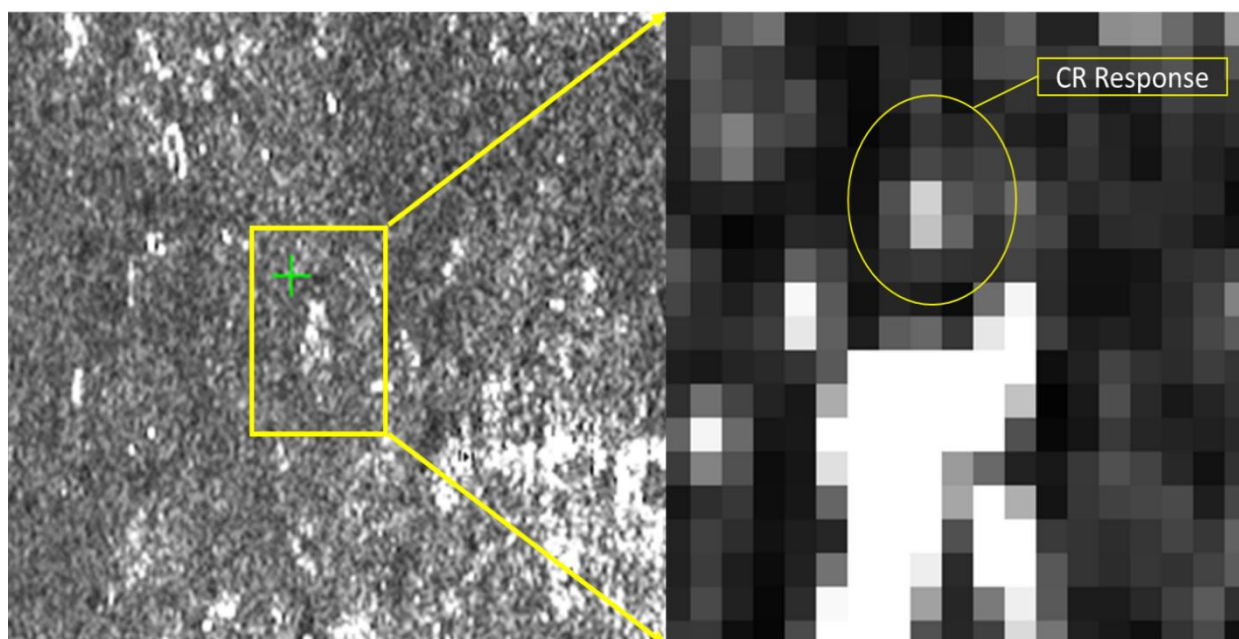
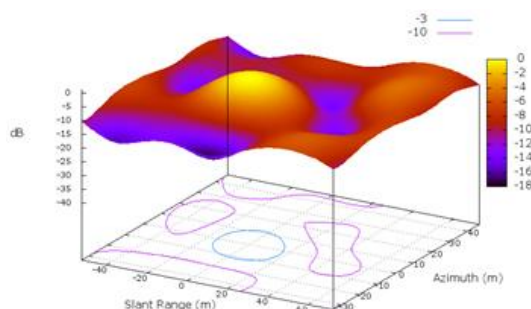


**Figure 5-6 Response of CR at SAC, Bopal, Ahmedabad site of MRS SAR intensity data on 05/07/15**



**CR\_Bopal\_7x7\_4x4**

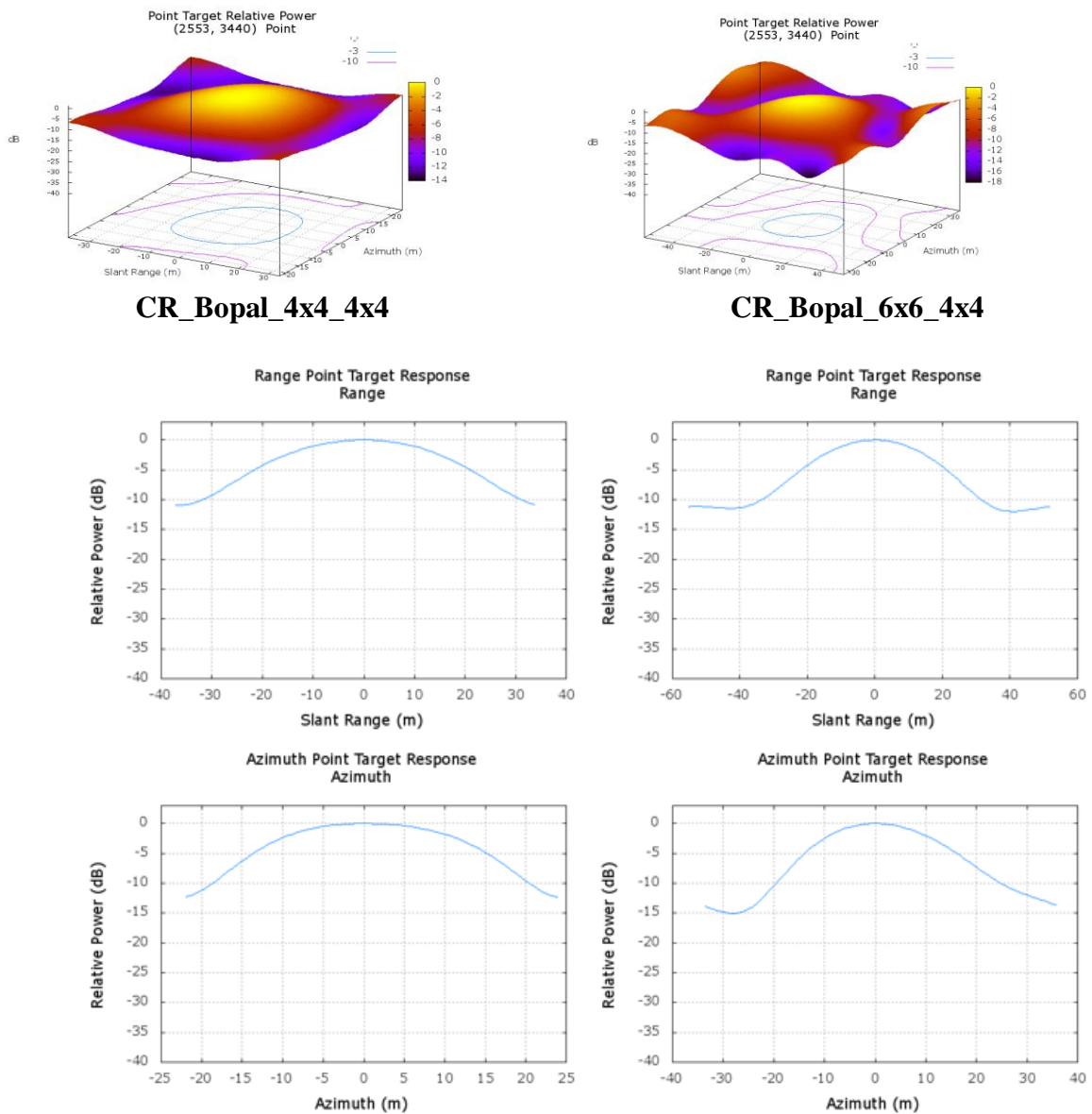
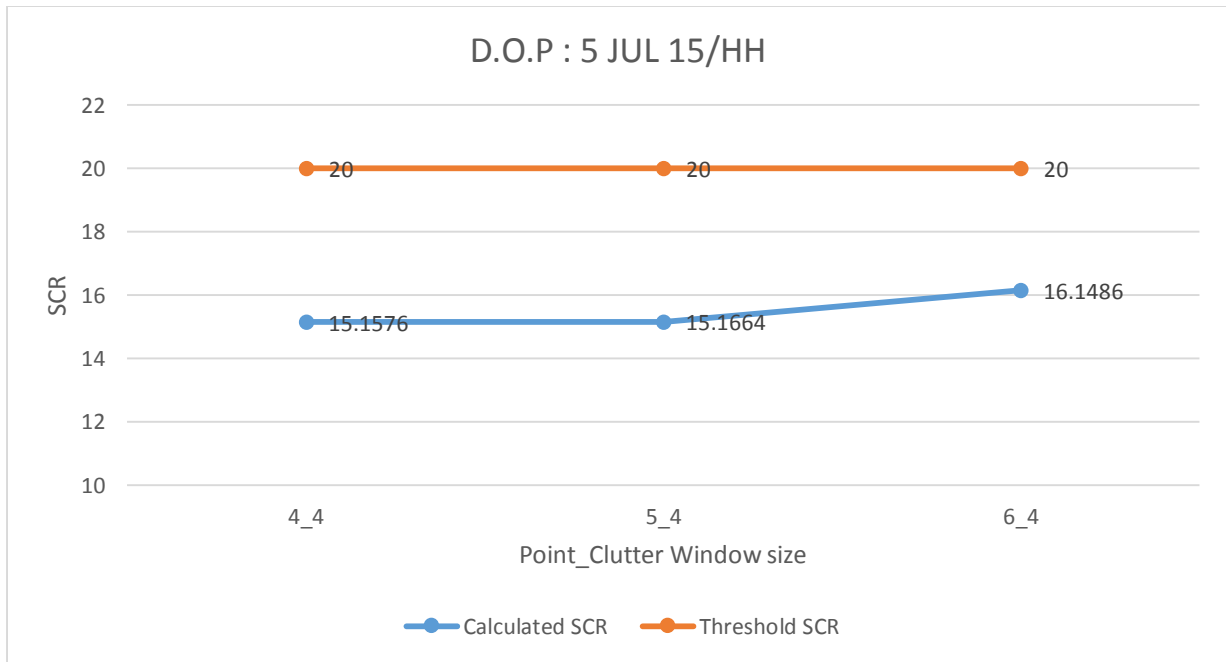


Figure 5-7 Impulse response function of the CR for 5<sup>th</sup> July 2015 MRS image for different target and clutter window sizes

Table 5-5 Estimated calibration constant for 5<sup>th</sup> July 2015

CR No	Location	Point window size	Clutter window size	Calibration Constant	Difference
1	Bopal	3x3	4x4	69.4380	-5.017
1	Bopal	4x4	4x4	69.5183	-4.9367
1	Bopal	5x5	4x4	69.5271	-4.9279
1	Bopal	6x6	4x4	70.5094	-3.9456
				<b>Average</b>	<b>-4.7068</b>

It can be seen from Table 5-5 that the estimated CC remains almost same as the target window size increases from 3 to 5, but with the further increase in the target window size, it starts increasing. The reason might be due to the presence of building near the CR. As the target window size increases, integrated power increases because of the inclusion of the power from the building response which in turn increases the estimated CC.



**Figure 5-8 Calculated SCR for different target and clutter window sizes**

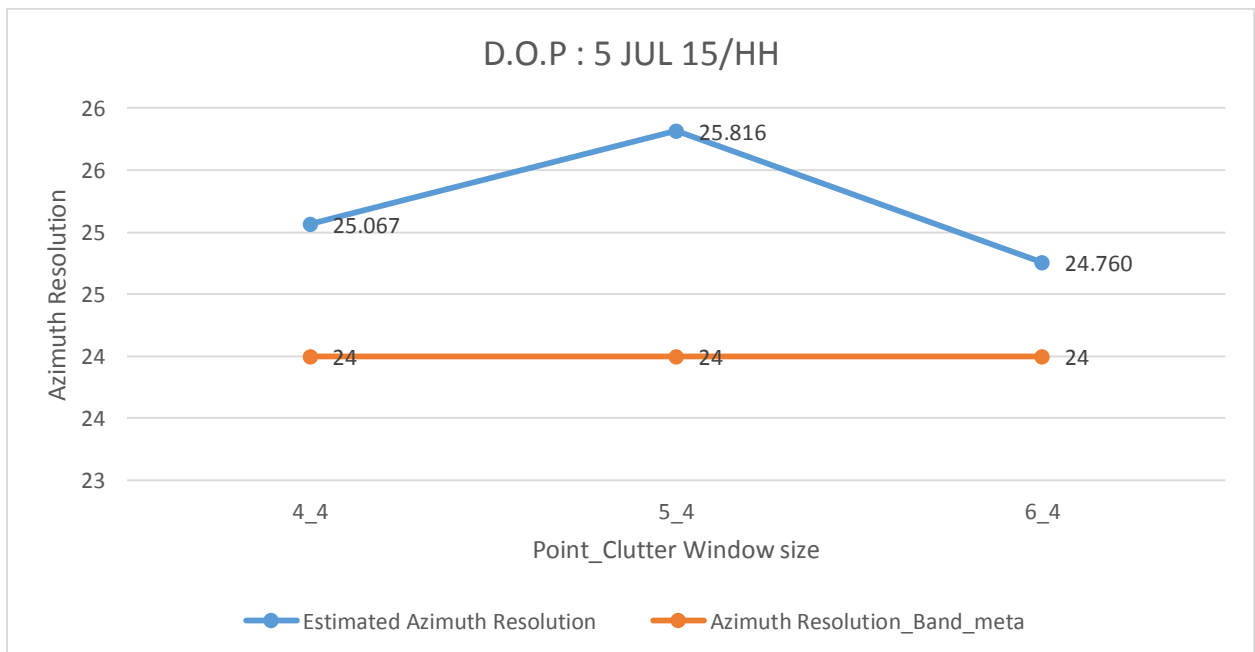


**Figure 5-9 Range and azimuth spatial resolution estimated from IRF**

### 5.2.1.4 30th July 2015: MRS-HH Polarization

Beam no - 87-89-91-93-95-97

Incidence angle at scene center – 36.79907

Calibration Constant\_Band Meta – 74.552

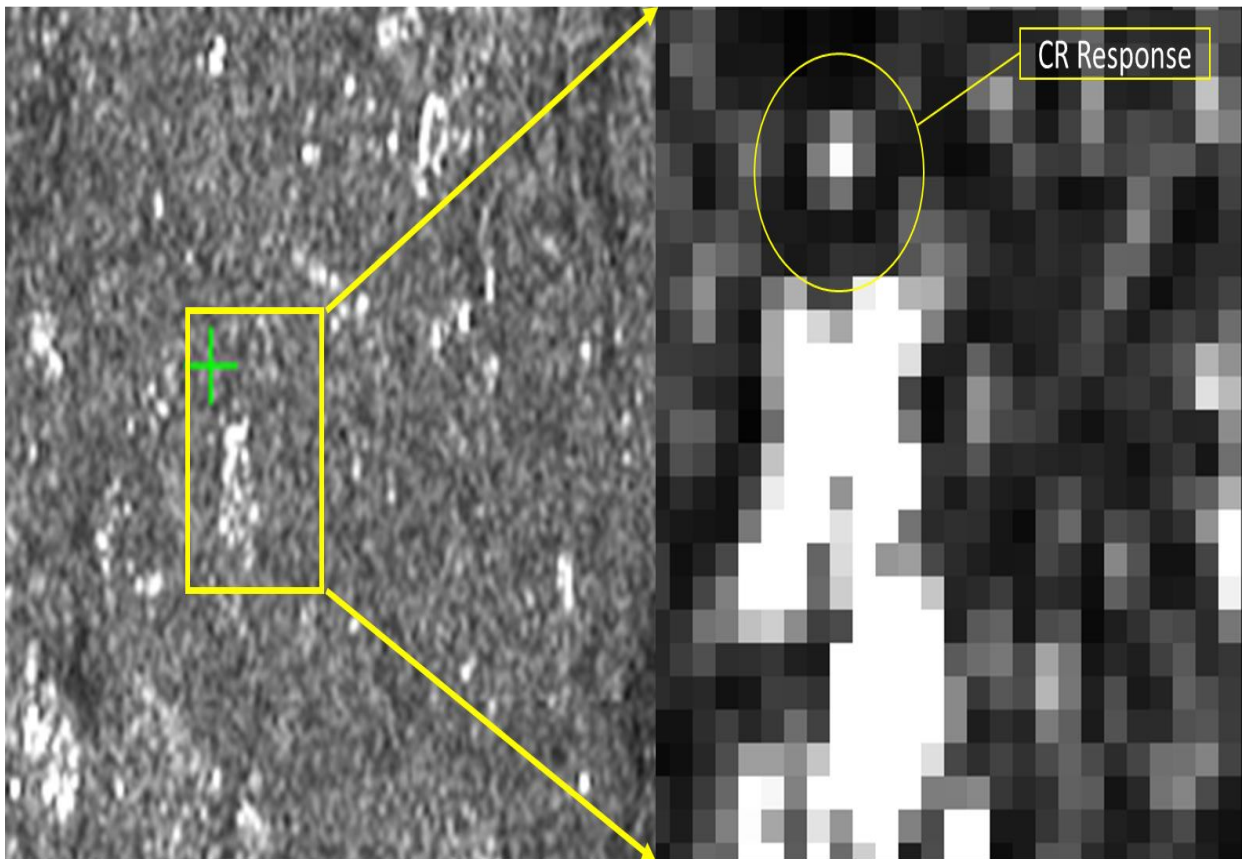
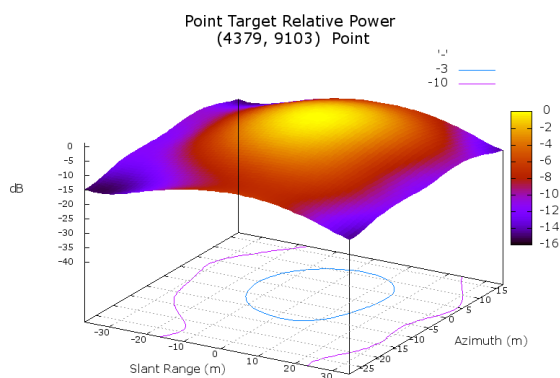
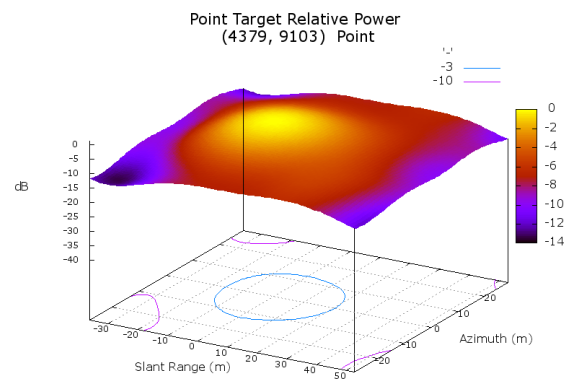


**Figure 5-10 Response of CR at SAC, Bopal, Ahmedabad site of MRS SAR intensity data on 30/07/15**



**CR\_Bopal\_4x4\_4x4**



**CR\_Bopal\_5x5\_4x4**

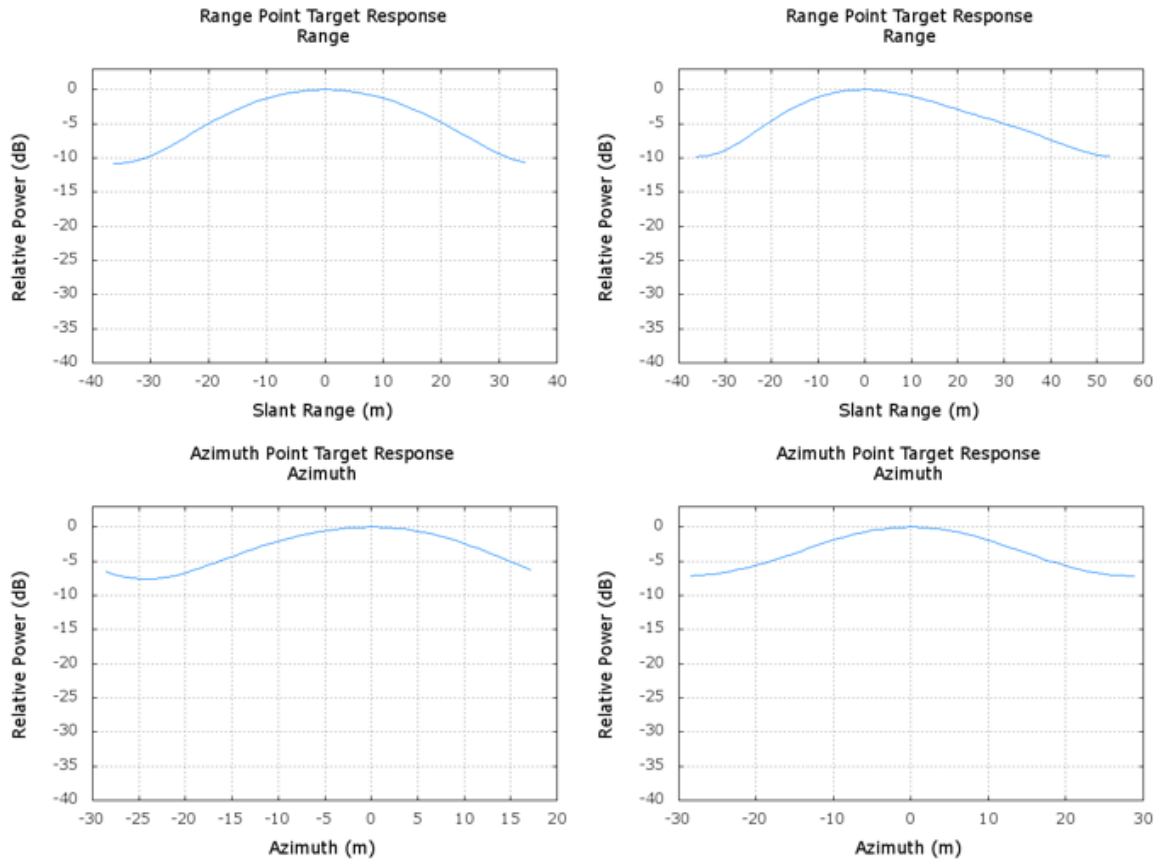
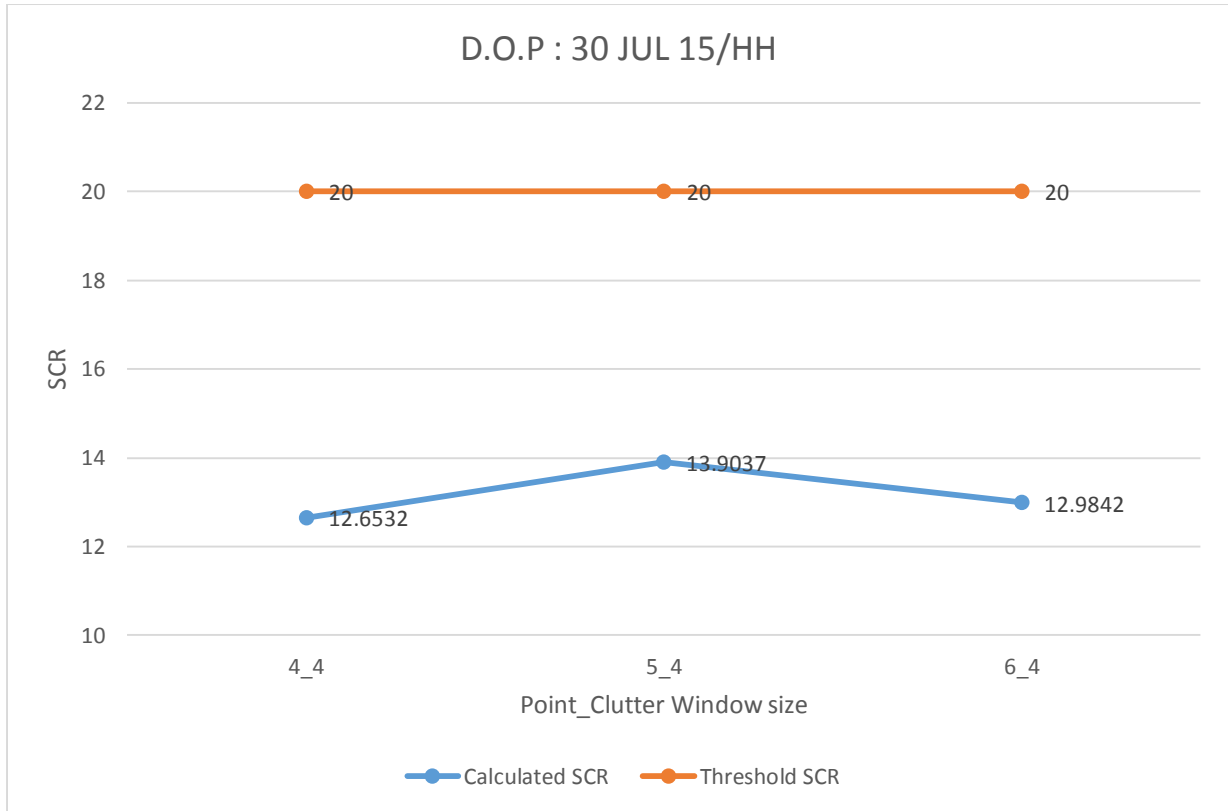


Figure 5-11 Impulse response function of the CR for 30<sup>th</sup> July 2015 MRS image for different target and clutter window sizes

Table 5-6 Estimated calibration constant for 30<sup>th</sup> July 2015

CR No.	Location	Point window size	Clutter window size	Calibration Constant	Difference
1	Bopal	3x3	4x4	71.4700	-3.082
1	Bopal	4x4	4x4	71.1390	-3.413
1	Bopal	5x5	4x4	72.3895	-2.1625
1	Bopal	6x6	4x4	72.5073	-2.0447
				<b>Average</b>	<b>-2.6755</b>

For this date, the same trend was observed as that in the case of 5<sup>th</sup> July 2015 MRS. It can be seen from Table 5-6 that in this case also, the estimated CC remains almost same as the target window size increases from 3 to 4, but with the further increase in the target window size, it starts increasing.



**Figure 5-12 Calculated SCR for different target and clutter window sizes**

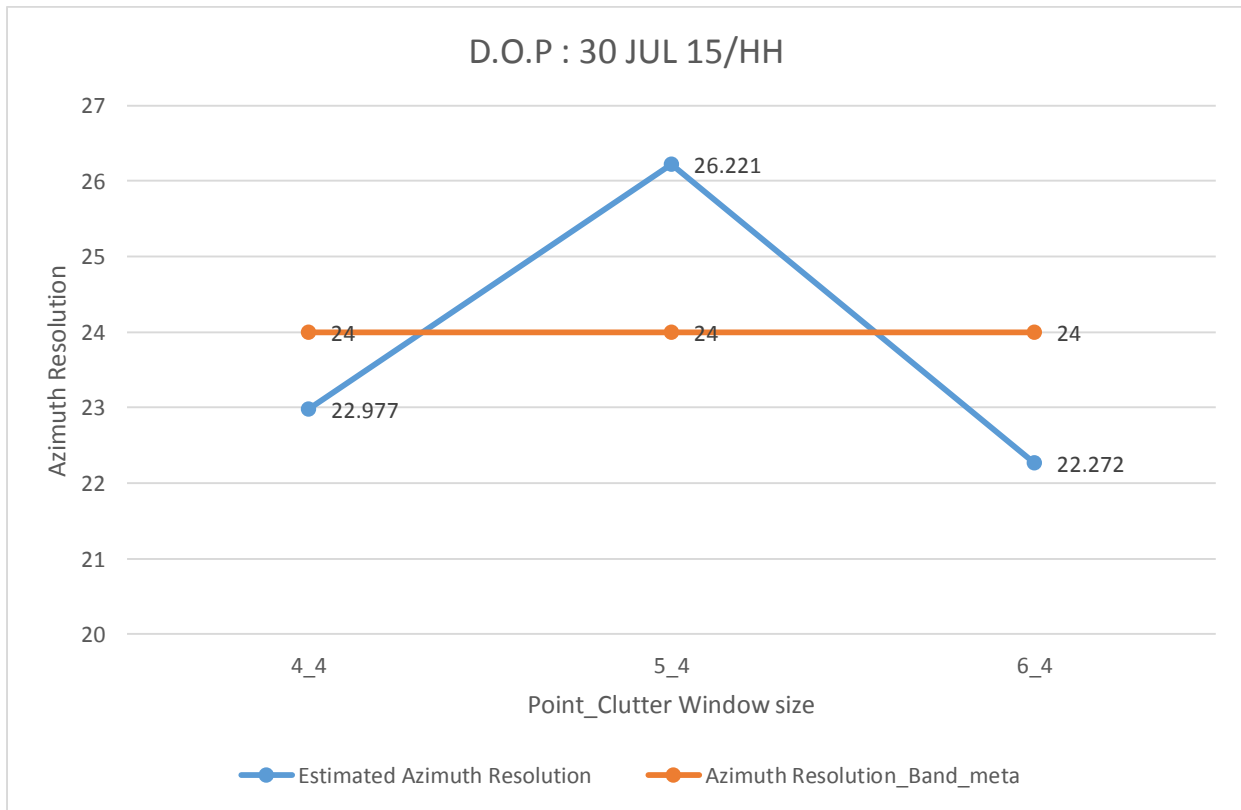


**Figure 5-13 Azimuth spatial resolution estimated from IRF**

### 5.2.1.5 24th August 2015: MRS-HH Polarization

Beam no - 87-89-91-93-95-97

Incidence angle at scene center – 36.77593

Calibration Constant\_Band Meta – 74.646

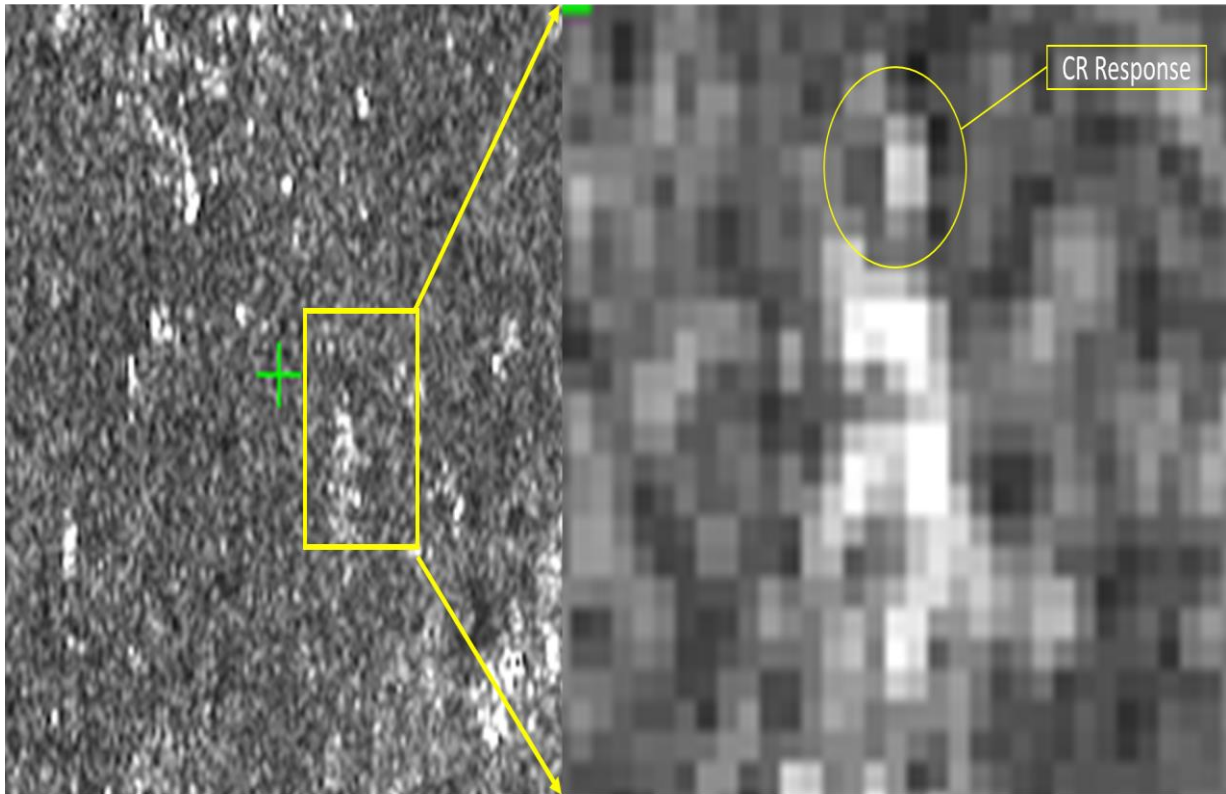
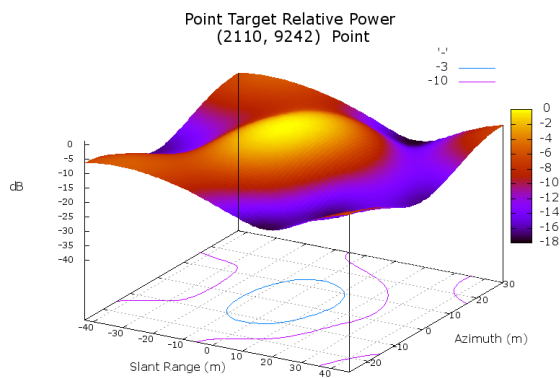
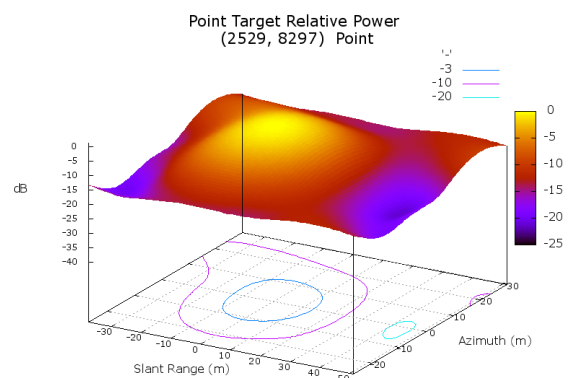


Figure 5-14 Response of CR at SAC, Bopal, Ahmedabad site of MRS SAR intensity data on 24/08/2015



CR\_Bopal\_5x5\_4x4



CR\_Nirma\_5x5\_4x4

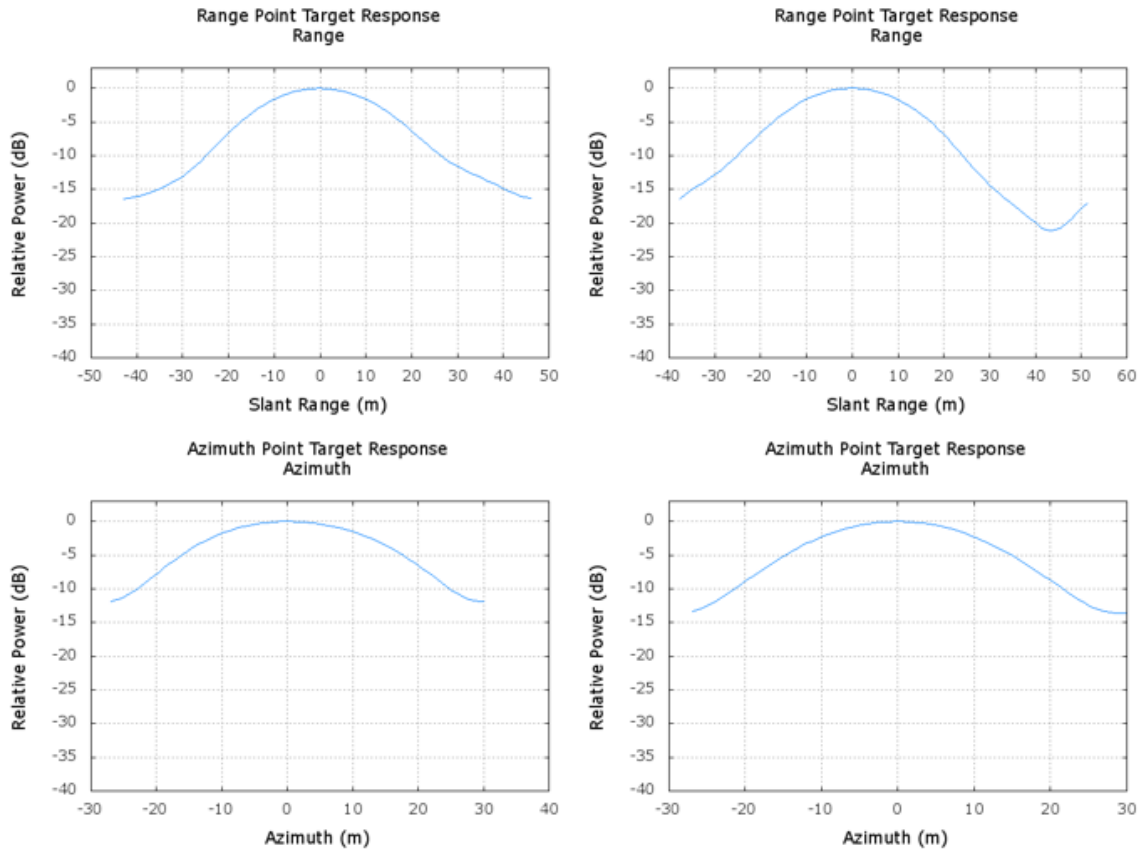


**Figure 5-15 Impulse response function of the CR for 24<sup>th</sup> August 2015 MRS image for different target and clutter window size**

**Table 5-7 Estimated calibration constant for 24<sup>th</sup> August 2015**

CR No.	Location	Point window size	Clutter window size	Calibration Constant	Difference
1	Bopal	4x4	4x4	74.1153	-0.5307
1	Bopal	5x5	4x4	74.5462	-0.0998
1	Bopal	6x6	4x4	75.2043	0.5583
				<b>Average (of first two cases)</b>	<b>-0.3152</b>

For this date again, the same trend was observed as that in the case of 5<sup>th</sup> and 30<sup>th</sup> July 2015 MRS. Table 5-7 shows that the estimated CC remains almost same as the target window size increases upto 5, but with the further increase in the target window size, it starts increasing for the case of CR deployed in SAC-Bopal campus. Whereas, for the case of the CR deployed in Nirma University ground, the difference found was very large. The SCR for the CR deployed in Nirma University ground was found to be very poor (less than 11dB), hence while reporting

the average value, it is not considered. Nirma University ground is surrounded by large number of buildings, error in locating the CR response might have happened.

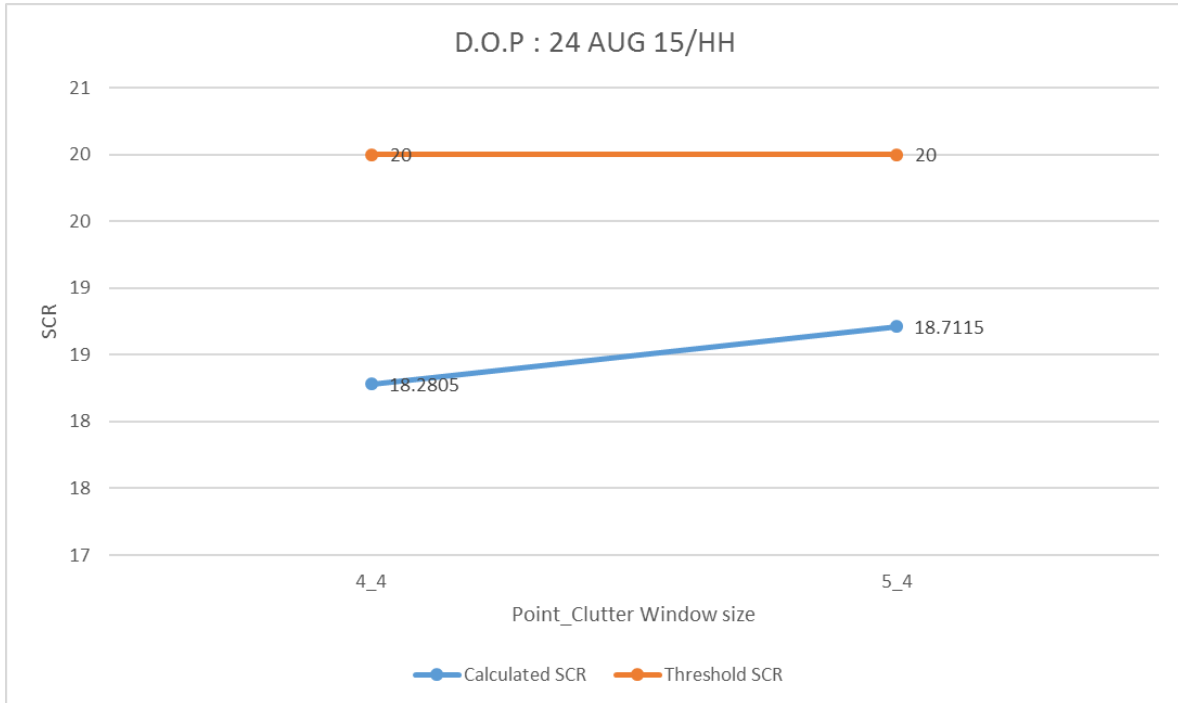


**Figure 5-16 Calculated SCR for different target and clutter window sizes**

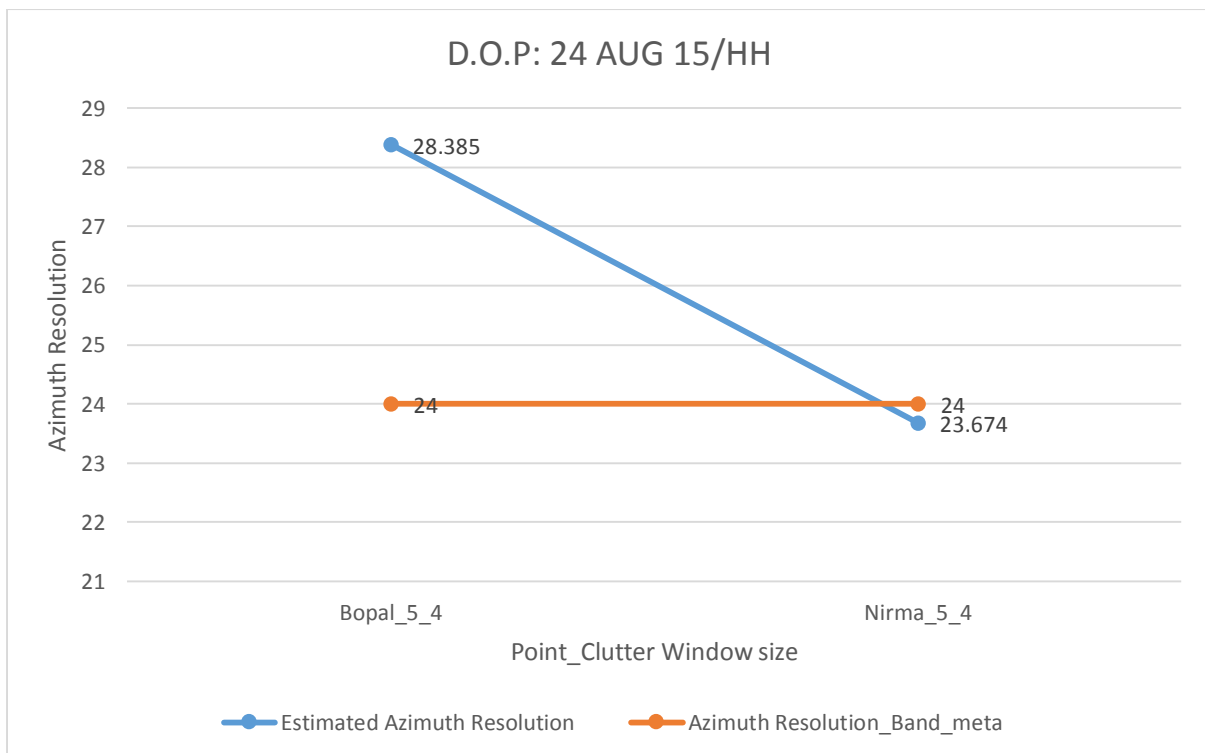


**Figure 5-17 Azimuth spatial resolution estimated from IRF**

### 5.2.1.6 18<sup>th</sup> September 2015: MRS-HH Polarization

Beam no - 87-89-91-93-95-97

Incidence angle at scene center – 36.79698

Calibration Constant\_Band Meta – 74.552

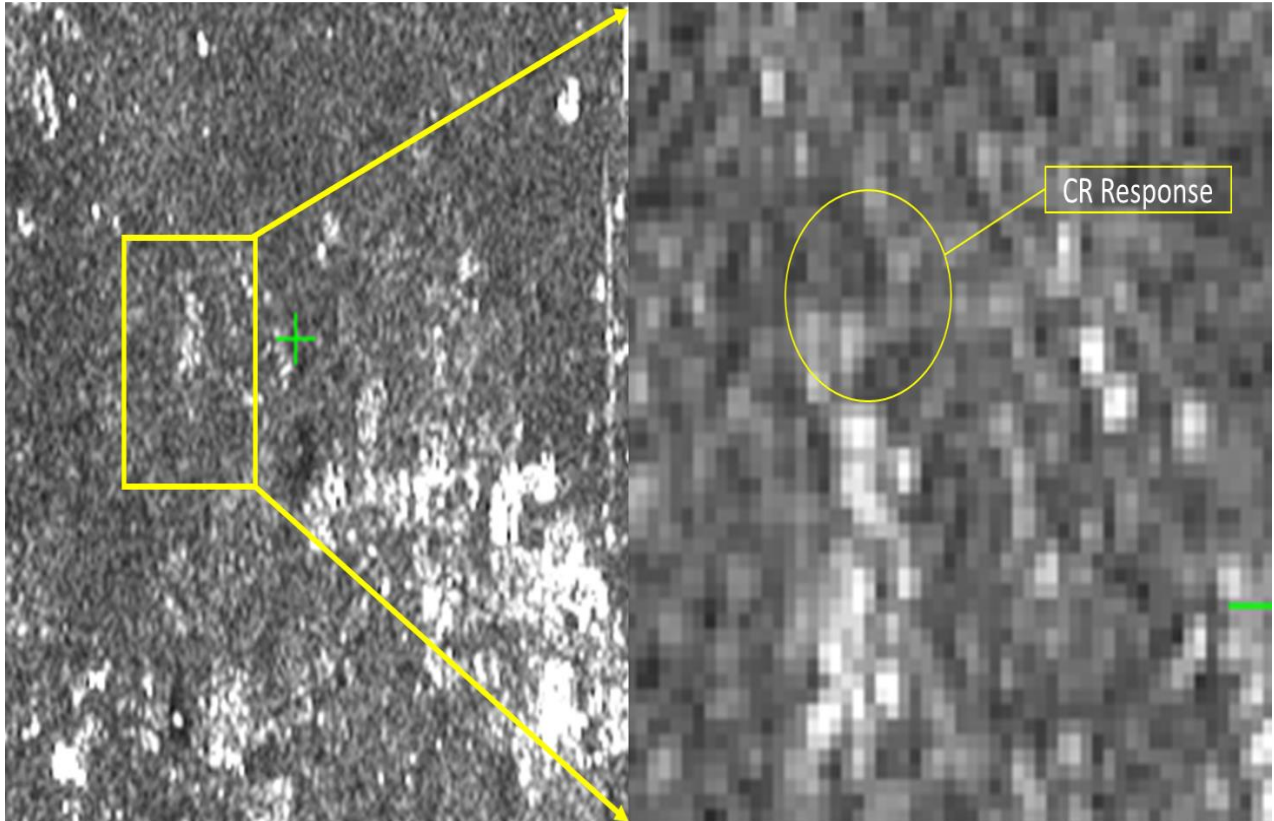
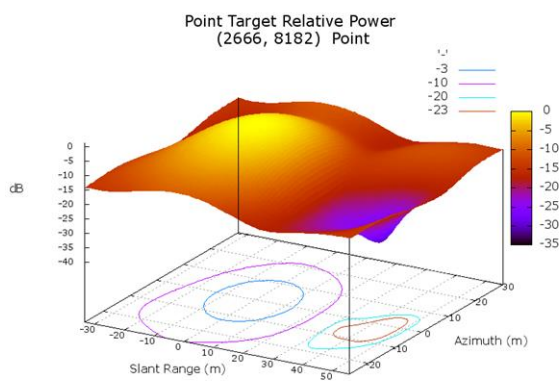
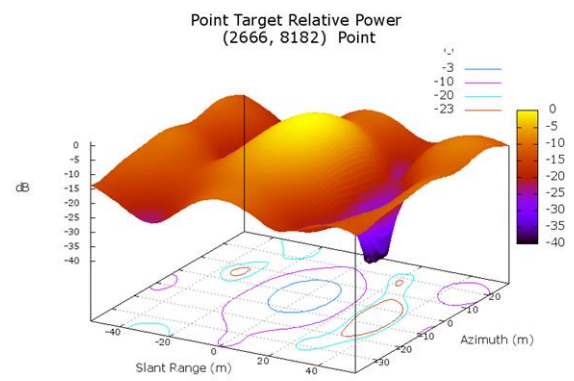


**Figure 5-18 Response of CR at SAC, Bopal, Ahmedabad site of MRS SAR intensity data on 18/09/2015**



**CR\_Nirma\_5x5\_4x4**



**CR\_Nirma\_6x6\_4x4**

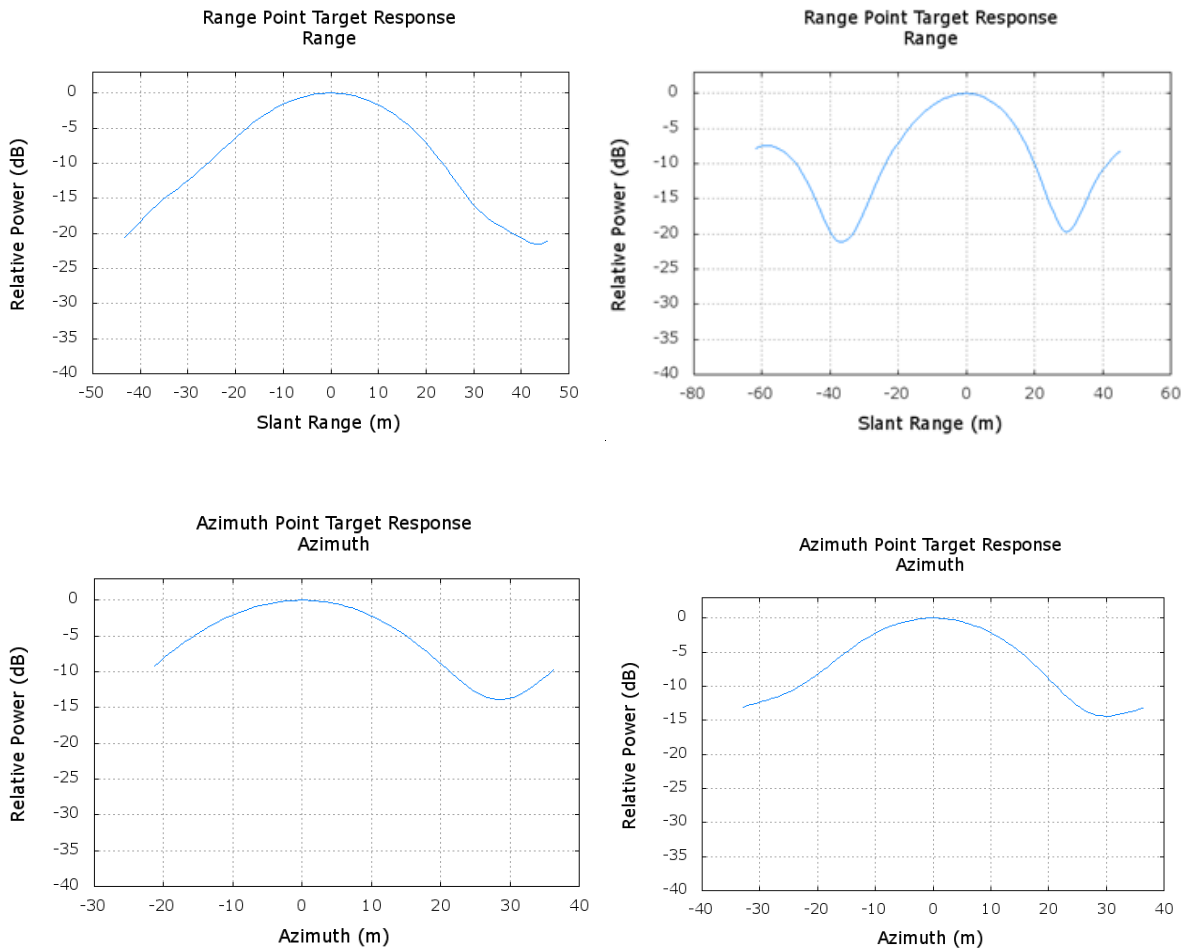


**Figure 5-19 Impulse response function of the CR for 18<sup>th</sup> September 2015 MRS image for different target and clutter window size**

**Table 5-8 Estimated calibration constant for 18<sup>th</sup> September 2015**

CR No	Location	Point target window size	Clutter window size	Calibration Constant	Difference (dB)
2	Nirma	4x4	4x4	75.6596	-1.1076
2	Nirma	5x5	4x4	75.4181	-0.8661
2	Nirma	6x6	4x4	75.6615	-1.1095
				<b>Average</b>	<b>-1.028</b>

On this date the CR deployed in Nirma University ground, the difference found was marginally less. The SCR for the CR deployed in Nirma University ground was found to be better as compared to SCR of the previous date deployment. Table 5-8 shows results of point target analysis of CR, which shows that with the change of point target window size the results remains almost same. Consistency in the estimated calibration constant indicates the uniformity of the site.

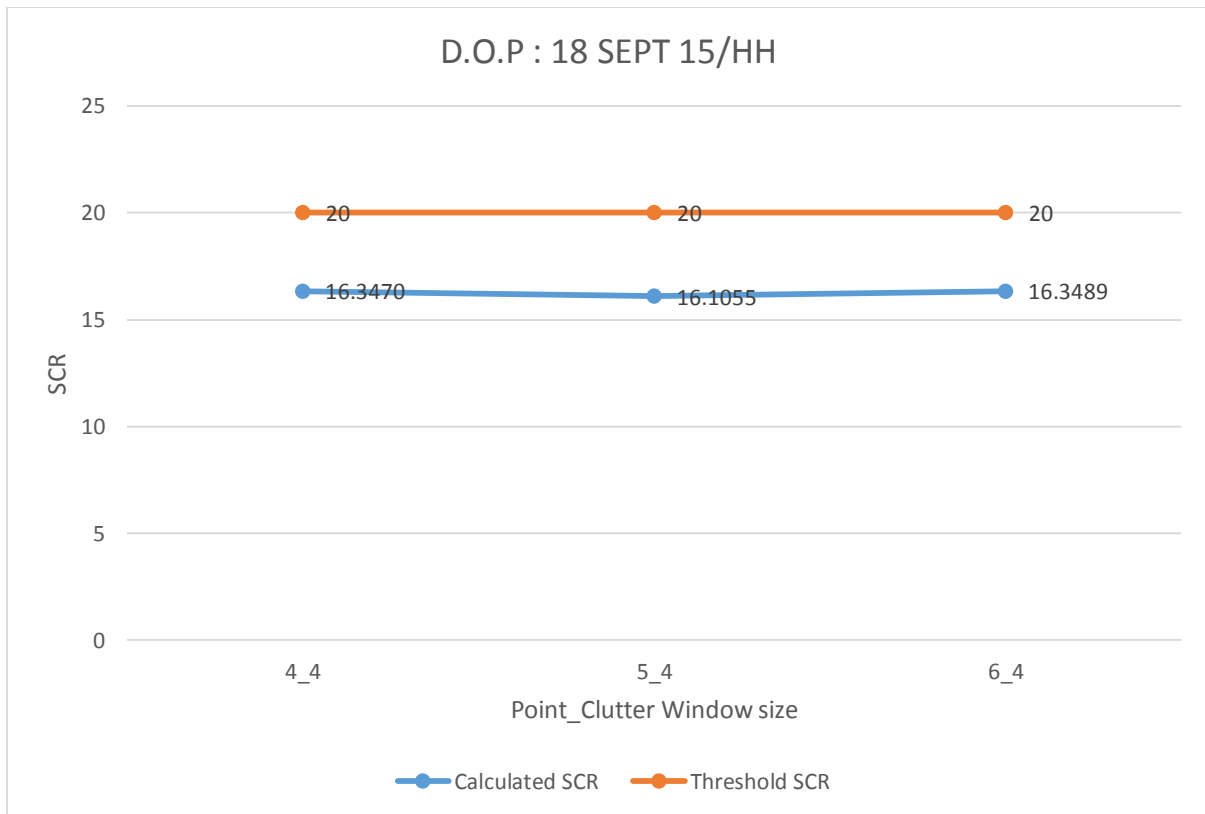


**Figure 5-20 Calculated SCR for different target and clutter window sizes**

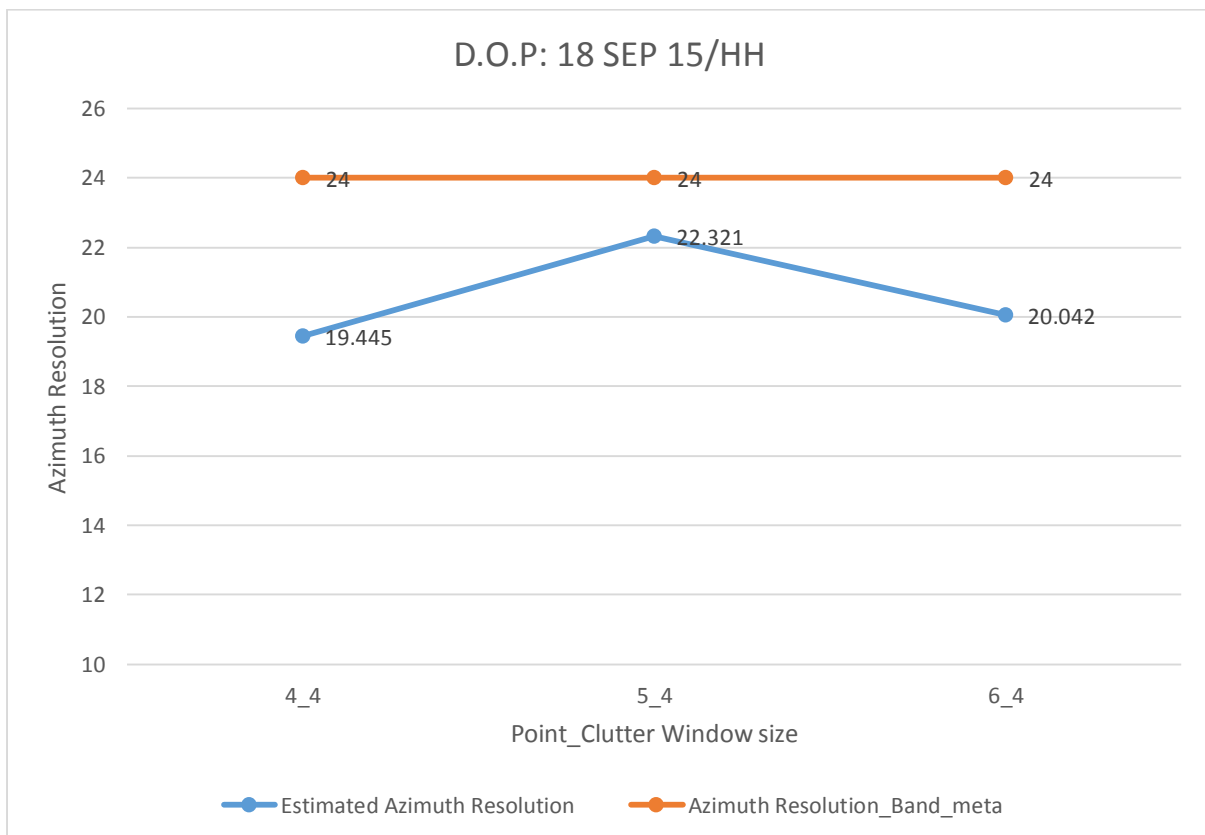


**Figure 5-21 Azimuth spatial resolution estimated from IRF**

### 5.2.1.7 13th October 2015: MRS-HH Polarization

Beam no - 87-89-91-93-95-97

Incidence angle at scene center – 36.81646

Calibration Constant\_Band Meta – 74.443

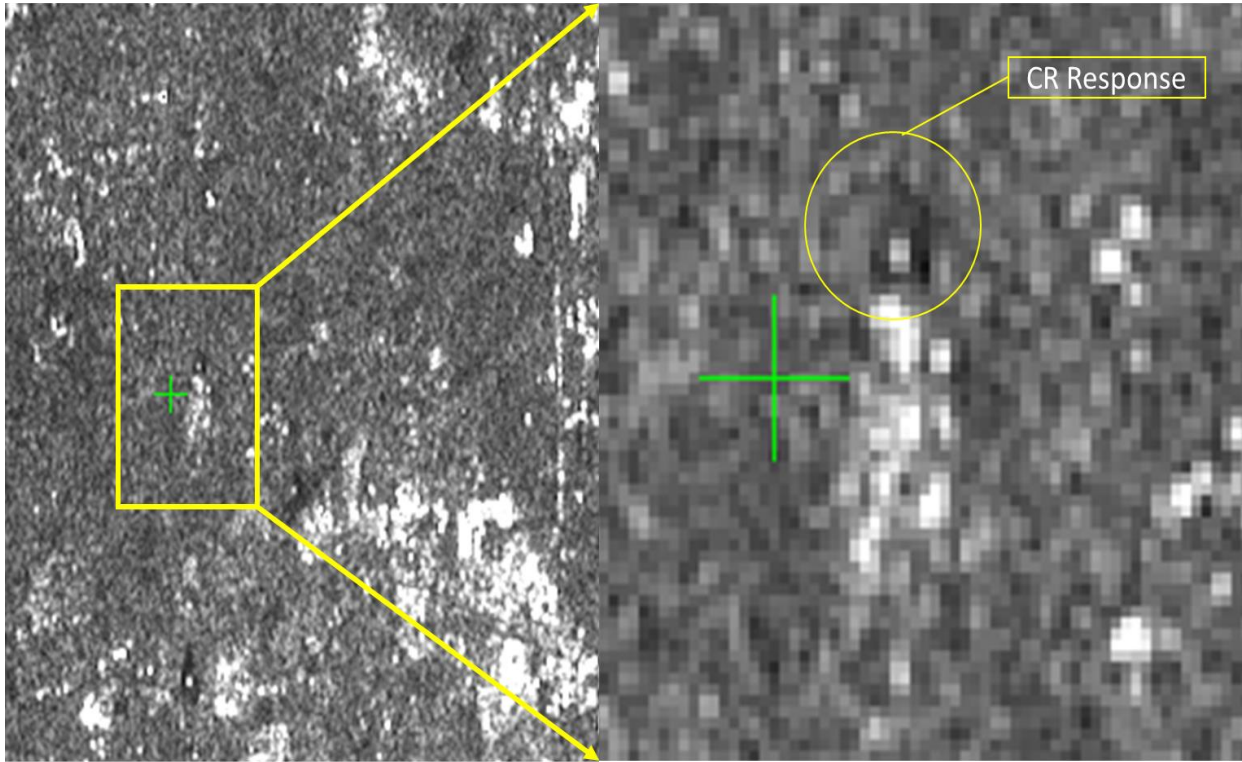
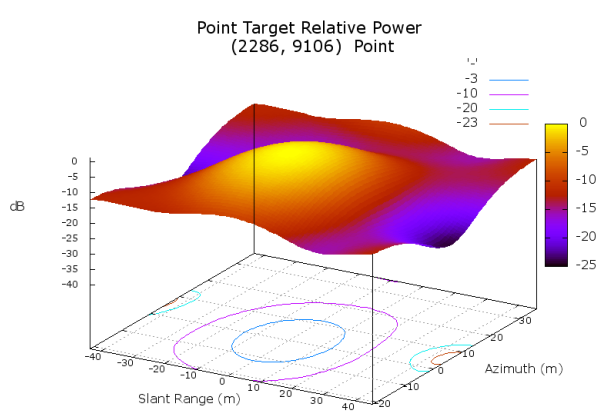
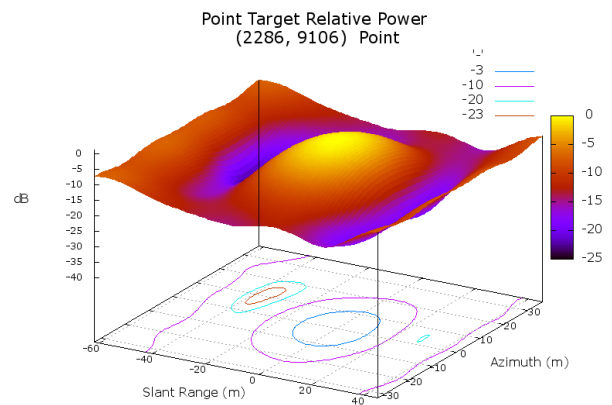


**Figure 5-22 Response of CR at SAC, Bopal, Ahmedabad site of MRS SAR intensity data on 13/10/2015**



**CR\_Bopal\_5x5\_4x4**



**CR\_Bopal\_6x6\_4x4**

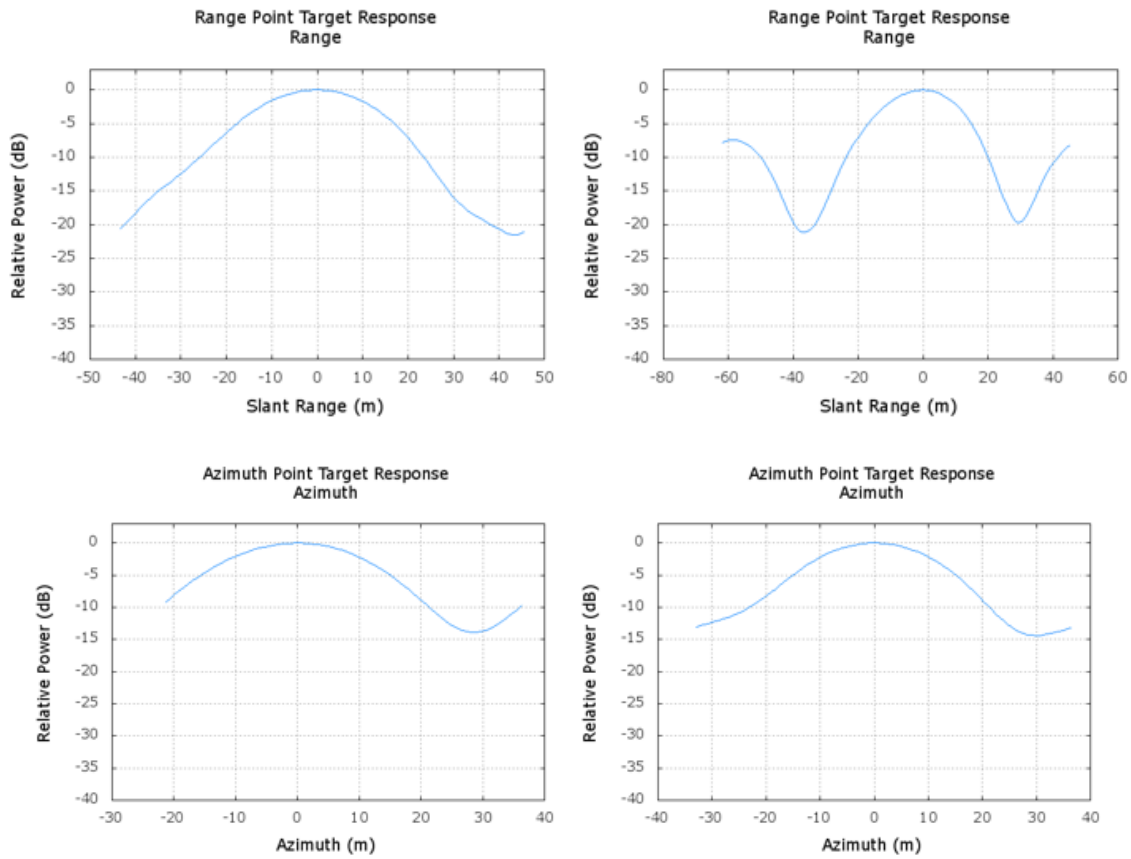


**Figure 5-23 Impulse response function of the CR for 13<sup>th</sup> October 2015 MRS image for different target and clutter window sizes**

**Table 5-9 Estimated calibration constant for 13<sup>th</sup> October 2015**

CR No	Location	Point window size	Clutter window size	Calibration Constant	Difference
1	Bopal	4x4	4x4	72.4705	-1.9725
1	Bopal	5x5	4x4	72.0711	-2.3719
1	Bopal	6x6	4x4	73.2046	-1.2384
				<b>Average</b>	<b>-1.86</b>

A different trend was observed for the case of 13<sup>th</sup> October MRS data. From Table-5-9, we see that as the target window size increases first the estimated CC increases and with further increase, it starts getting decrease. This trend was unlike to the previous trends observed for the same location.

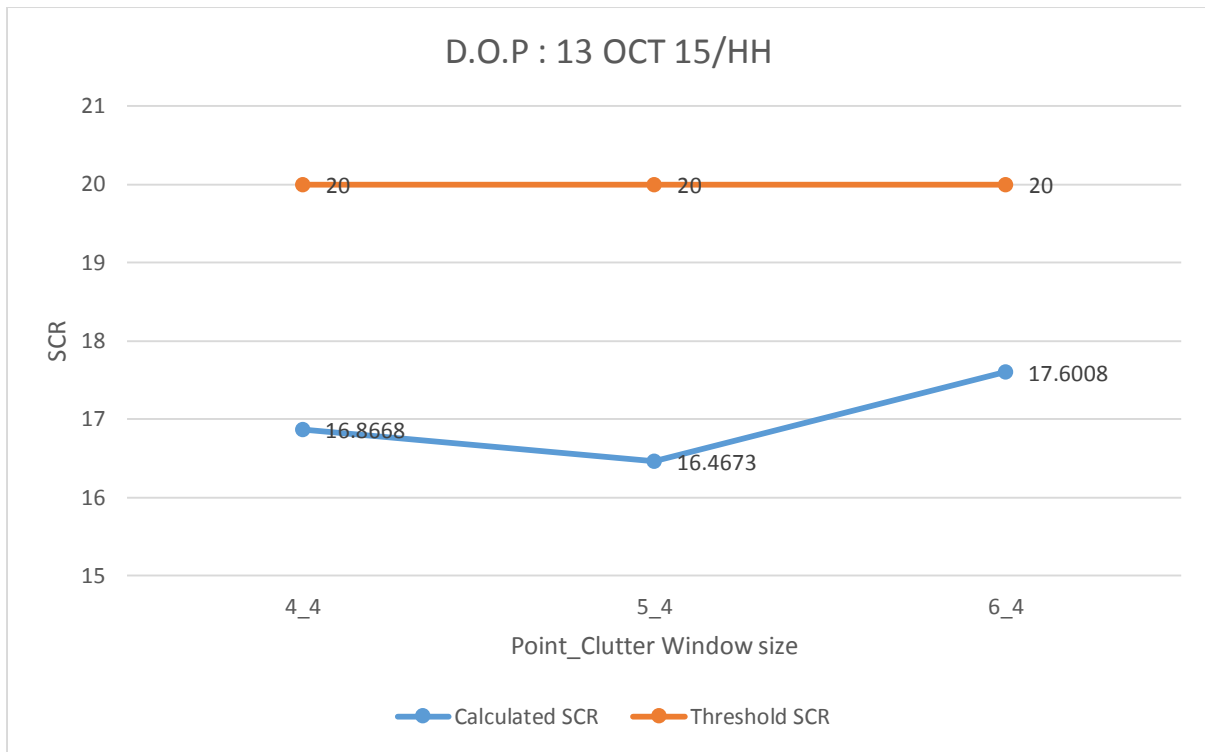


**Figure 5-24 Calculated SCR for different target and clutter window sizes**

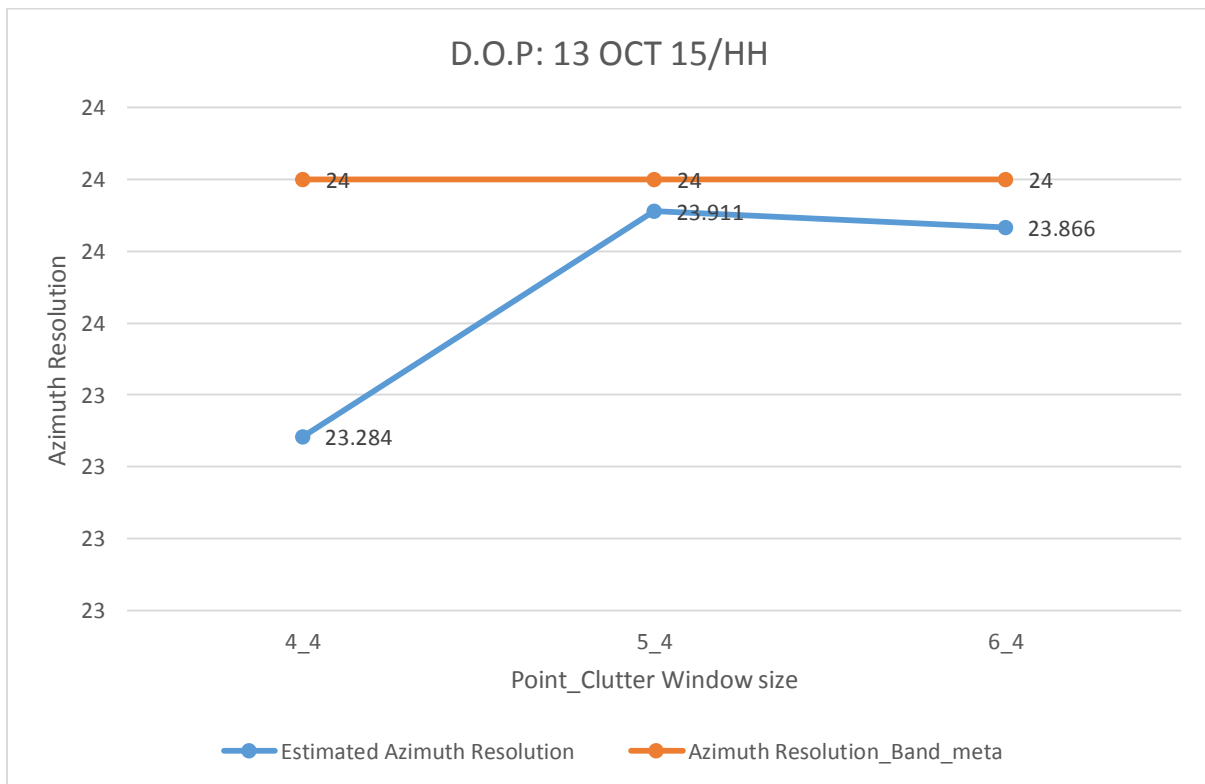


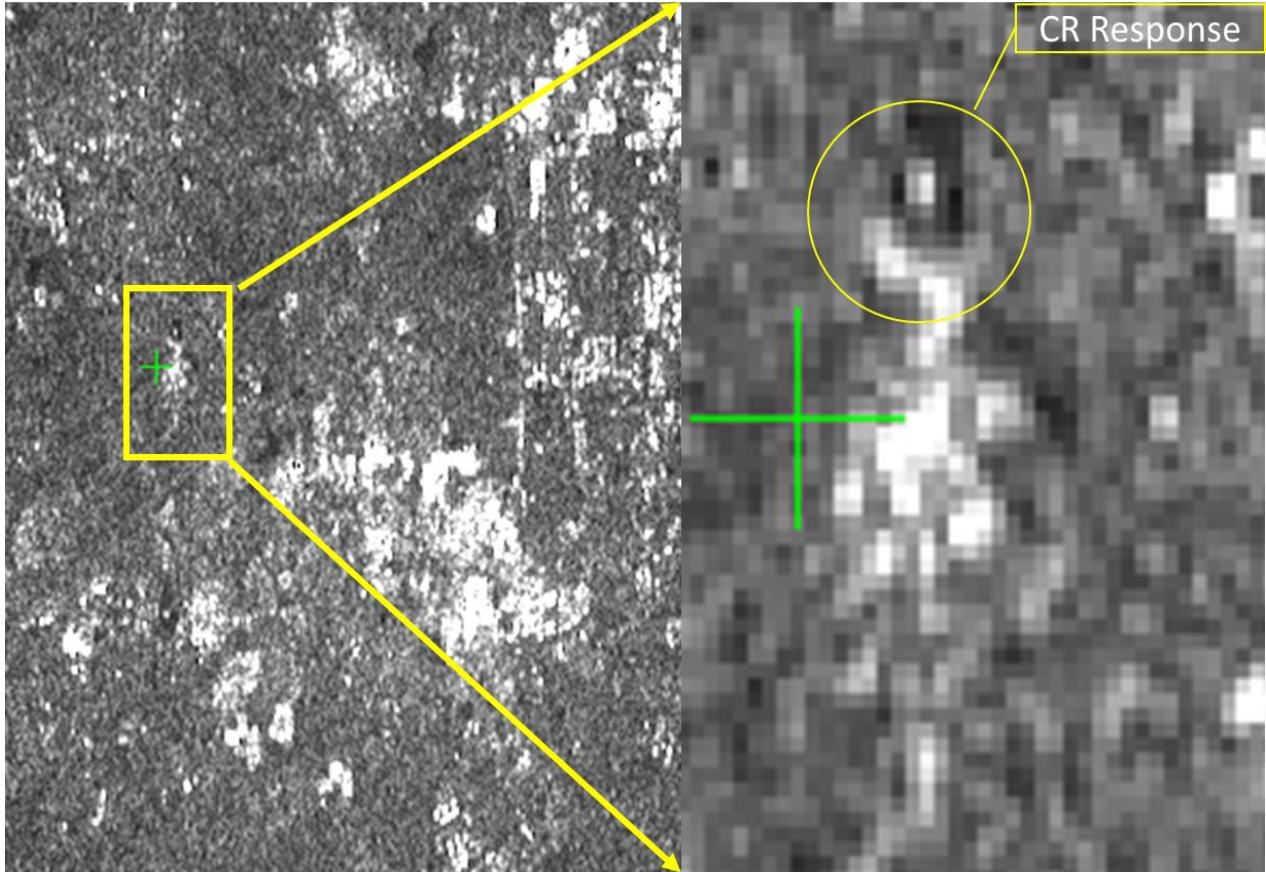
**Figure 5-25 Azimuth spatial resolution estimated from IRF**

### 5.2.1.8 7th November 2015: MRS-HH Polarization

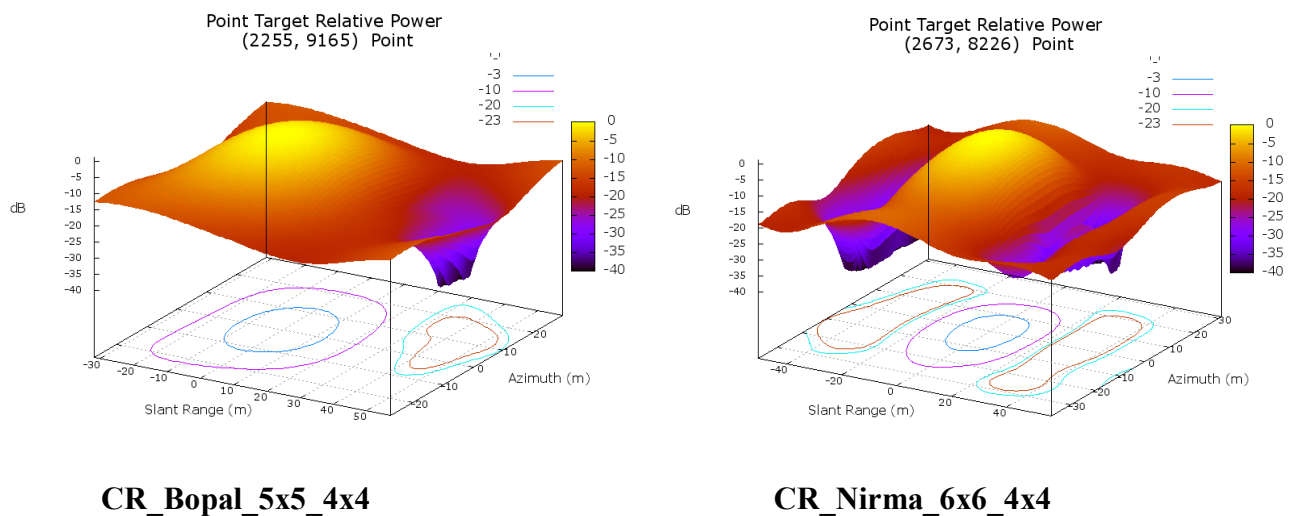
Beam no - 87-89-91-93-95-97

Incidence angle at scene center – 36.78942

Calibration Constant\_Band Meta – 74.522



**Figure 5-26 Response of CR at SAC, Bopal, Ahmedabad site of MRS SAR intensity data on 07/11/2015**



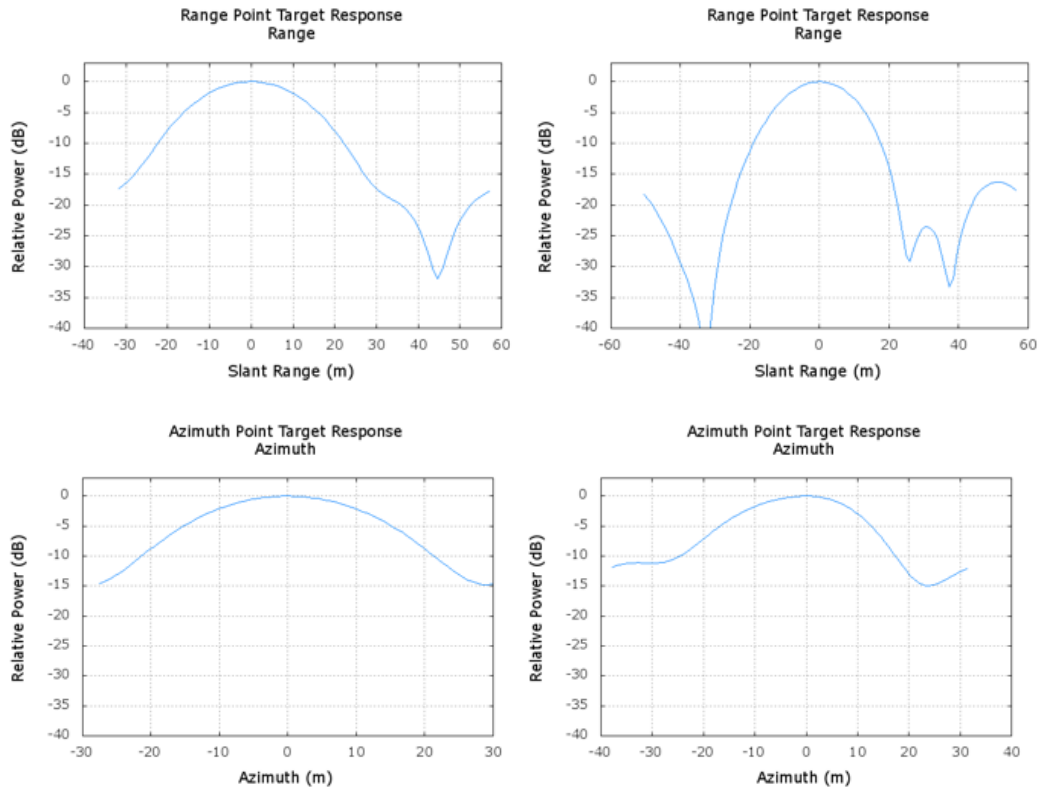


**Figure 5-27 Impulse response function of the CR for 7<sup>th</sup> November 2015 MRS image for different target and clutter window sizes**

**Table 5-10 Estimated calibration constant for 7<sup>th</sup> November 2015**

CR No	Location	Point window size	Clutter window size	Calibration Constant	Difference
1	Bopal	4x4	4x4	72.4653	-2.0567
1	Bopal	5x5	4x4	72.4737	-2.0483
1	Bopal	6x6	4x4	72.7546	-1.7674
2	Nirma	4x4	4x4	72.9868	-1.5352
				<b>Average</b>	<b>-1.8519</b>

The same trend as that of 13<sup>th</sup> October MRS was also observed in this case. From Table-5-10, it can be seen that as the target window size increases first the estimated CC increases and with further increase, it decreases. The reason for this might be attributed to the different background conditions. There might be inclusion of some bright pixel (because of the increased vegetation at the site) in the clutter window size, because of which the background corrected point target energy got decreased which in turn decreased the estimated CC.

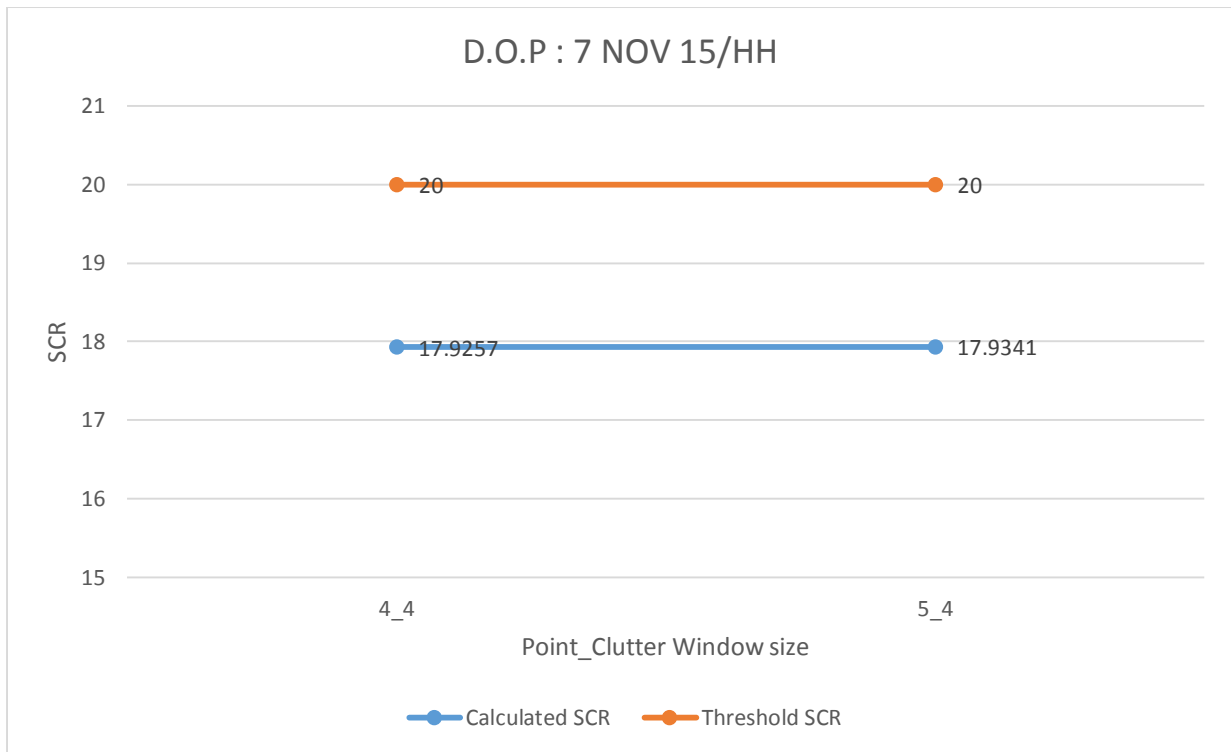


**Figure 5-28 Calculated SCR for Bopal site and for different target and clutter window sizes**

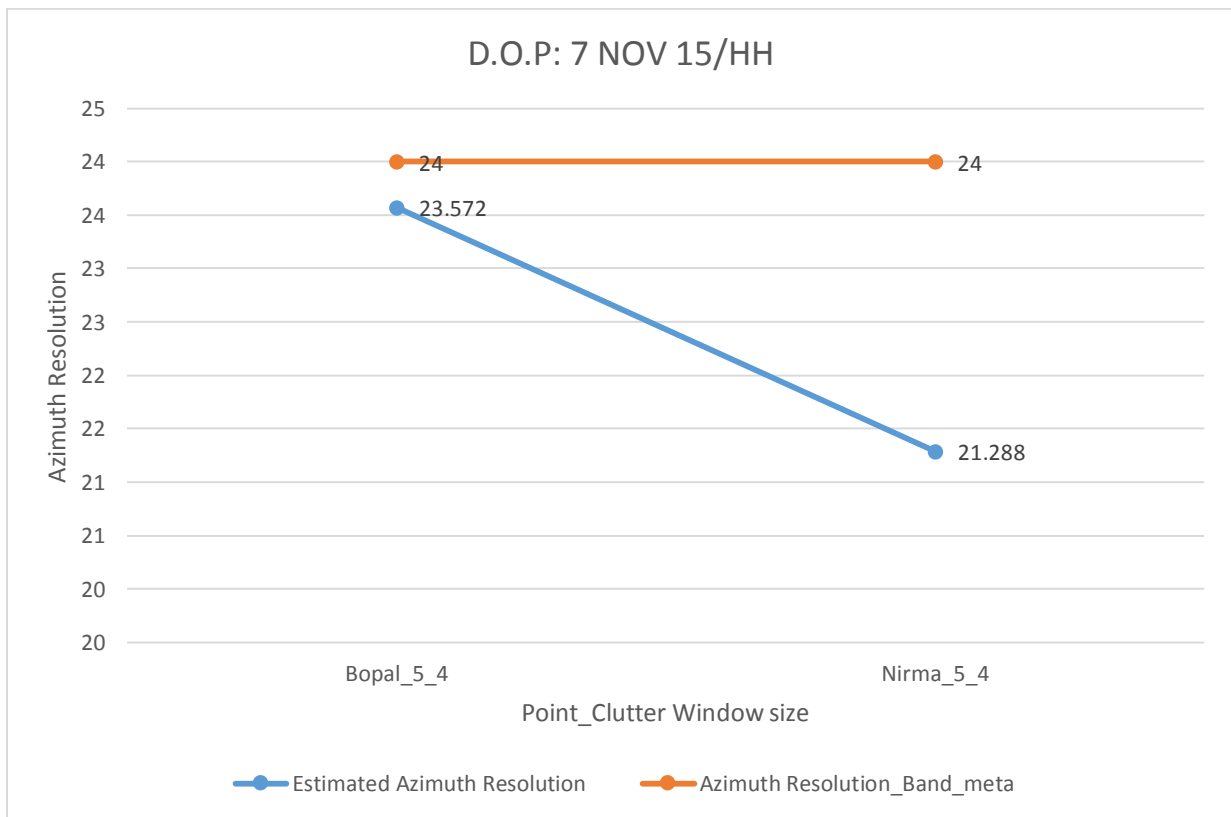


**Figure 5-29 Azimuth spatial resolution estimated from IRF**

### 5.2.1.9 2nd December 2015: MRS-HH Polarization

Beam no - 87-89-91-93-95-97

Incidence angle at scene center – 36.76666

Calibration Constant\_Band Meta – 74.653

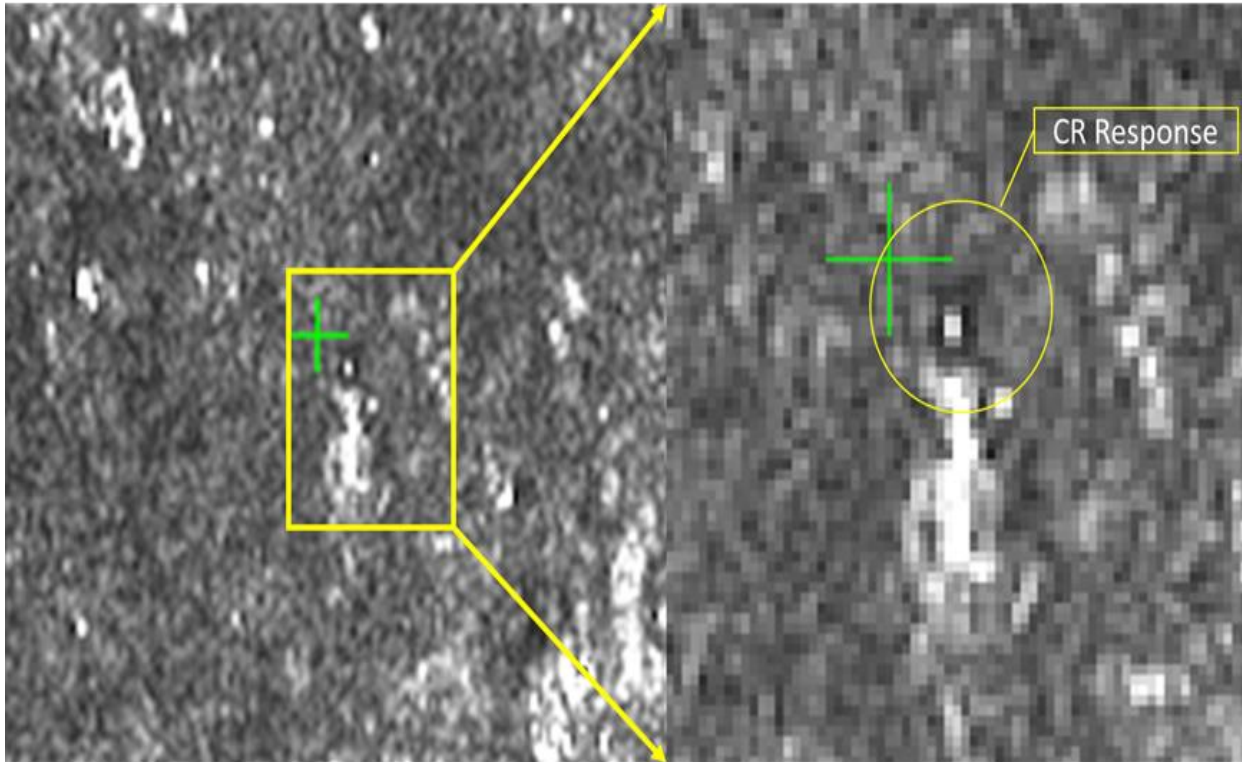
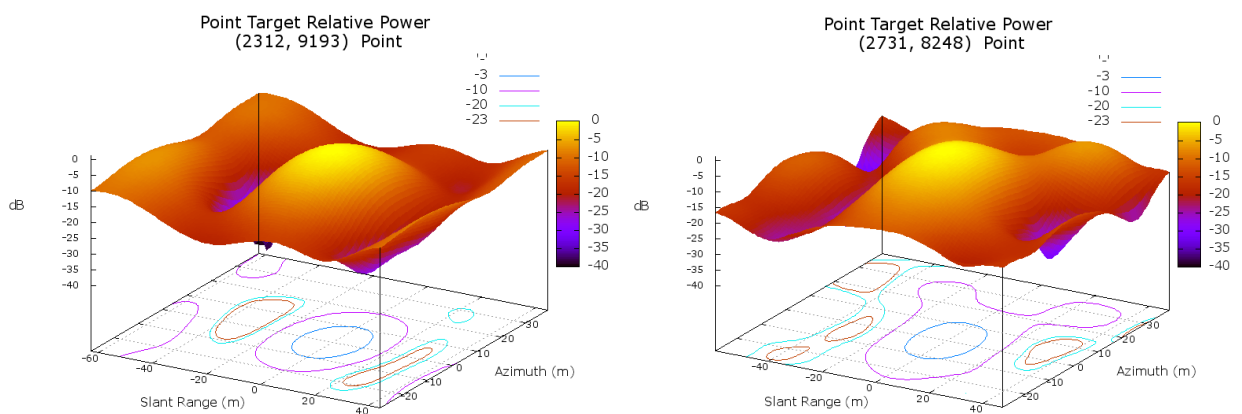


Figure 5-30 Response of CR at SAC, Bopal, Ahmedabad site of MRS SAR intensity data on 02/12/2015



CR\_Bopal\_6x6\_4x4

CR\_Nirma\_6x6\_4x4

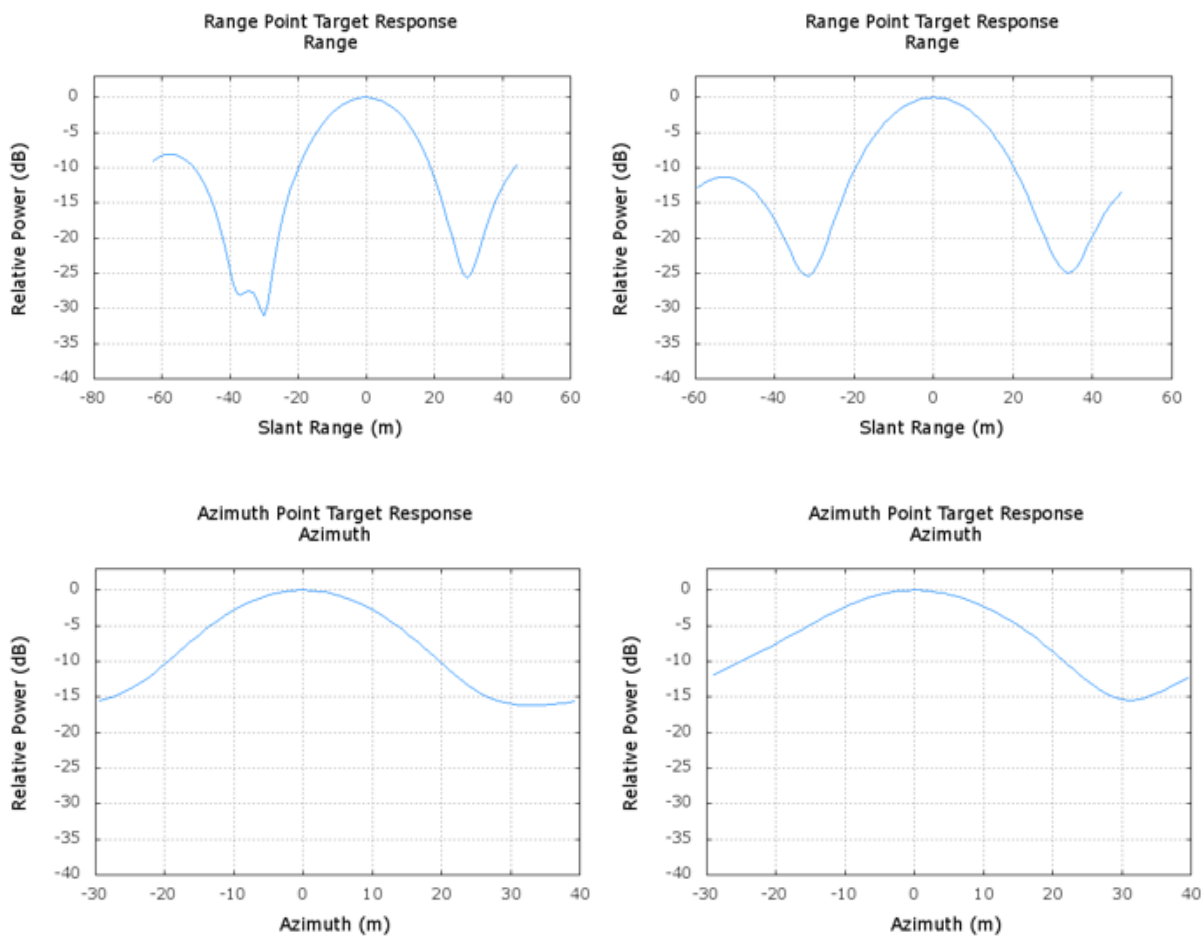
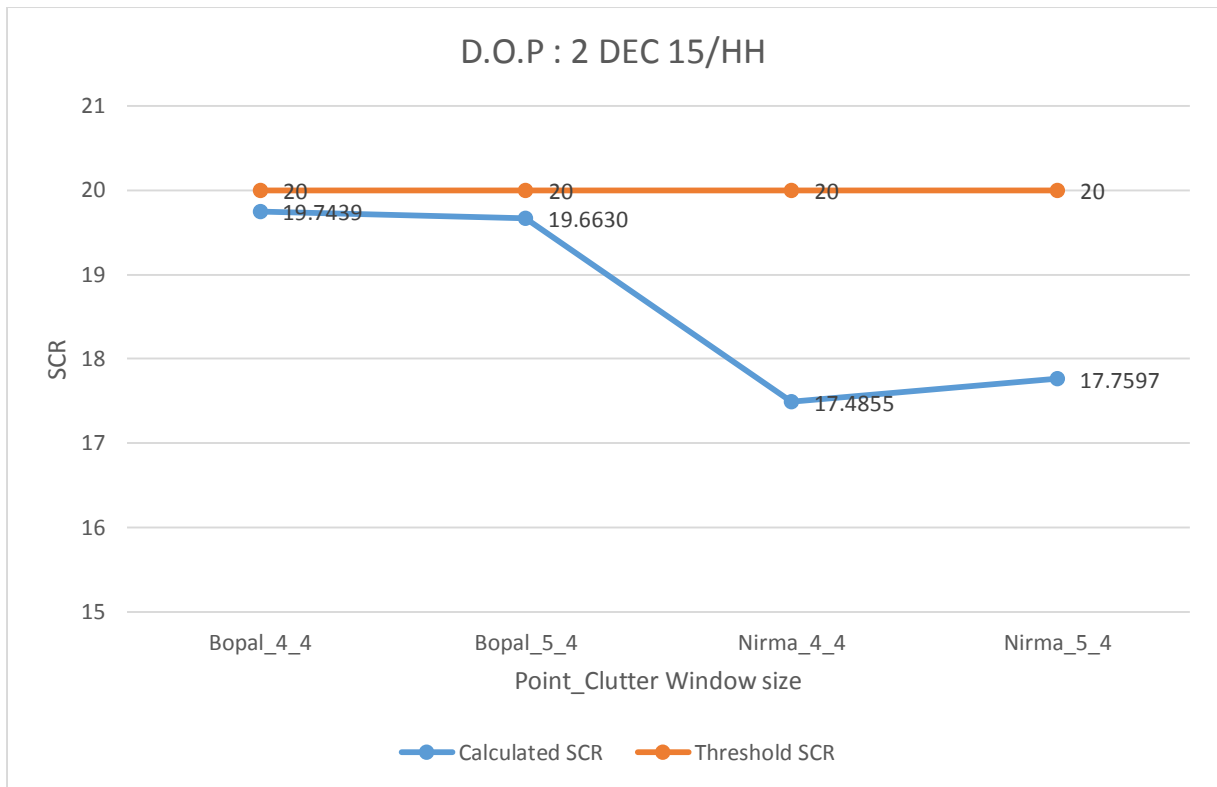


Figure 5-31 Impulse response function of the CR for 2<sup>nd</sup> December 2015 MRS image for different target and clutter window sizes

Table 5-11 Estimated calibration constant for 2<sup>nd</sup> December 2015

CR No	Location	Point window size	Clutter window size	Calibration Constant	Difference
1	Bopal	4x4	4x4	73.9449	-0.7081
1	Bopal	5x5	4x4	73.9449	-0.7081
1	Bopal	6x6	4x4	74.7315	0.0785
2	Nirma	4x4	4x4	75.3430	0.69
				<b>Average</b>	<b>-0.6688</b>

The results obtained from point target analysis for corenr reflector deployment on December 02, 2016 is shown in table 5-11. The results shows that very marginal difference of calibration constant obtained and claibration constant of header file is obtained. Once again, it was identified that sites having SCR near threshold value of SCR shows consistent results.



**Figure 5-32 Calculated SCR for Bopal and Nirma University sites and for different target and clutter window sizes**

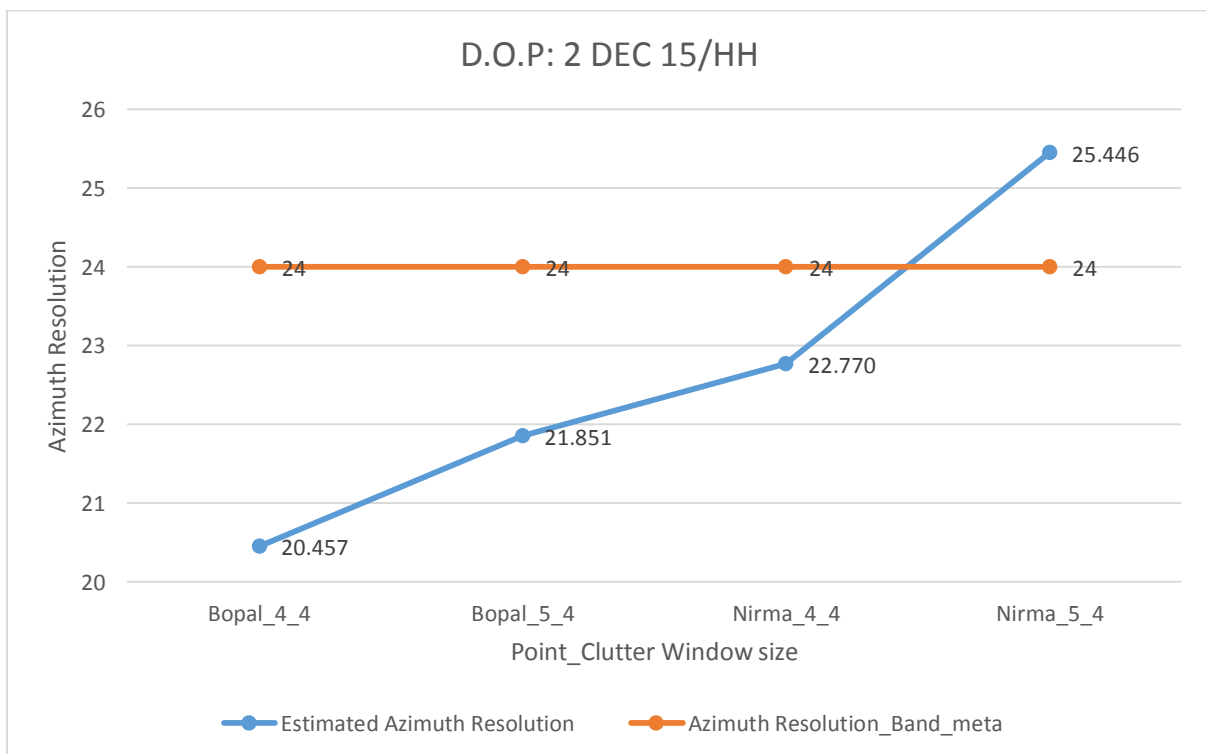


**Figure 5-33 Azimuth spatial resolution estimated from IRF**

### 5.2.1.10 27th December 2015: MRS-HH Polarization

Beam no - 87-89-91-93-95-97

Incidence angle at scene center – 36.76462

Calibration Constant\_Band Meta – 74.602

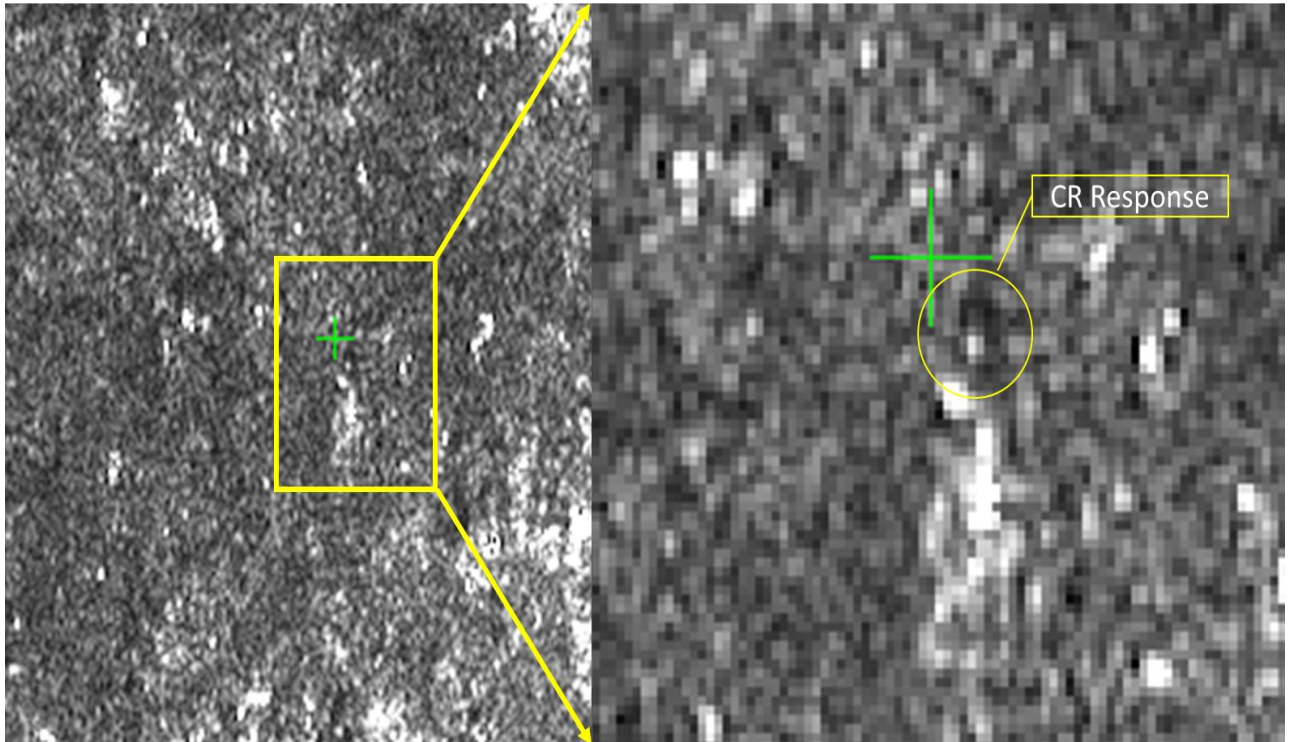
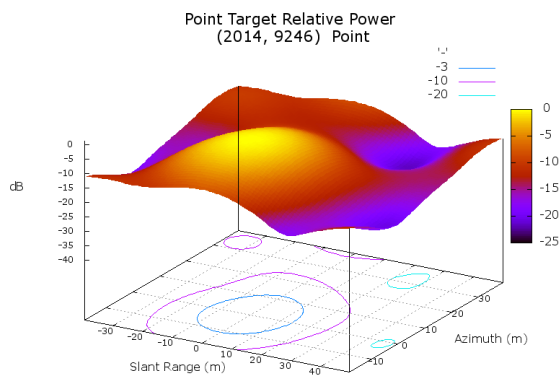
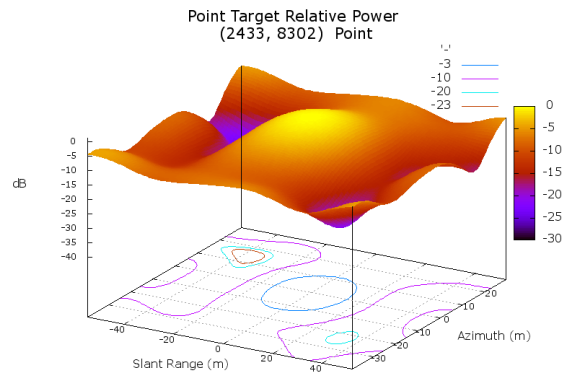


Figure 5-34 Response of CR at SAC, Bopal, Ahmedabad site of MRS SAR intensity data on 27/12/2015



CR\_Bopal\_5x5\_4x4



CR\_Nirma\_6x6\_4x4

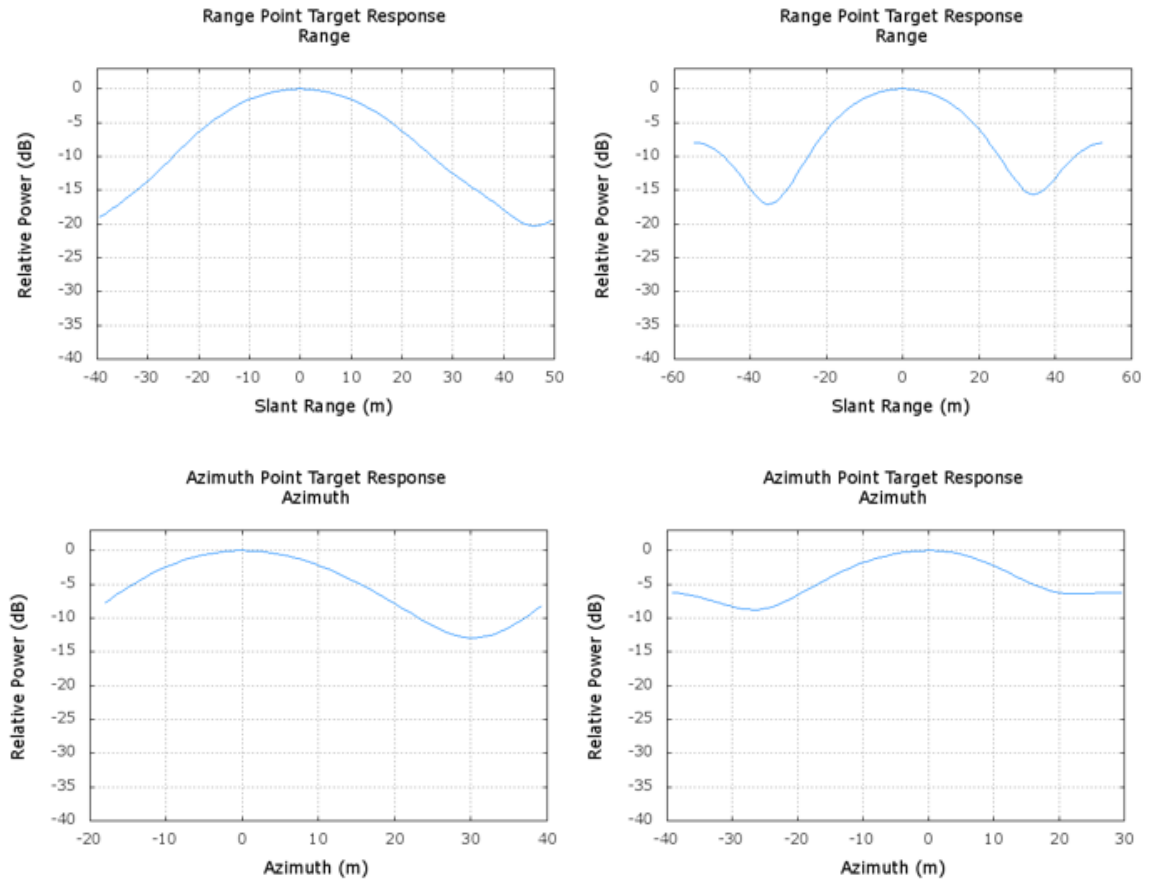


**Figure 5-35 Impulse response function of the CR for 27<sup>th</sup> December 2015 MRS image for different target and clutter window sizes**

**Table 5-12 Estimated calibration constant for 27<sup>th</sup> December 2015**

CR No.	Location	Point window size	Clutter window size	Calibration Constant	Difference
1	Bopal	4x4	4x4	71.5897	-3.0123
1	Bopal	5x5	4x4	70.9925	-3.6095
1	Bopal	6x6	4x4	71.2500	-3.352
2	Nirma	4x4	4x4	71.0639	-3.5381
2	Nirma	6x6	4x4	71.6281	-2.9739
				<b>Average</b>	<b>-3.297</b>

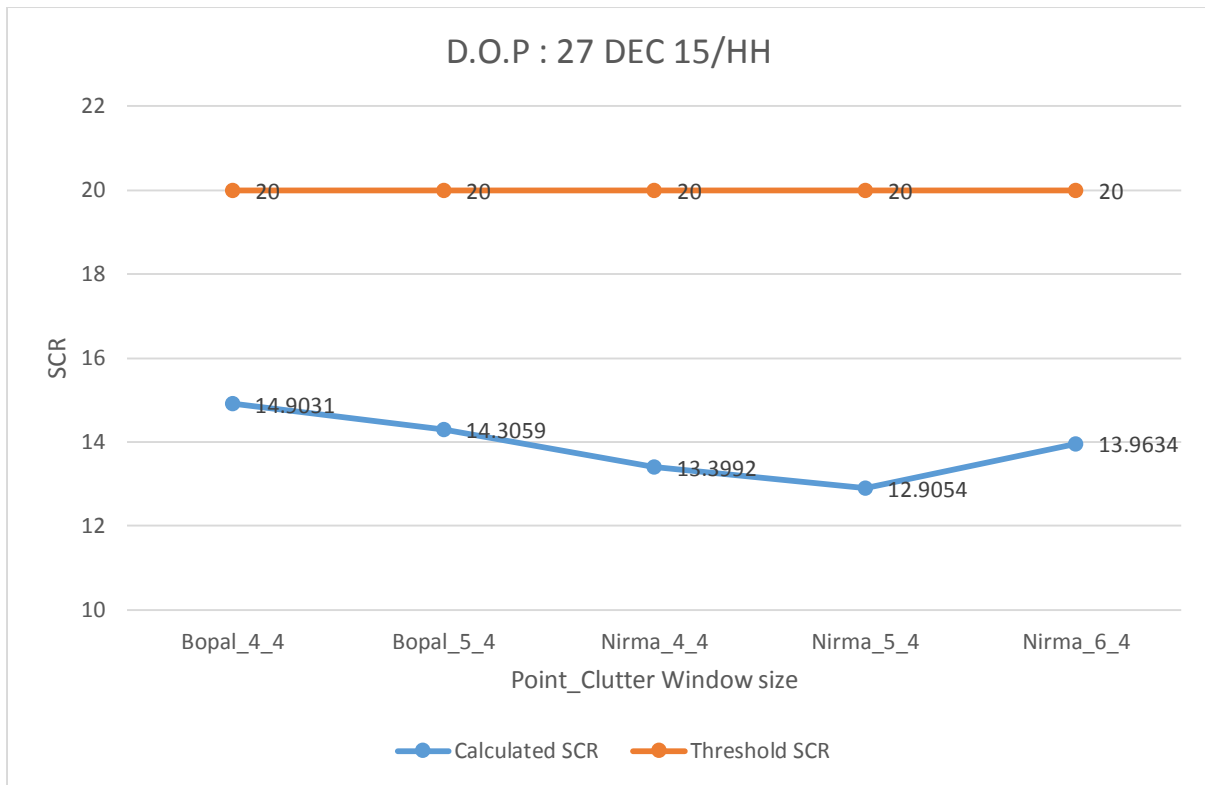


**Figure 5-36 Calculated SCR for Bopal and Nirma University sites and for different target and clutter window sizes**

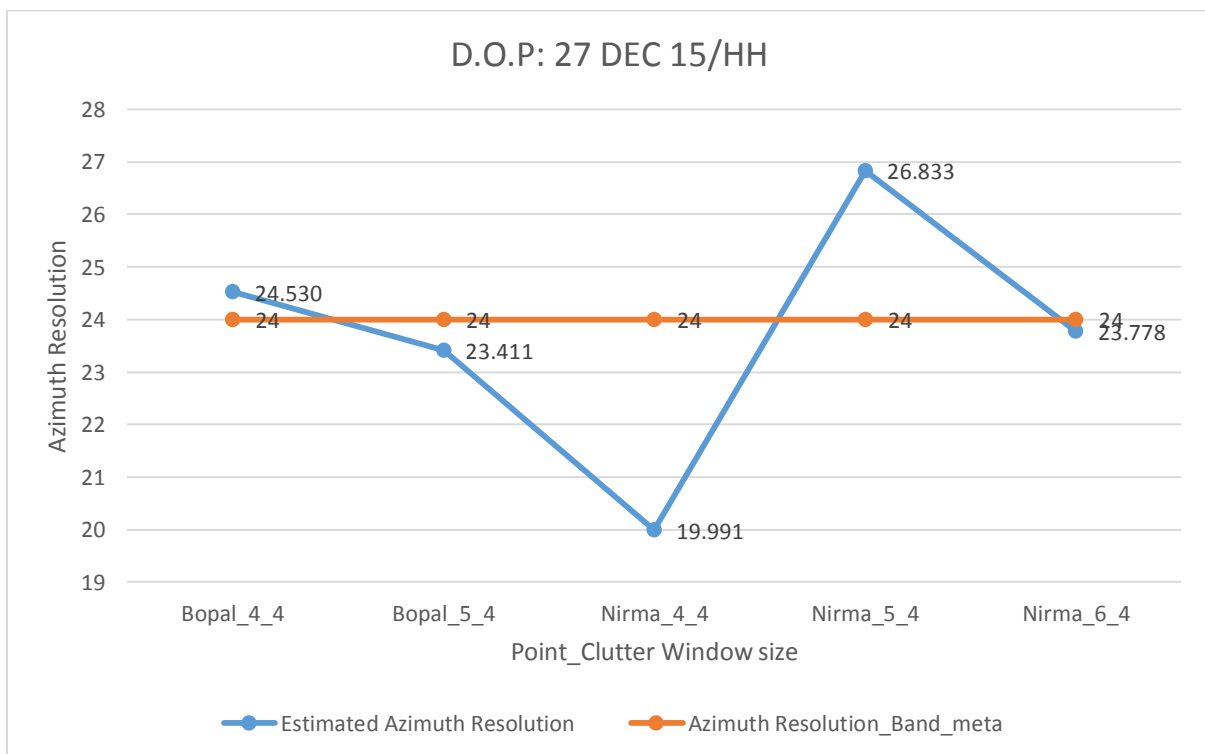


**Figure 5-37 Azimuth spatial resolution estimated from IRF**

### Summary of the results for Ahmedabad sites and discussion

The summary of the radiometric calibration results obtained for Ahmedabad sites is shown in Table 5-13 & Table 5-14 for MRS and FRS-1 mode data respectively. It can be seen from Table that the calibration constant difference between average estimated and provided values was found to be within 1dB for FRS-1 beam 104 and beam 21 respectively. However, for MRS data the difference was found to be within the range of 0.3-4.9 dB. The reason of getting such large difference is might be due to the SCR values. The SCR value should be at least 20dB in order to minimize errors in computation of the calibration factor [32]. But it was found that the calculated Signal to clutter ratio (SCR) values for Ahmedabad sites (Bopal and Nirma University ground) were less than 20 dB for MRS data (as can be seen from Table 5-13). The variation of SCR for this site was found to be within the range of 13-20 dB. The reason of such variation is the varying amount of vegetation as can be seen from the ground pictures of the sites at different dates, for some dates when the background is clean, the value of SCR approaches the specified value of 20dB, whereas, for the cases when there is large amount of vegetation present on the site (30<sup>th</sup> July 2015), signal to clutter ratio was found to be very poor (13.2dB).

Time series variation of the average estimated calibration constant, provided calibration constant and SCR is shown in Figure 5-38. It is clearly visible from the figure that for cases where SCR value is near to 20dB (for 2<sup>nd</sup> December ~19dB and for 24<sup>th</sup> August ~20dB), the estimated constant was found to be approaching the provided value and the difference of the estimated and provided CC was within 1dB. For the cases where the SCR value is between 16-18 dB range (13<sup>th</sup> Oct and 7<sup>th</sup> Nov 2015), the difference was found to be less than 2dB. For SCR values less than or equal to 15dB, the difference found was much higher (5<sup>th</sup> July, 30<sup>th</sup> July and 27<sup>th</sup> December 2015). Although, the SCR values for the same sites for FRS-1 data was found to be well above the threshold value of 20dB (Table-5-13).

**Table 5-13 Difference between average estimated CC and provided CC along with the calculated value of SCR for MRS**

S.No.	Date	Average Estimated Calibration Constant (CC)	Provided calibration constant	Difference (dB)	SCR
1.	5-07-2015	69.494	74.455	4.961	15.16
2.	30-07-2015	71.305	74.552	3.247	13.28

3.	24-08-2015	74.331	74.646	<b>0.315</b>	<b>18.50</b>
4.	13-10-2015	72.582	74.443	1.861	16.98
5.	07-11-2015	72.670	74.522	1.852	16.01
6.	2-12-2015	73.945	74.653	<b>0.708</b>	<b>19.70</b>
7.	27-12-2015	71.305	74.602	3.297	13.9

**Table 5-14 Calculated value of SCR for FRS-1**

S.No.	Date and Beam	Average Estimated CC	Provided CC	Difference (in dB)	SCR
1.	21 <sup>st</sup> April 2015 (FRS-1) Beam No. 104, HH	79.117	79.699	0.582	35.6329
2.	25 <sup>th</sup> April 2015 (FRS-1) Beam No. 21, HH	75.072	76.053	0.981	32.2518

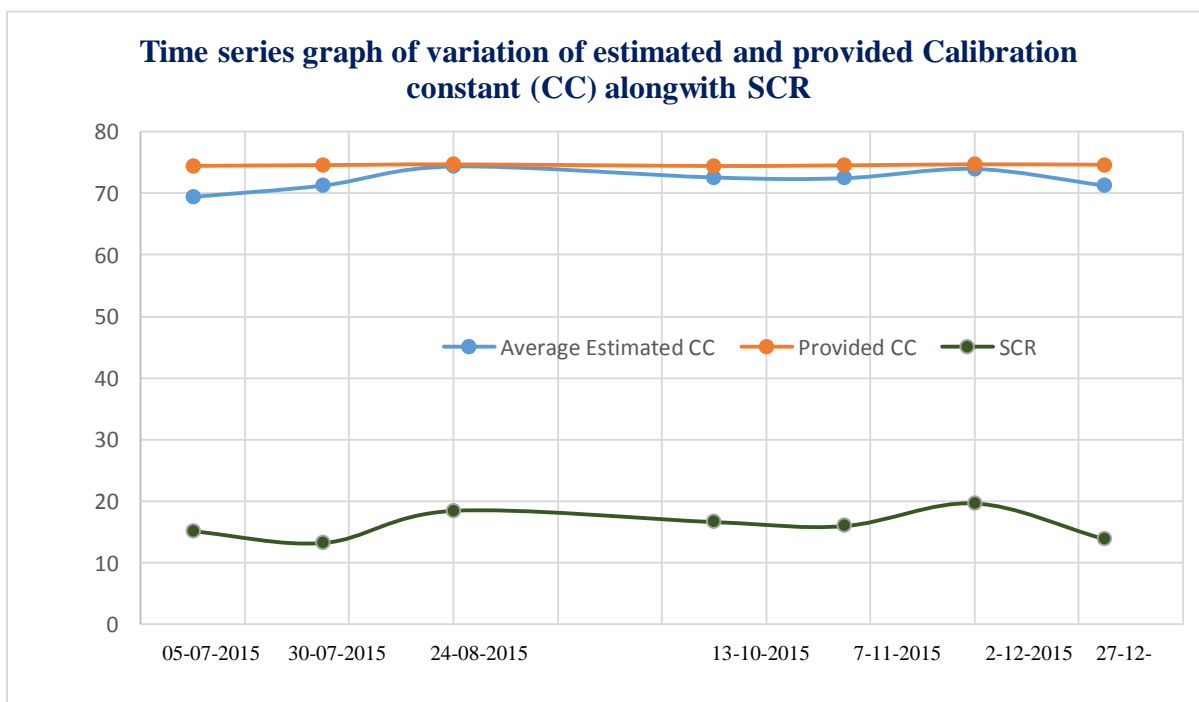


**Figure 5-38 Time series variation of average estimated and provided calibration constant along with SCR**

The sites in Ahmedabad was found to be behaving well in terms of SCR for FRS-1 data, however for MRS data, it was observed that SCR was not meeting the required specifications. Because of the variation in the vegetation amount, the results differ from date to date. So, alternate site for MRS data calibration was required and hence, Desalpar, Rann of Kutch site was selected for the study as this site is large in size, having very uniform background and devoid of any vegetation or buildings.

## **5.2.2 Results for Desalpar, Rann of Kutch site**

While deploying the CRs in Desalpar, Rann of Kutch site, a further consideration when choosing site locations for CR deployment was to ensure that the side-lobe response of adjacently sited CR would not overlap and they have clear distinction of their responses in the image. Generally, the baselines between all CR sites should be greater than 20 times the pixel size so for MRS mode data the distance between two adjacent CRs should be greater than around 500m, whereas for FRS-1, the baseline should be at least 60m. Maintaining large distance between CRs for MRS mode was possible due to the availability of large parcel of uniform land in Desalpar site. Deployed CRs were identified in the image and analysis was done. The results obtained for each date is as follows:

### **5.2.2.1 22nd January 2016, FRS-1 (RH)**

Beam no - 66

Incidence angle at scene center – 14.24753

Calibration Constant\_Band Meta – 71.832

The locations of the deployed CRs at Desalpar, Rann of Kutch site, on Google Earth image are shown in Figure 5-39 and their responses in RISAT-1 FRS-1 image of 22nd January 2016 are shown in Figure 5-40. The FRS-1 data of 21st January 2016 was not available due to some downlinking problem in the Antarctica station.

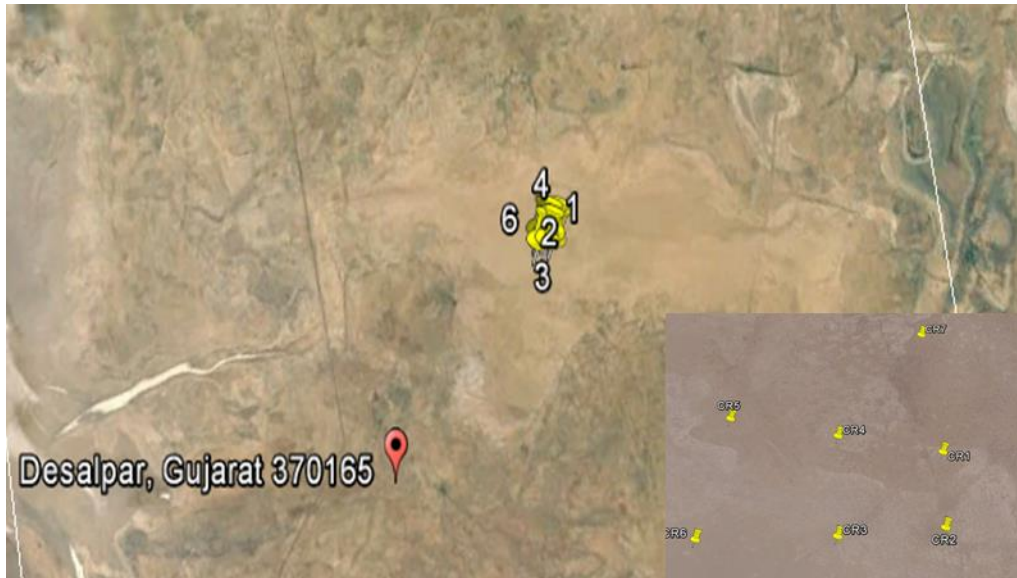


Figure 5-39 Locations of deployed CRs on Google Earth Image (common for 21<sup>st</sup> January 2016 FRS-1 pass and 22<sup>nd</sup> January 2016 FRS-1 pass)

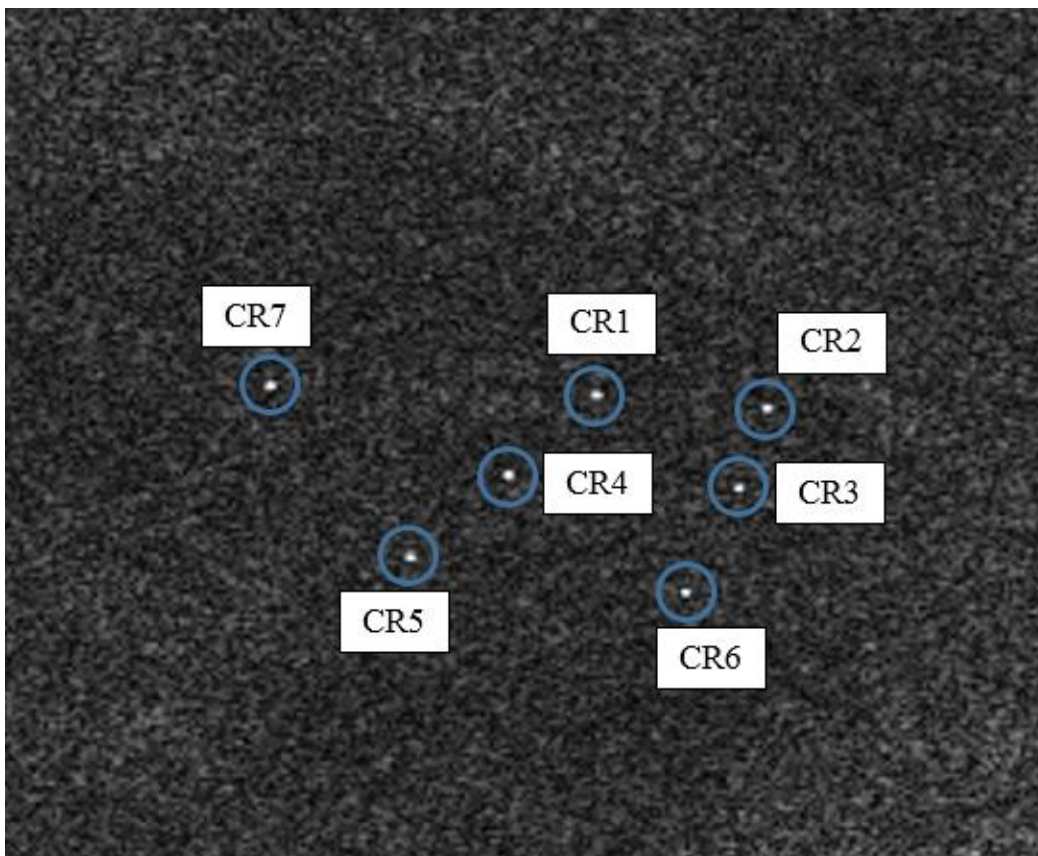


Figure 5-40 Response of deployed CRs as seen on 22<sup>nd</sup> January 2016 FRS-1 image)

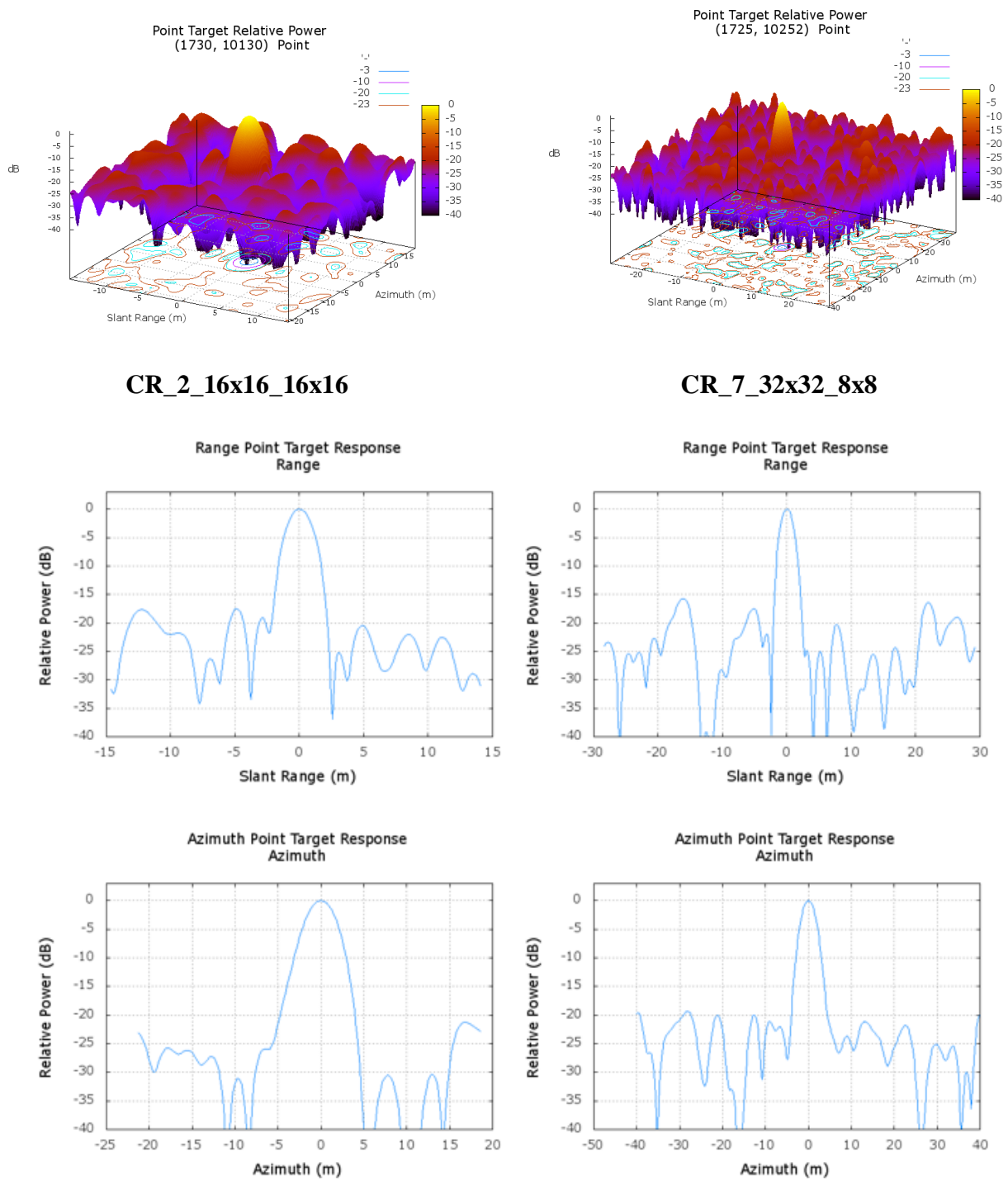


Figure 5-41 Impulse response function of the CR (2 & 7) for 22<sup>nd</sup> January 2016 MRS

**Table 5-15 Estimated Calibration Constant for different CRs**

<b>Corner Reflector No.</b>	<b>Point window size</b>	<b>Clutter window size</b>	<b>Calibration Constant estimated</b>	<b>Difference (dB)</b>
1	7x7	6x6	70.1759	1.6561
1	7x7	7x8	70.0051	1.8269
2	6x6	6x6	70.7810	1.0510
2	6x6	8x8	70.7416	1.0904
3	6x6	6x6	68.9699	2.8621
3	6x6	6x8	69.1153	2.7167
4	4x5	6x6	70.0408	1.7912
4	4x5	9x10	70.0528	1.7792
5	4x5	6x6	69.3391	2.4929
5	11x10	17x4	69.0744	2.7576
6	8x8	6x6	69.3578	2.4742
6	4x4	8x8	69.3287	2.5033
7	7x8	6x6	70.6016	1.2304
7	4x5	4x4	70.5760	1.2560
			<b>Average</b>	<b>1.9634</b>

The difference between estimated and provided calibration constant was found to be within 2dB for all CRs except CR 3, 5 and 6 for which the difference was slightly higher. The reason of this comparatively large difference might be because of the improper elevation setting of these CRs which was due to the faulty mount. However, the average difference value was found to be within 2dB.

### **5.2.2.2 14th February 2016, MRS (HH)**

Beam no - 87-89-91-93-95-97

Incidence angle at scene center – 36.80517

Calibration Constant\_Band Meta – 74.491

The locations of the deployed CRs at Desalpar, Rann of Kutch site, on Google Earth image are shown in Figure 5-42, 5-43, 5-44 & 5-45 and their responses in RISAT-1 MRS image of 14<sup>th</sup> February 2016 are shown in Figure 5-47 and 5-48.

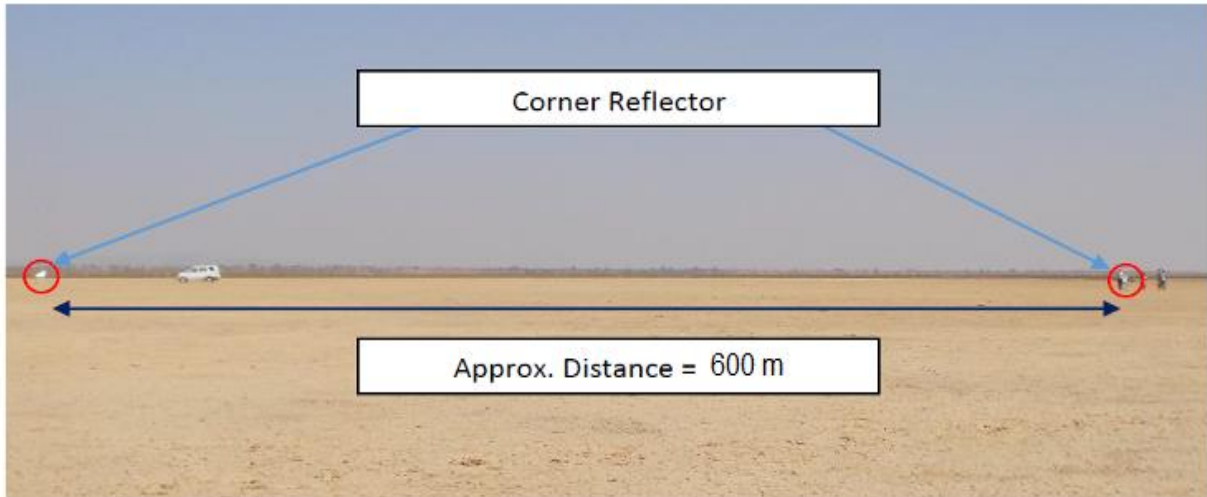


**Figure 5-42 Snap showing the distance between deployed CRs**

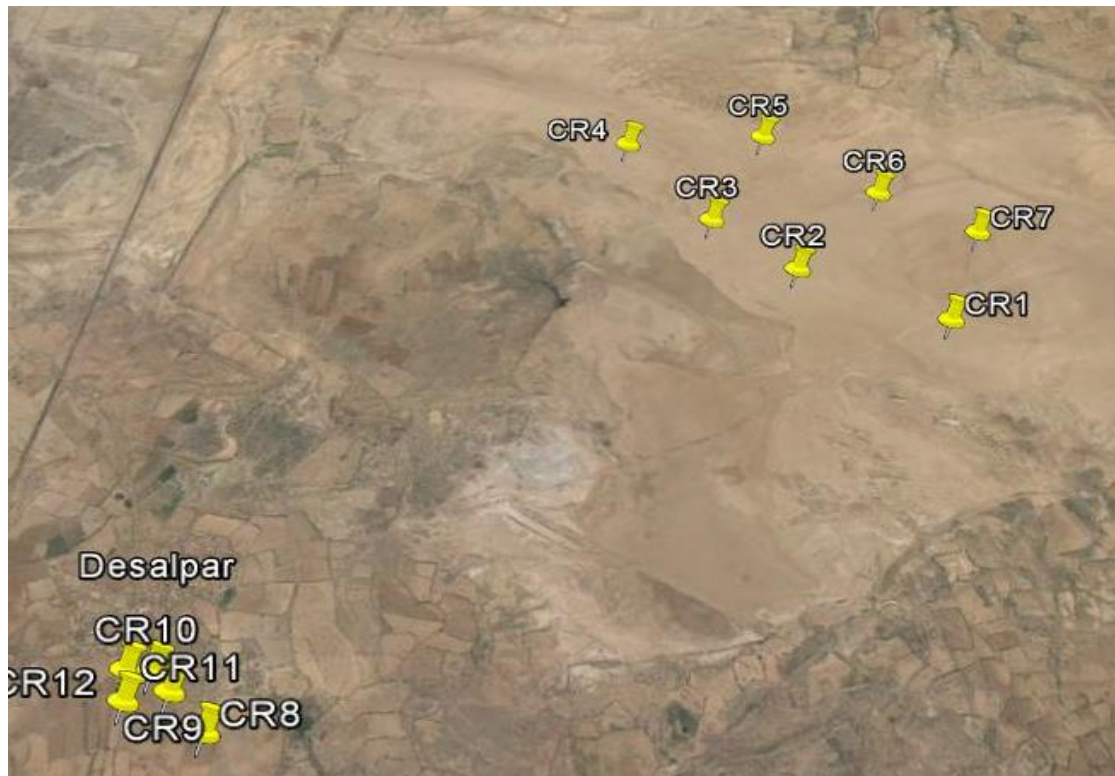


**Figure 5-43 Locations of deployed CRs on Google Earth Image (common for 14<sup>th</sup> February MRS pass and 15<sup>th</sup> February 2016 FRS-1 pass)**

In order to study the effect of the background on SCR, this time, an experiment was done by using the black cloth as a background for CR. CR was deployed on black cloth of size (5×5) m which was greater than the size of one pixel of FRS-1 (CR 11 in Figure 5-45 and deployed CR in Figure 5-46).

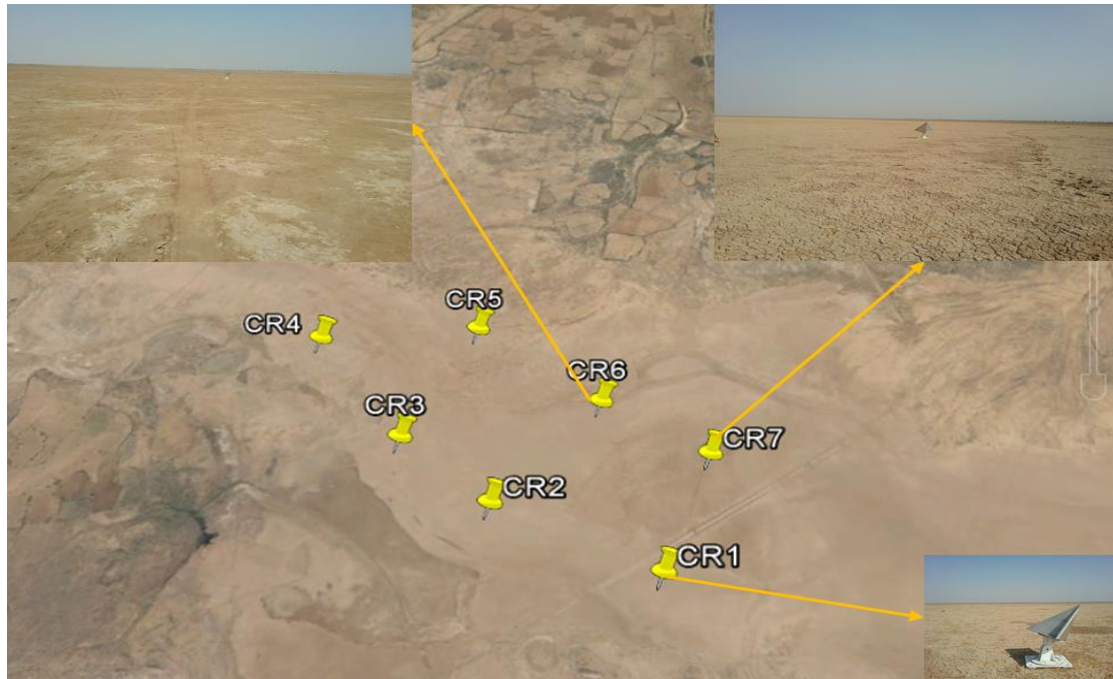


**Figure 5-44** Locations of deployed CRs at Rann of Kutch (with field photographs) on Google Earth Image (common for 14<sup>th</sup> February MRS pass and 15<sup>th</sup> February 2016 FRS-1 pass)

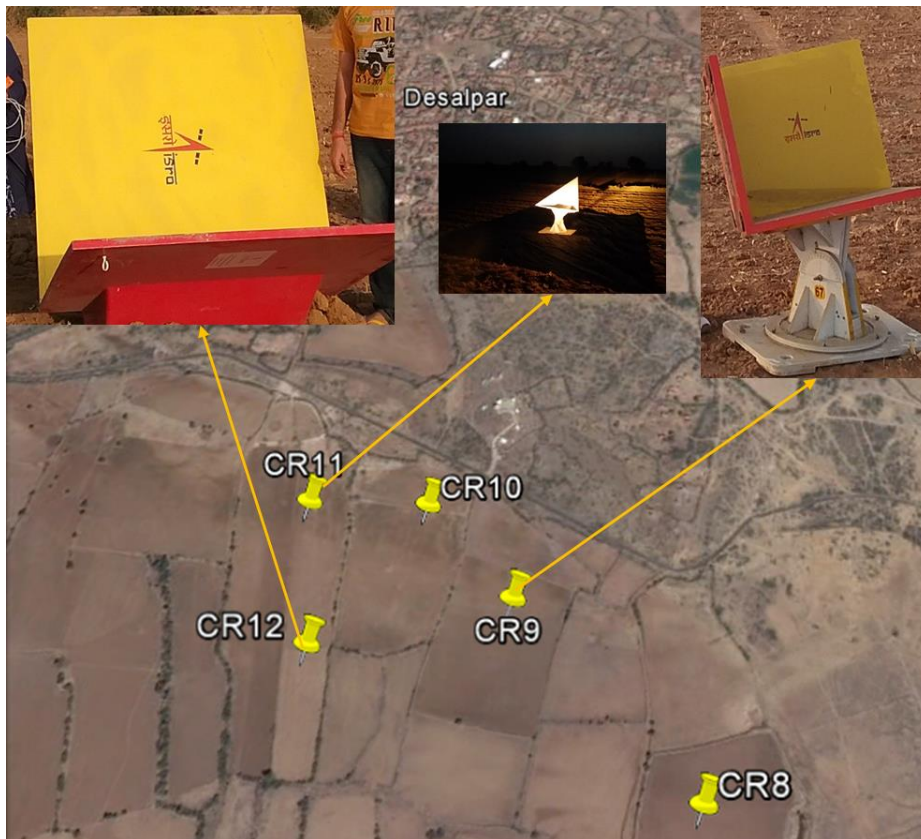


**Figure 5-45** Locations of deployed CRs at the fields in front of ISR cabin (with field photographs) on Google Earth Image (common for 14<sup>th</sup> February MRS pass and 15<sup>th</sup> February 2016 FRS-1 pass)



Figure 5-46 CR deployed on black cloth background

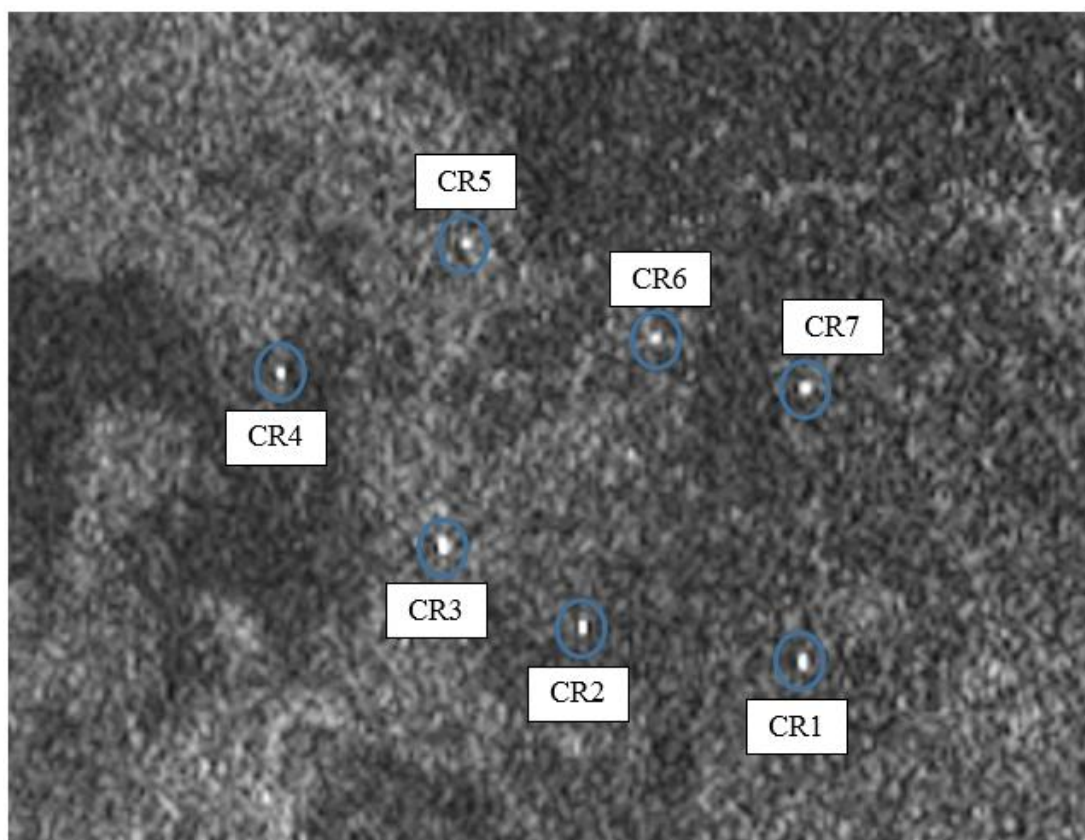


Figure 5-47 Response of CRs (1-7) as seen in RISAT-1 MRS image of 14<sup>th</sup> Feb 2016

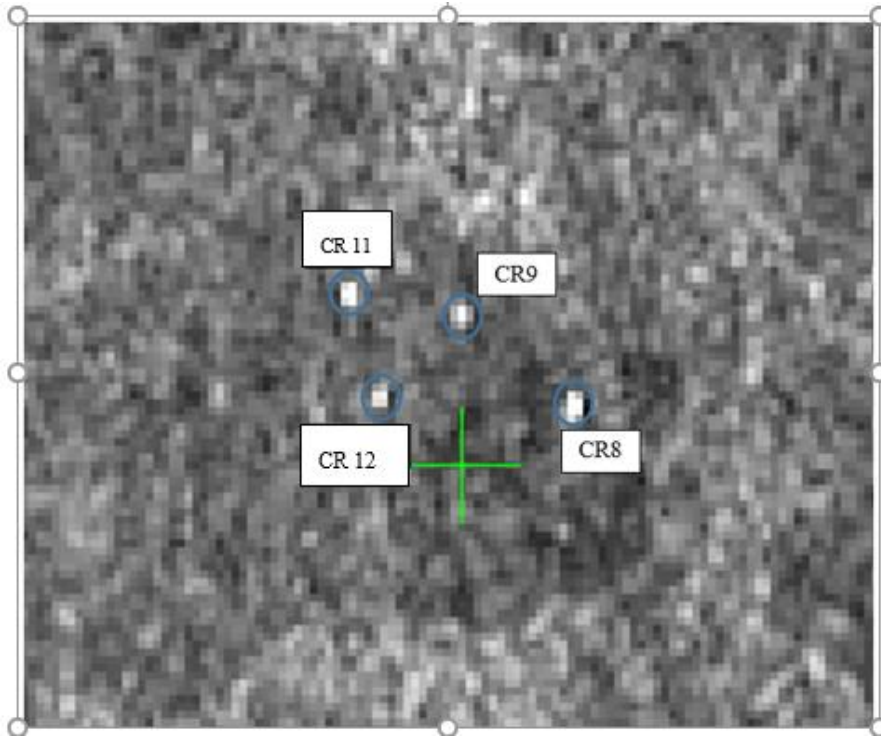
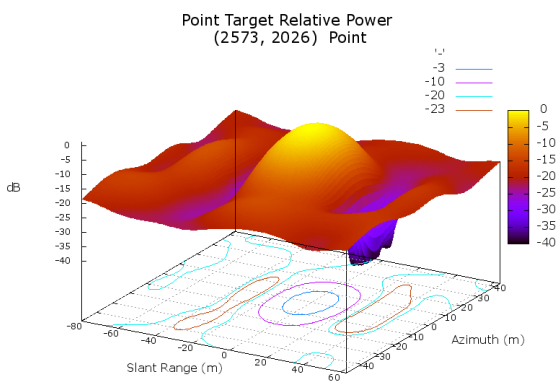
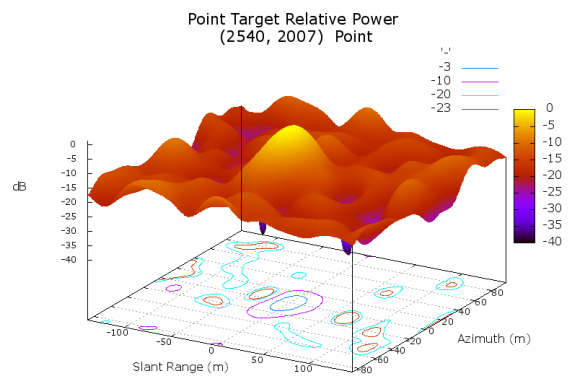


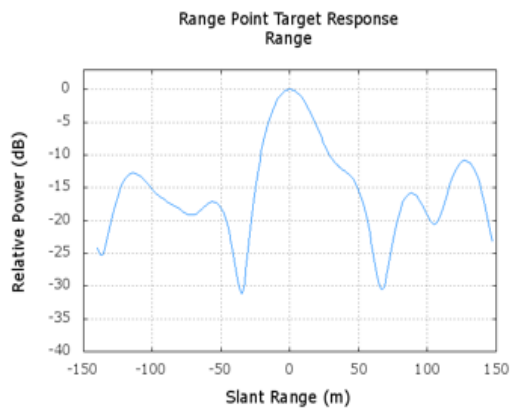
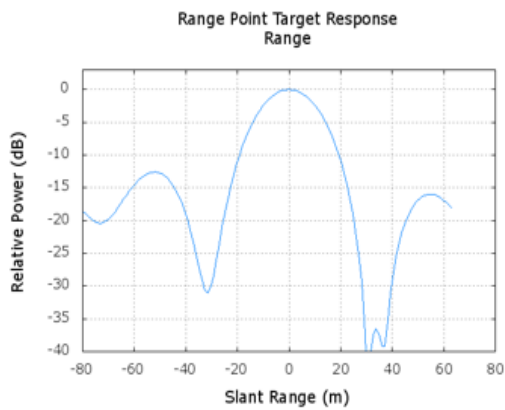
Figure 5-48 Response of CRs (8-10) as seen in RISAT-1 MRS image of 14<sup>th</sup> Feb 2016



CR\_2\_8x8\_8x8



CR\_3\_16x16\_8x8



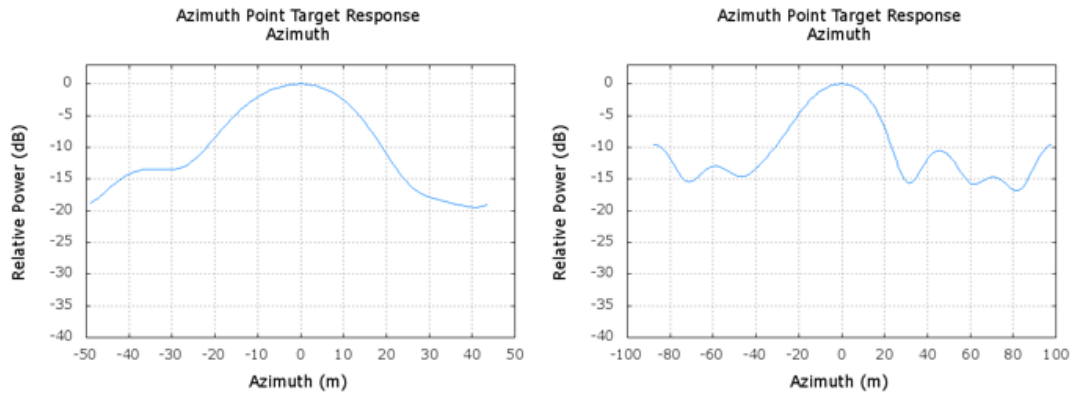
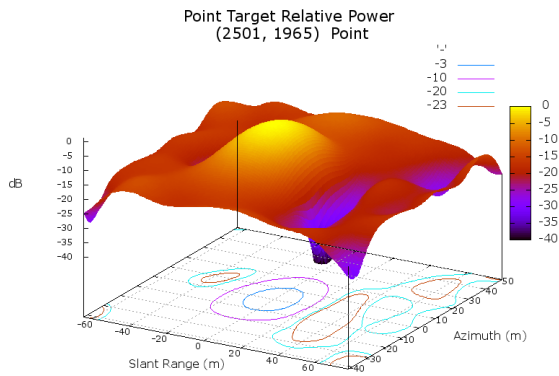
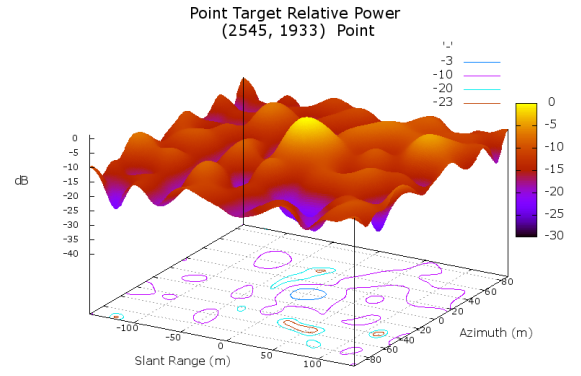


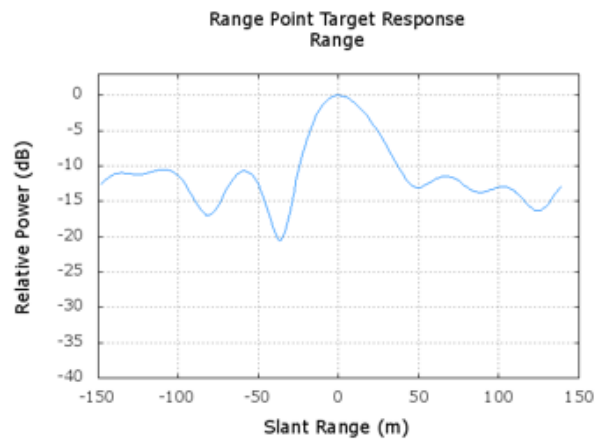
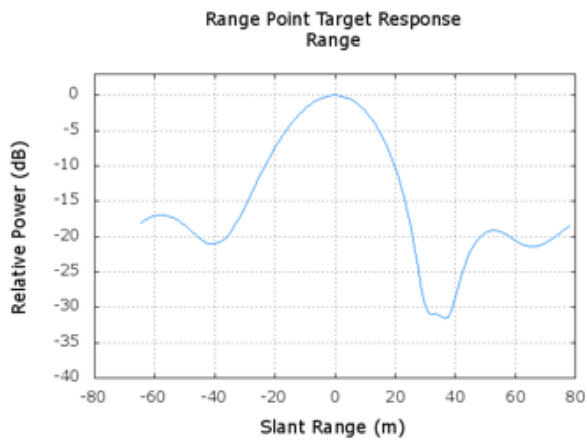
Figure 38a: Impulse response function of the CR (2 & 3) for 14<sup>th</sup> February 2016 MRS



CR\_4\_8x8\_8x8



CR\_5\_16x16\_8x8



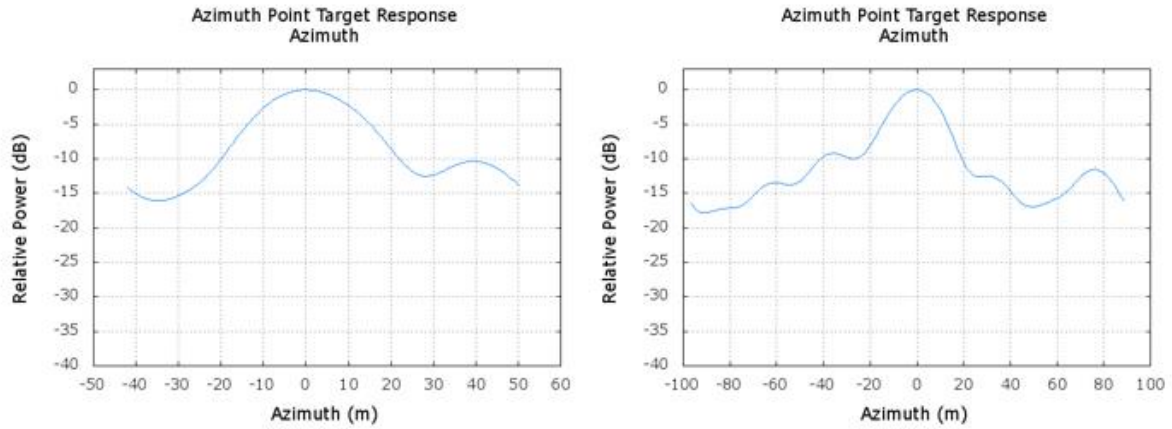
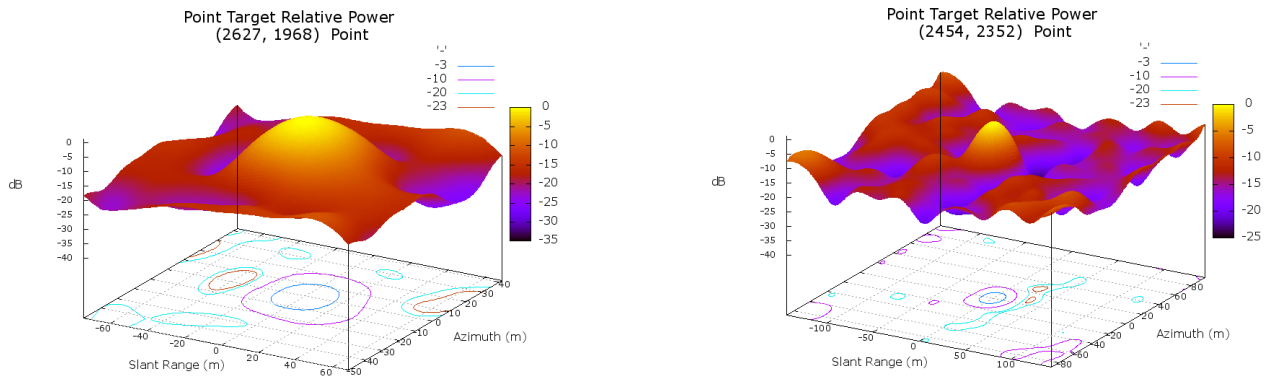
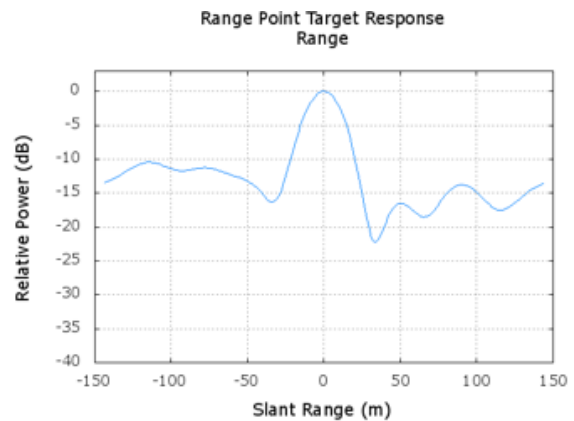
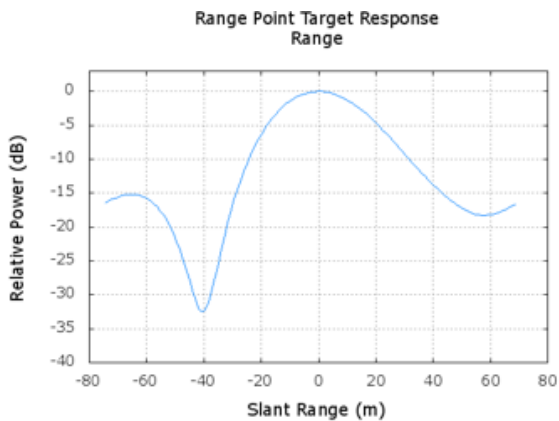


Figure 38b: Impulse response function of the CR (4 & 5) for 14<sup>th</sup> February 2016 MRS



CR\_7\_8x8\_8x8

CR\_9\_16x16\_8x8



Azimuth Point Target Response  
Azimuth

Azimuth Point Target Response  
Azimuth

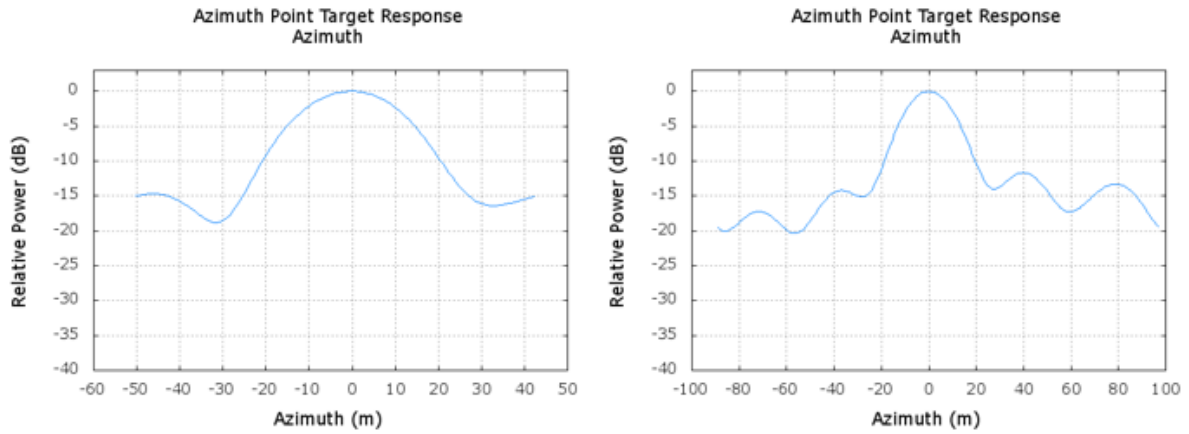


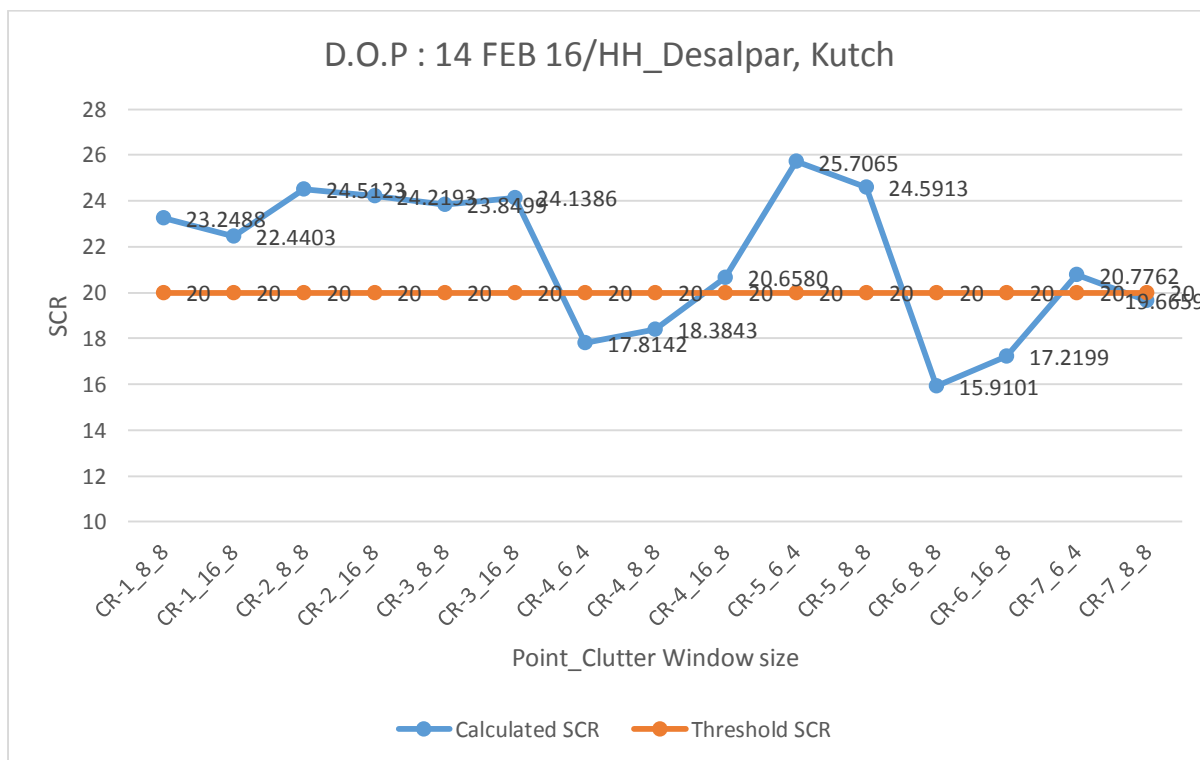
Figure 5-49 Impulse response function of the CR (7 & 9) for 14<sup>th</sup> February 2016 MRS

Table 5-16 Estimated Calibration Constant for different CRs

CR No.	Point window size	Clutter window size	Calibration Constant	Difference (dB)
2	6x6	4x4	75.4853	0.9943
2	8x8	8x8	75.4169	0.9259
2	16x16	8x8	74.6084	0.1174
3	6x6	4x4	77.0940	2.603
3	8x8	8x8	77.1914	2.7004
3	16x16	8x8	77.1358	2.6448
4	6x6	4x4	72.9016	-1.5894
4	8x8	6x6	73.2849	-1.2061
4	8x8	8x8	73.3436	-1.1474
5	6x6	4x4	71.9716	-2.5194
5	8x8	8x8	72.1713	-2.3197
5	16x16	8x8	74.4449	-0.0461
7	6x6	4x4	74.5097	0.0187
7	8x8	8x8	74.6374	0.1464
8*	6x6	4x4	73.8315	-0.6595
8*	8x8	8x8	73.8511	-0.6399
8*	16x16	8x8	73.4956	-0.9954
9	16x16	8x8	72.2960	-2.195
11	6x6	4x4	75.0826	0.5916
11	8x8	8x8	75.0342	0.5432

\*Square Trihedral CR

The calibration constant was estimated using the IRF of the deployed CRs. It can be seen from Table 5-14 that the calibration constant difference between estimated and provided is within 2.5 dB. Because of the improper elevation setting of square trihedral (CR6) due to the faulty mount, the results obtained utilizing the IRF of this CR are not included. Results obtained from CR 12 (dihedral) are being analyzed. It is interesting to note that CR 11 (with the background of black cloth) and CR 8 (square trihedral) both are showing the difference within 1dB.



**Figure 5-50 Calculated SCR for different CRs and for different target and clutter window sizes**

Signal to clutter ratio was calculated for all the CRs with different target and clutter window sizes and plotted in Figure 5-50. In most of the cases, the SCR value was found to be greater than 20dB, which was not the case with Ahmedabad sites for MRS data. It shows the potential of this site for the calibration of MRS data.

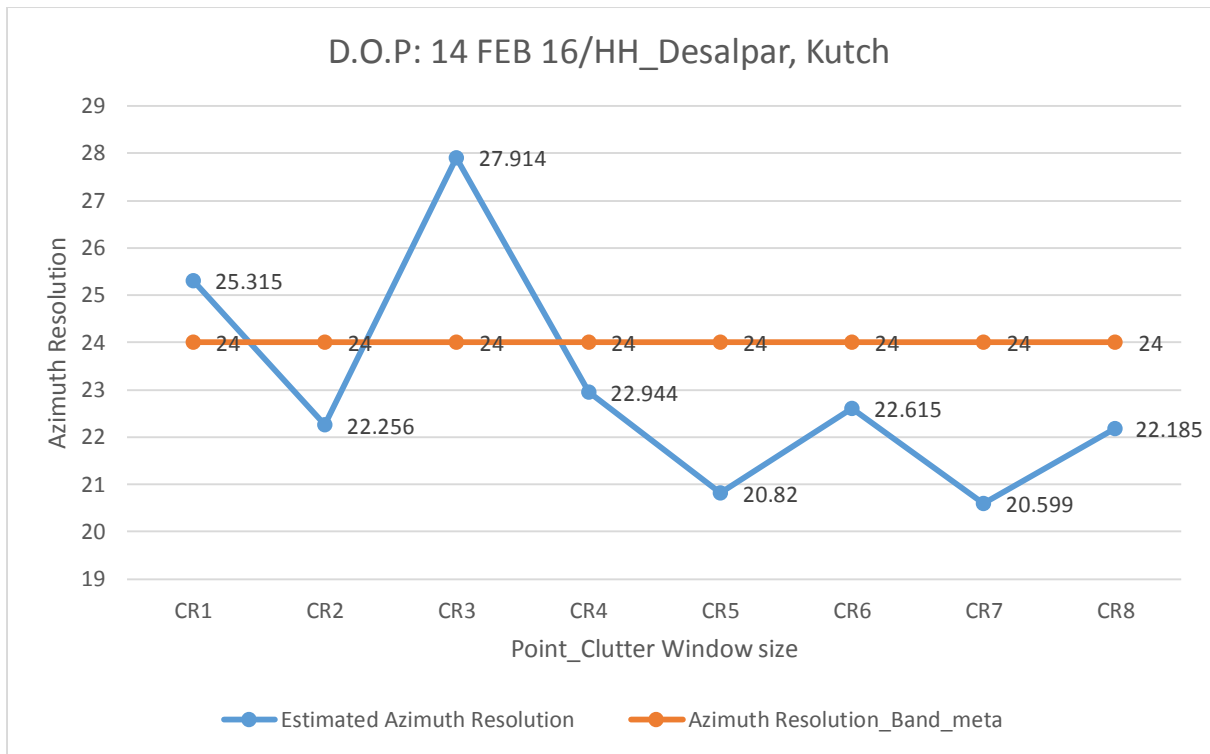


**Figure 5-51 Azimuth spatial resolution estimated from IRF for different target and clutter window sizes**

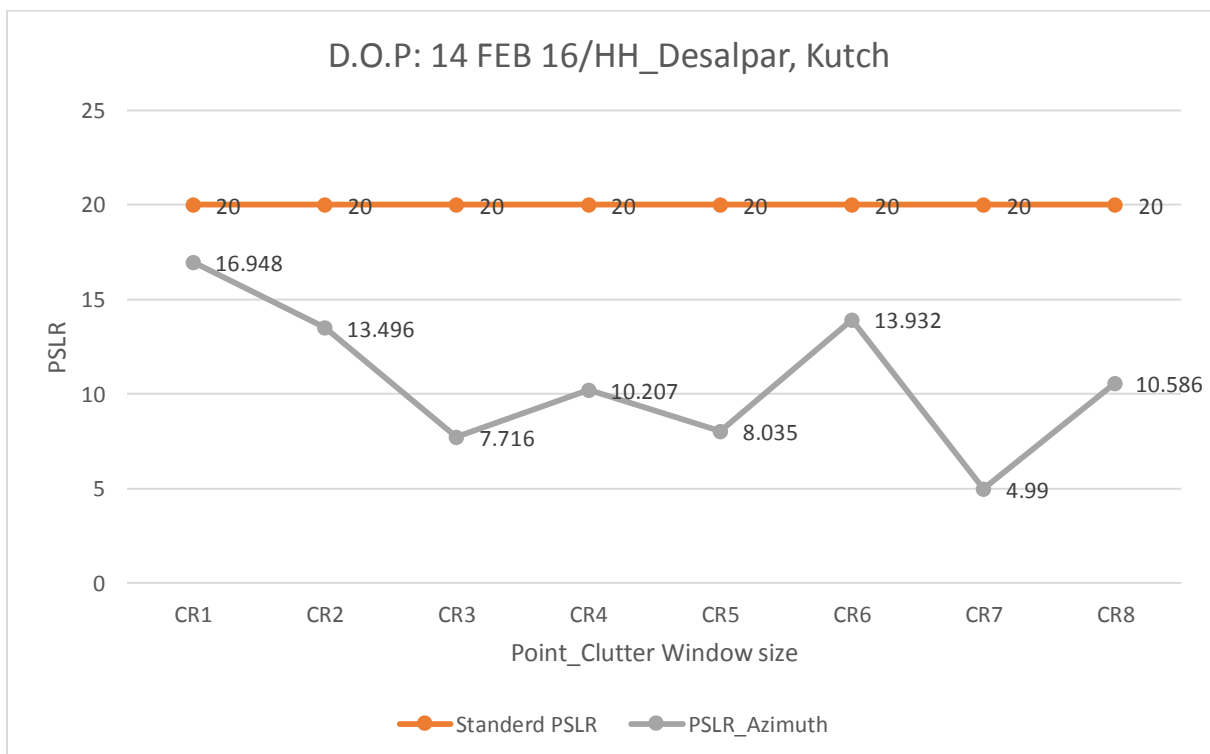


**Figure 5-52 PSLR in azimuth estimated from IRF for different target and clutter window sizes**

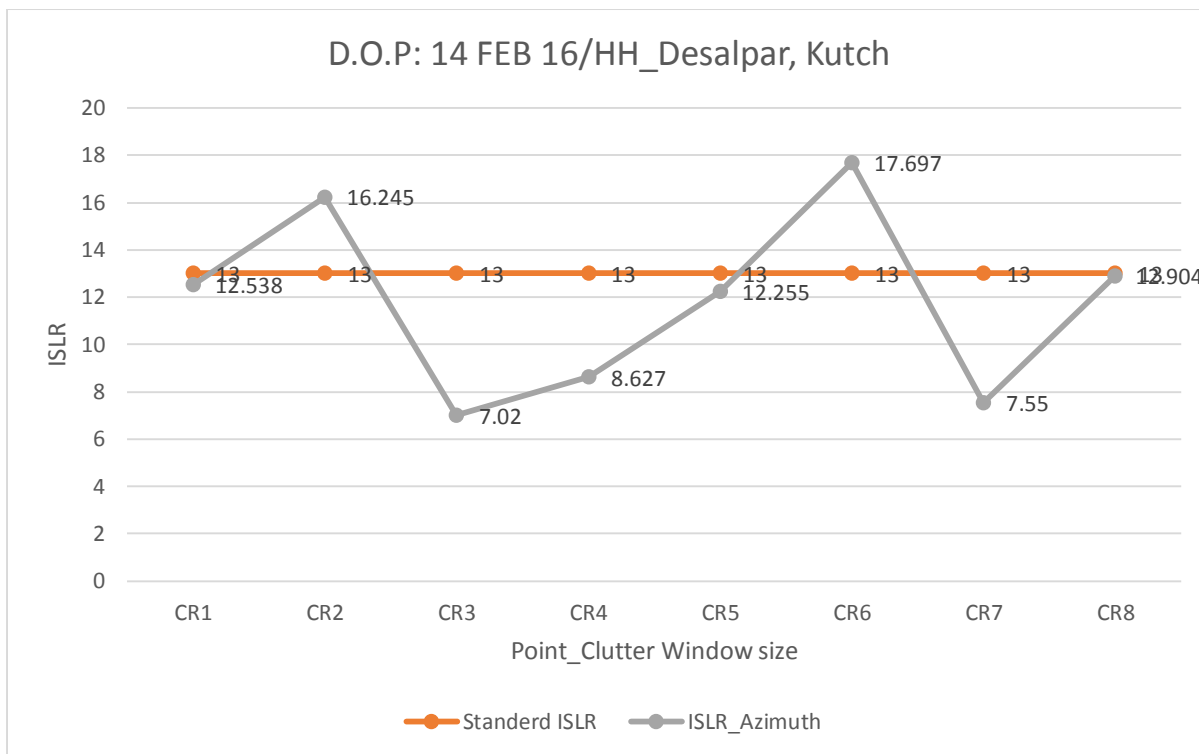


**Figure 5-53 PSLR in azimuth estimated from IRF for different target and clutter window sizes**

The spatial resolution in azimuth and the PSLR (azimuth) along with ISLR (azimuth) are shown in Figures 5-51, 5-52 and 5-53 respectively.

### 5.2.2.3 15th February 2016, FRS-1 (RH)

Beam no - 87

Incidence angle at scene center – 32.98252

Calibration Constant\_Band Meta – 70.645

The locations of CRs deployed on 15<sup>th</sup> February 2016 are common to 14<sup>th</sup> February 2016 locations. The response of CRs on FRS-1 image is seen in Figures 5-42 and 5-43.

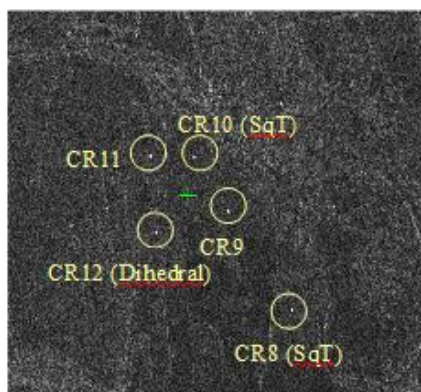


**Figure 5-54 Response of CRs (8-12) as seen in RISAT-1 FRS-1 image of 15<sup>th</sup> Feb 2016**

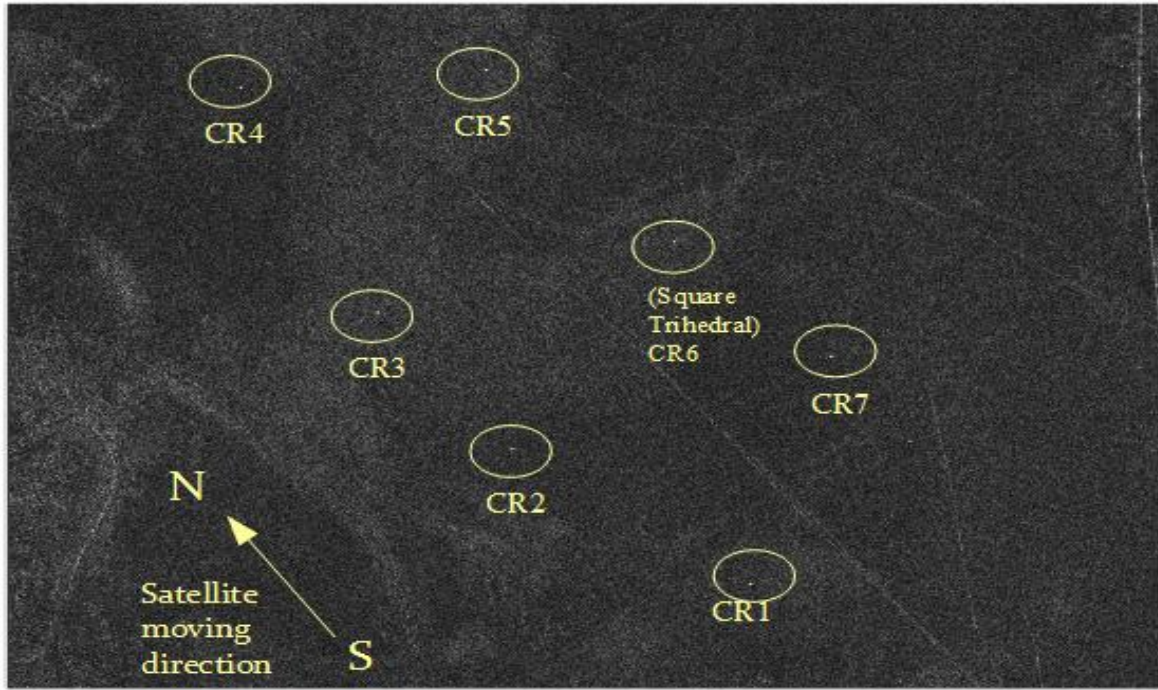
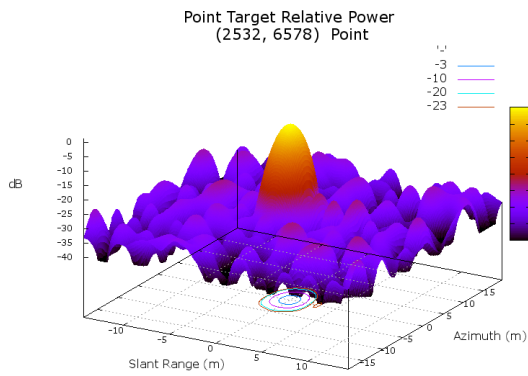
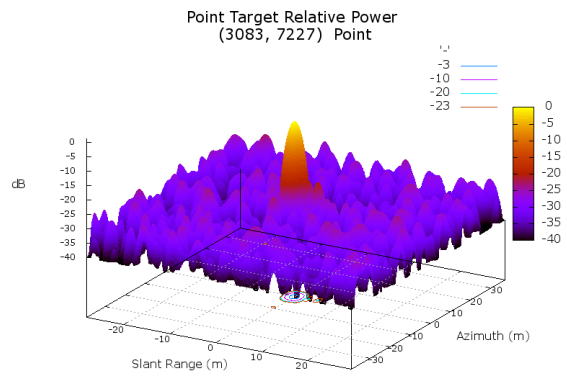


Figure 5-55 Response of CRs (1-7) as seen in RISAT-1 FRS-1 image of 15<sup>th</sup> Feb 2016

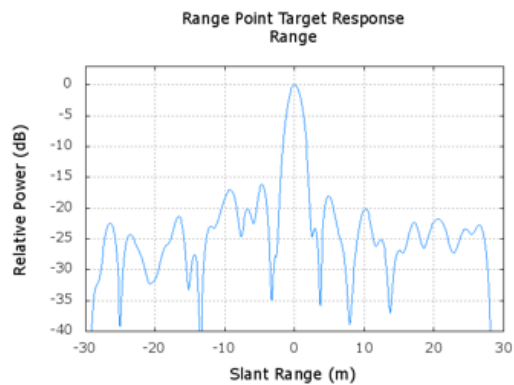
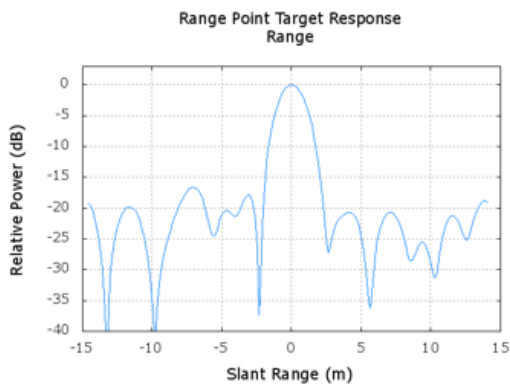
The impulse response functions of CRs are shown in Figure 43.



CR\_5\_16x16\_16x16



CR\_1\_32x32\_8x8



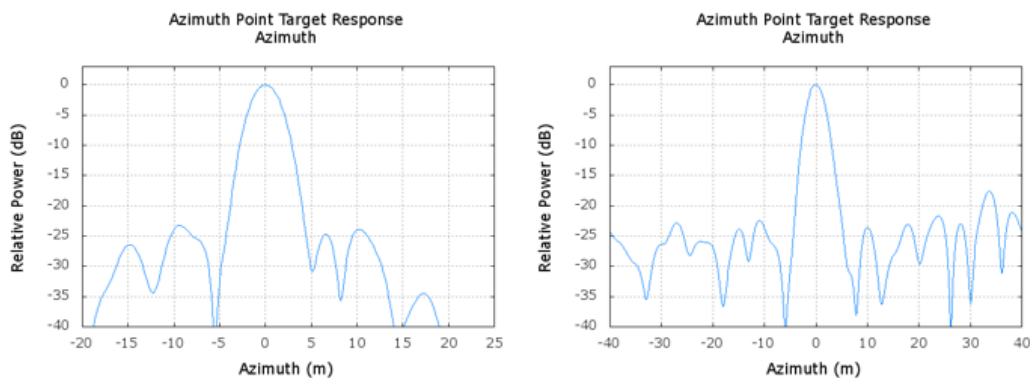


Figure 5-56 Impulse response function of the CR (5 & 1) for 15<sup>th</sup> February 2016 FRS-1

Table 5-17 Estimated Calibration Constant for different CRs

CR No	Point window size	Clutter window size	Calibration Constant	Difference (dB)
1	8x8	8x8	70.4883	0.1567
1	16x16	16x16	70.4956	0.1494
1	32x32	8x8	70.5711	0.0739
1	32x32	16x16	70.6204	0.0246
2	8x8	8x8	69.7779	0.8671
2	16x16	16x16	69.8265	0.8185
2	32x32	8x8	69.8634	0.7816
2	32x32	16x16	69.8075	0.8375
3	8x8	8x8	69.8579	0.7871
3	16x16	16x16	69.8661	0.7789
3	32x32	8x8	69.5504	1.0946
4	8x8	8x8	69.9817	0.6633
4	16x16	16x16	69.9395	0.7055
4	32x32	8x8	70.1200	0.5250
4	32x32	16x16	70.0140	0.6310
5	8x8	8x8	70.2391	0.4059
5	16x16	16x16	70.0534	0.5916
5	32x32	8x8	70.5195	0.1255
7	8x8	8x8	70.3743	0.2707
7	16x16	16x16	70.4073	0.2377
7	32x32	8x8	69.9278	0.7172
7	32x32	16x16	70.3168	0.3282

9	8x8	8x8	69.3047	1.3403
9	16x16	16x16	69.2361	1.4089
9	32x32	8x8	68.8672	1.7778
9	32x32	16x16	68.7015	1.9435
11	8x8	8x8	69.7738	0.8712
11	16x16	16x16	69.7655	0.8795
11	32x32	8x8	69.9039	0.7411
11	32x32	16x16	69.9146	0.7304
			<b>Average</b>	<b>0.5689</b>

The estimated calibration constants for different CRs and for different target and window sizes are shown in Table-5-17. The calibration constant difference was found to be almost within 1dB for all the CRs except CR 9, which is a triangular trihedral CR and for which comparatively high value was observed. It is interesting to note that for MRS pass of 14<sup>th</sup> February 2016, the same CR 9 showed comparatively higher difference between estimated and the provided calibration factor. This shows that there is some problem with the alignment or background of the CR itself, not with the result. So, while reporting the average calibration constant for this date, the constants estimated using CR9 was not taken into account.

The summary of the average difference of calibration constant estimated for each date FRS-1 and MRS data is shown in Table 5-18 and Table 5-19.

**Table 5-18 Estimated Average Calibration Constant for FRS-1**

Sr. No	Location	Date	Difference (dB)	Signal to Clutter ratio (SCR)
1.	Ahmedabad	21 <sup>st</sup> April 2015 Beam No. 104, HH	<b>0.5817</b>	35.6329
2.	Ahmedabad	25 <sup>th</sup> April 2015 Beam No. 21, HH	<b>0.9811</b>	32.2518
3.	Desalpar, Rann of Kutch	22 <sup>nd</sup> January 2016 Beam No. 66 , RH	<b>1.9634</b>	26.1109
4.	Desalpar, Rann of Kutch	15 <sup>th</sup> February 2016 Beam No. 87 RH	<b>0.5689</b>	32.0483

**Table 5-19 Estimated Average Calibration Constant for MRS**

Sr. No	Location	Date	Difference (in dB)	Signal to Clutter ratio (SCR)
1.	Bopal	5th July 2015	4.961	15.16
2.	Bopal	30th July 2015	3.247	13.28
3.	Bopal	24th August 2015	<b>0.315</b>	<b>18.50</b>
4.	Bopal	13th October 2015	1.861	16.98
5.	Bopal	7 <sup>th</sup> November 2015	1.852	16.01
6.	Bopal	2 <sup>nd</sup> December 2015	<b>0.708</b>	<b>19.70</b>
7.	Bopal	27 <sup>th</sup> December 2015	3.297	13.9

In the present study, as already mentioned in the methodology section that while calculating the scattering area,  $\sin \Theta$  term was not taken into account and also the output pixel spacing in range and azimuth was used. However, the results were also calculated using input resolution as well as including  $\sin \Theta$  term. Figures 5-56-1 and 5-56-2 show the results obtained for all the four cases (with  $\sin \Theta$ , output pixel spacing i.e. pixel area, without  $\sin \Theta$  and input pixel spacing i.e. resolution area).

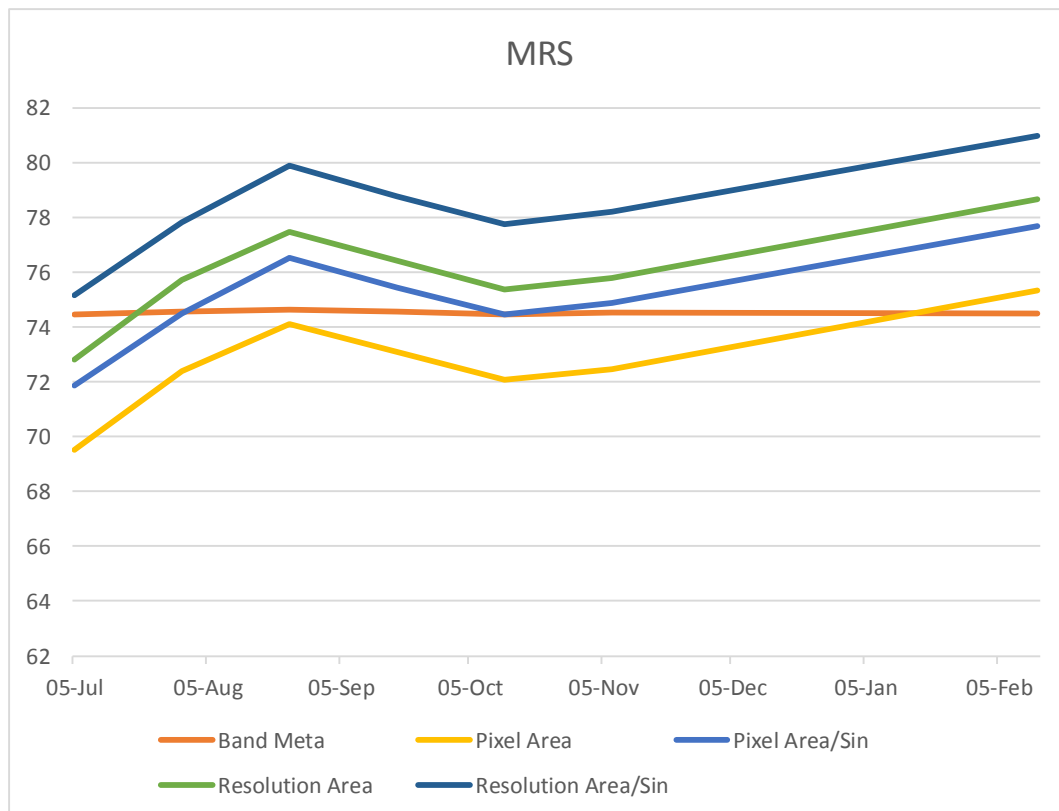


**Figure 5-56-1: Estimated CC for all the four cases for MRS (with  $\sin\theta$ , output pixel spacing i.e. pixel area, without  $\sin\theta$  and input pixel spacing i.e. resolution area)**

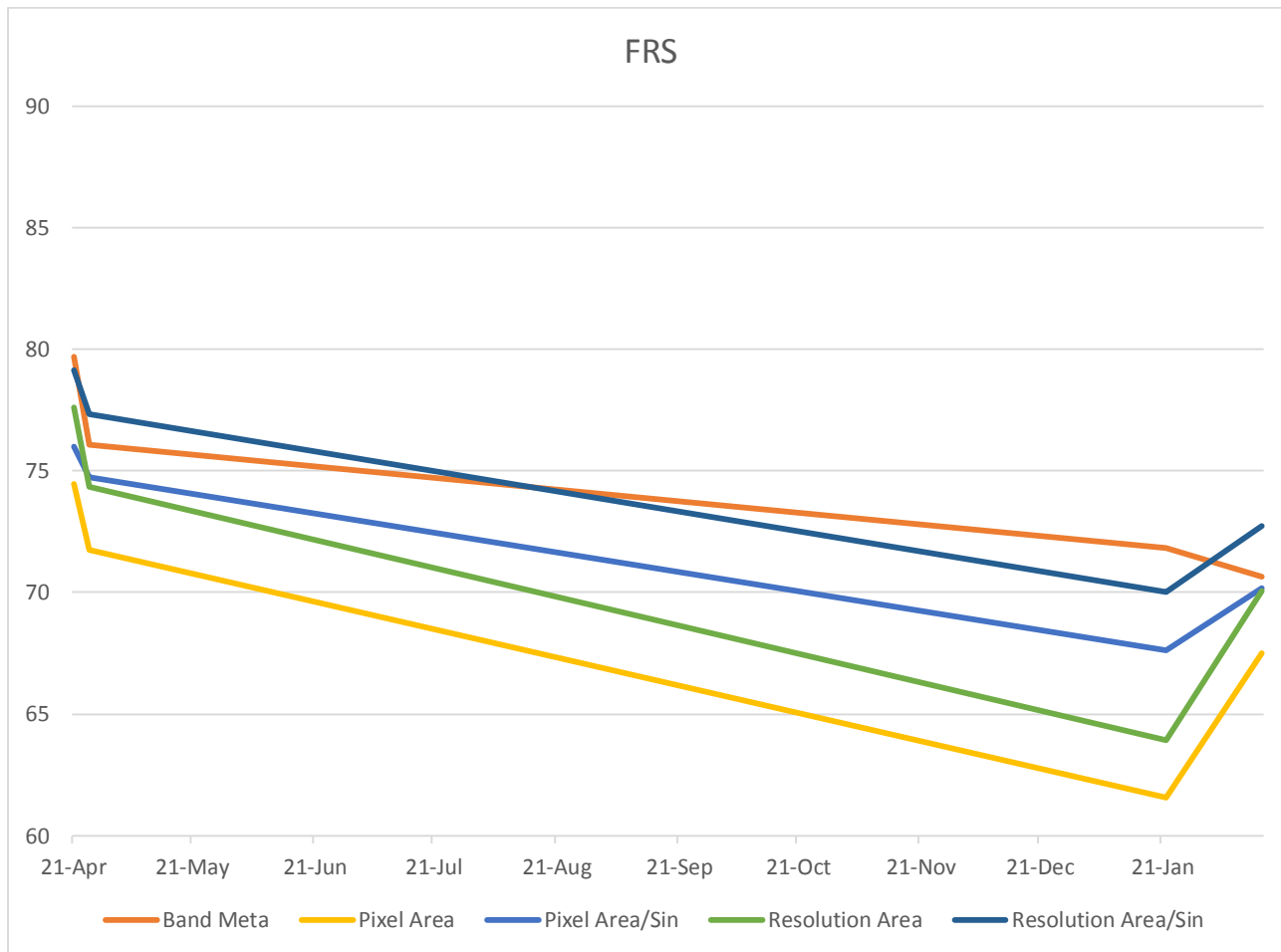


**Figure 5-56-2: Estimated CC for all the four cases for FRS (with  $\sin\theta$ , output pixel spacing i.e. pixel area, without  $\sin\theta$  and input pixel spacing i.e. resolution area)**

### 5.3 Results of radiometric calibration using distributed targets

Image of FRS Mode of RISAT-1 satellite of 22<sup>nd</sup> January 2016 was obtained in SLC format for AMAZON Rainforest region. Figures 5-57 shows the location map of amazon rainforest on world map and 5-58 show the Amazon forest on Google earth image and its response on FRS-1 image.

Latitude of the image center= -7.313441

Longitude of the image center= -69.645032

Incidence angle= 19.14404°

Location:  
Amazon rainforest,  
South America

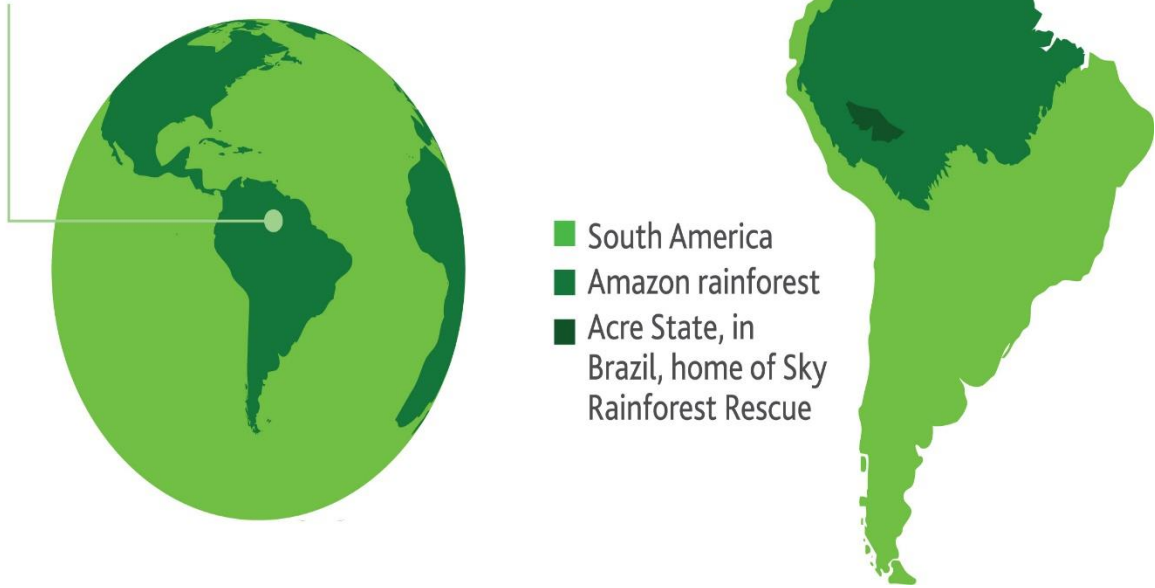


**Figure 5-57 Study Area map for distributed target analysis**

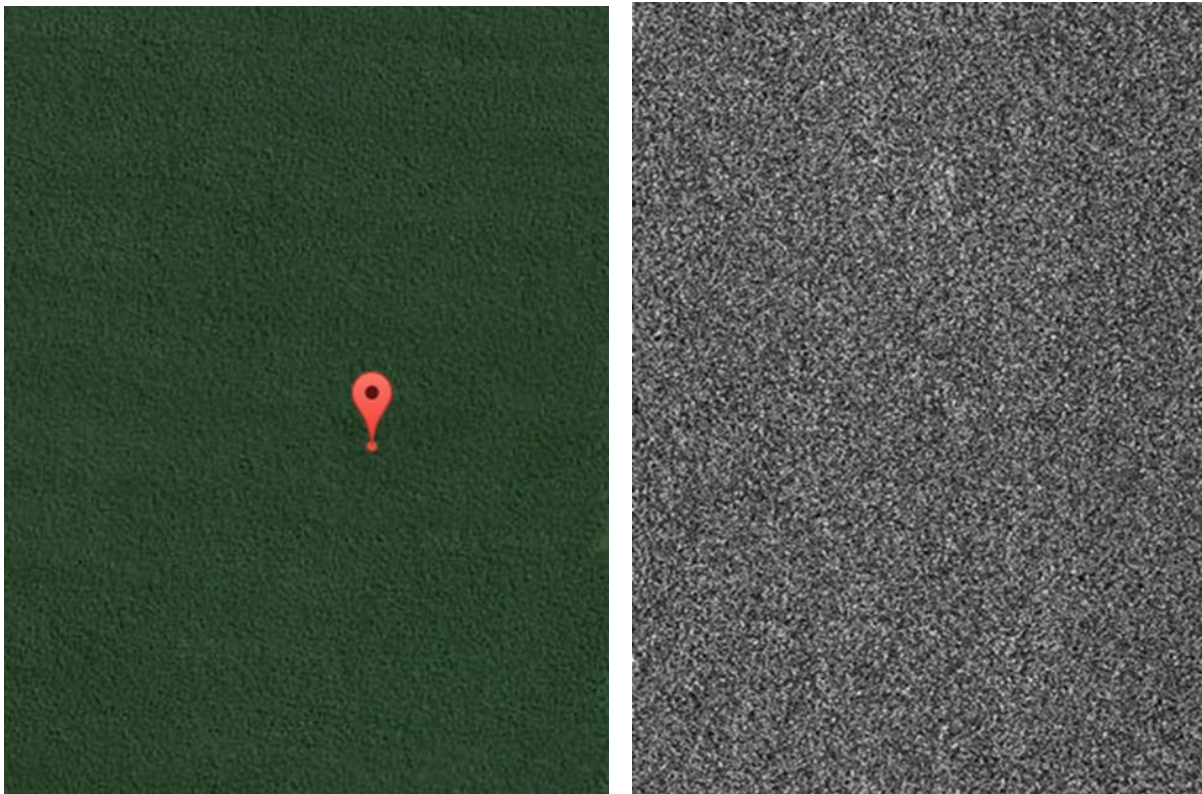


**Figure 5-58 Amazon Forest in Google Earth Image and Response of Amazon Forest in FRS Mode SAR Image**

This image was checked for the calibration as per the methodology described in the methodology section and results obtained are shown in Table-5-20.

**Table 5-20 Estimated Calibration constant (CC) using distributed target method**

Date	No of Pixels	Intensity	Gamma	Sigma	K_ Calculated	K_ Band Meta	K_ Difference
22/1/16	13998386	70.11764	-6.5	-6.7468	76.86446	76.576	-0.288465
22/1/16	7635936	70.20730	-6.5	-6.7468	76.95412	76.576	-0.378121
22/1/16	146680	70.13342	-6.5	-6.7468	76.88024	76.576	-0.304244
22/1/16	1158638	70.17767	-6.5	-6.7468	76.92448	76.576	-0.348488
						HH	-0.329830
Date	No of Pixels	Intensity	Gamma	Sigma	C_ Calculated	K_ Band Meta	K_ Difference
22/1/16	2539133	59.3788905	-12.5	-12.7468	72.125709	73.011	0.885290
22/1/16	5708541	59.3575923	-12.5	-12.7468	72.104411	73.011	0.906588
22/1/16	108169	59.4463268	-12.5	-12.7468	72.193145	73.011	0.817854
						HV	0.86991131

It can be clearly seen from Table 5-18 that the difference in calibration constant between the Manually calculated and provided in the Band Meta file along with the data are found to be quite similar. Average difference of 0.33 dB was obtained for HH Polarization and 0.87 dB was obtained for HV polarization which is within the specifications of the satellite. Further validation of the calibration constant can be performed by performing similar exercise over other dates of data and also for different distributed target sites like Congo forest and Valdivian Rainforest.

#### 5.4 Results of geometric calibration using point targets

Geometric calibration of Geo-Tiff images of FRS-1 and MRS data was attempted. Using handheld GPS location of deployed CRs were noted. The location of these CRs in the Geo-Tiff images of RISAT data was found out using ENVI software and then the difference was reported. Co-ordinates of each corner reflector recorded at the time of deployment for FRS-1 data are given in Table 5-21.

**Table 5-21 Coordinates of deployed CRs**

Co-ordinates of Point Target								
Date	Location	CR No	Lat_GPS			Long_GPS		
22/1/2016	Desalpar	CR1	23	46	14.1	70	43	19.3
22/1/2016	Desalpar	CR2	23	46	10.6	70	43	19.2
22/1/2016	Desalpar	CR3	23	46	10.2	70	43	14.1
22/1/2016	Desalpar	CR4	23	46	14.9	70	43	14
22/1/2016	Desalpar	CR5	23	46	15.8	70	43	8.4
22/1/2016	Desalpar	CR6	23	46	10.1	70	43	7.4
22/1/2016	Desalpar	CR7	23	46	20.5	70	43	18.5
15/2/2016	Desalpar	CR1	23	46	2.9	70	43	25
15/2/2016	Desalpar	CR2	23	46	11.4	70	42	53
15/2/2016	Desalpar	CR3	23	46	23	70	42	33
15/2/2016	Desalpar	CR4	23	46	42	70	42	12
15/2/2016	Desalpar	CR5	23	46	49	70	42	42
15/2/2016	Desalpar	CR6	23	46	35.7	70	43	9
15/2/2016	Desalpar	CR7	23	46	27.6	70	43	31
15/2/2016	Fields	CR8	23	44	17.4	70	41	22
15/2/2016	Fields	CR9	23	44	23.1	70	41	14
15/2/2016	Fields	CR10	23	44	26.3	70	41	9.8
15/2/2016	Fields	CR11	23	44	25.6	70	41	5
15/2/2016	Fields	CR12	23	44	20.4	70	41	6.7

Geometric error calculated for each corner reflector using RH and RV images is shown in Tables 5-22 and Table 5-23 respectively.

**Table 5-22 Estimated Geometric error for FRS-1, RH**

Geometric Error									
		GeoTiff						Difference (seconds)	
	Polarization	Lat_GeoTiff			Long_GeoTiff			Diff_Lat	Diff_Long
<b>22-1-2016</b>									
1	RH	23	46	16.57	70	43	12.72	-2.47	6.58
2	RH	23	46	13.21	70	43	12.67	-2.61	6.53

3	RH	23	46	12.83	70	43	7.58	-2.6	6.52
4	RH	23	46	17.51	70	43	7.48	-2.61	6.52
5	RH	23	46	18.45	70	43	1.93	-2.65	6.47
6	RH	23	46	12.61	70	43	0.9	-2.51	6.5
7	RH	23	46	23.16	70	43	12.01	-2.66	6.49
<b>15-2-2016</b>									
1	RH	23	46	0.56	70	43	22.9	2.34	2.55
2	RH	23	46	9.04	70	42	50.4	2.36	2.52
3	RH	23	46	19.9	70	42	30.7	3.14	2.57
4	RH	23	46	39.6	70	42	9.05	2.45	2.55
5	RH	23	46	46.5	70	42	39.4	2.47	2.58
6	RH	23	46	33.2	70	43	6.35	2.49	2.65
7	RH	23	46	25.1	70	43	28.3	2.53	2.44
8	RH	23	44	14.8	70	41	19.6	2.56	2.42
9	RH	23	44	20.6	70	41	11.4	2.54	2.61
10	RH	23	44	23.8	70	41	7.06	2.55	2.74
11	RH	23	44	23	70	41	2.44	2.6	2.56
12	RH	23	44	17.8	70	41	4.12	2.61	2.58

**Table 5-23 Estimated Geometric error for FRS-1, RV**

<b>Geometric Error</b>									
		<b>GeoTiff</b>						<b>Difference (seconds)</b>	
	<b>Polarization</b>	<b>Lat_GeoTiff</b>			<b>Long_GeoTiff</b>			<b>Diff_Lat</b>	<b>Diff_Long</b>
<b>22-1-2016</b>									
1	RV	23	46	16.86	70	43	13.51	-2.76	5.79
2	RV	23	46	13.21	70	43	12.67	-2.61	6.53
3	RV	23	46	12.83	70	43	7.58	-2.6	6.52
4	RV	23	46	17.51	70	43	7.32	-2.61	6.68
5	RV	23	46	18.45	70	43	1.77	-2.65	6.63
6	RV	23	46	12.61	70	43	0.9	-2.51	6.5
7	RV	23	46	23.02	70	43	11.85	-2.52	6.65
<b>15-2-2016</b>									
1	RV	23	46	0.56	70	43	22.85	2.34	2.55
2	RV	23	46	8.96	70	42	50.3	2.44	2.6
3	RV	23	46	19.86	70	42	30.73	3.14	2.57
4	RV	23	46	39.48	70	42	8.97	2.52	2.63
5	RV	23	46	46.46	70	42	39.42	2.54	2.58
6	RV	23	46	33.29	70	43	6.35	2.41	2.65

7	RV	23	46	25	70	43	28.18	2.6	2.52
8	RV	23	44	14.77	70	41	19.5	2.63	2.5
9	RV	23	44	20.56	70	41	11.39	2.54	2.61
10	RV	23	44	23.68	70	41	7.06	2.62	2.74
11	RV	23	44	23	70	41	2.44	2.6	2.56
12	RV	23	44	17.79	70	41	4.12	2.61	2.58

Co-ordinates of each corner reflector recorded at the time of deployment for MRS data are given in Table 5-24. Geometric error calculated for each corner reflector using HH image is shown in Table 5-25.

**Table 5-24 Coordinates of deployed CRs for 14<sup>th</sup> February 2016 MRS pass**

Co-ordinates of Point Target								
Date	Location	CR No	Lat_GPS			Long_GPS		
14/2/2016	Desalpar	CR1	23	46	3.1	70	43	25
14/2/2016	Desalpar	CR2	23	46	11.6	70	42	53
14/2/2016	Desalpar	CR3	23	46	22.4	70	42	33
14/2/2016	Desalpar	CR4	23	46	42	70	42	12
14/2/2016	Desalpar	CR5	23	46	49	70	42	42
14/2/2016	Desalpar	CR6	23	46	35.8	70	43	9
14/2/2016	Desalpar	CR7	23	46	27.6	70	43	31
14/2/2016	Fields	CR8	23	44	17.3	70	41	22
14/2/2016	Fields	CR9	23	44	23.2	70	41	14
14/2/2016	Fields	CR10	23	44	26.3	70	41	9.7
14/2/2016	Fields	CR11	23	44	25.7	70	41	5
14/2/2016	Fields	CR12	23	44	20.4	70	41	6.7

**Table 5-25 Estimated Geometric error for MRS, HH**

Geometric Error								
	GeoTiff						Difference (seconds)	
	Lat_GeoTiff			Long_GeoTiff			Diff_Lat	Diff_Long
1	23	46	4.7	70	43	25.4	-1.6	0.05
2	23	46	13.3	70	42	52.4	-1.65	0.5
3	23	46	24	70	42	32.8	-1.6	0.47
4	23	46	43.6	70	42	11.5	-1.55	0.23

5	23	46	50.8	70	42	41.5	-1.82	0.55
6	23	46	37.1	70	43	8.61	-1.27	0.39
7	23	46	29.2	70	43	30.1	-1.62	0.68
8	23	44	19	70	41	21.3	-1.69	0.82
9	23	44	24.3	70	41	13.1	-1.14	0.81
10	23	44	27.9	70	41	8.68	-1.6	1.02
11	23	44	26.8	70	41	4.22	-1.08	0.78
12	23	44	21.5	70	41	6.06	-1.09	0.64

Design specifications of the RISAT-1 Satellite are listed in Table 5-26. As the specifications mentions that the Geolocation Accuracy (RMSE) has to be 300 m for plain areas. Geolocation Accuracy (RMSE) was calculated after converting the geometric error into meters. RMSE error thus obtained is shown in Table 5-27.

**Table 5-26 Design Specifications of RISAT-1 satellite**

RISAT-1 Parameters	Values
Radiometric Resolution (SLC)	3.1 dB
Relative Radiometric Accuracy	1 dB
Absolute Radiometric Accuracy	2 dB
PSLR	-17 dB
Geolocation Accuracy (RMSE)	300 m (plain areas)
Geometric Distortions	FRS-1 100 m MRS 150 m CRS 300 m
Noise Equivalent Sigma-0 (NESZ)	-18 dB

It should be noted that the accuracy of handheld GPS is 3m which shows that the results of geometric calibration using handheld GPS holds good only for MRS mode data. For precise results, differential GPS (DGPS) should be used.

**Table 5-27 Estimated RMSE for FRS-1 and MRS**

Date	Mode	RMSE (in meters)			
		RH (Lat)	RH (Long)	RV (Lat)	RV (Long)
22 <sup>nd</sup> January 2016	FRS (Beam No. 66)	79.62	184.48	80.28	184.21
15th February 2016	FRS (Beam No. 87)	78.78	72.64	79.67	73.78
		HH (Lat)		HH (Long)	
14th February 2016	MRS	42.84		15.35	

### 5.5 Effect of Clutter window on ISLR

Integrated sidelobe ratio (ISLR) is an important parameter other than peak sidelobe ratio (PSLR), to assess the quality of a SAR Images. ISLR has been determined for SAR image performance analysis by taking into account the various clutter window sizes for RISAT-1 FRS data. ISLR is depends on the characteristics of the standard target and the clutter background at which the target is deployed. The data used in this study is of different dates as 28 June 2013 & 11 September 2015 having beam number 95 and 12 September 2013 & 16 June 2013 having beam number 74. Point target analysis was carried out to identify the variation ISLR value for different clutter sizes. The ISLR is determined by modified European Space Agency (ESA) method. Once the ISLR is determined, plot between ISLR and clutter window size is plotted to analyzed the trend of ISLR. In this study, clutter sizes are varied from 7X7 to 11X11 by keeping same target window size for various corner reflectors of different geospatial locations. Graphical results show consistent value of ISLR for same beam of data observations for different clutter backgrounds window sizes. Plot between ISLR and different window size show increasing trend. The results of this study may be utilized to assess the characteristics of ISLR and Image evaluation for RISAT-1 data. The plot between ISLR and clutter window size for various sate of pass, beam number and polarization is shown in figure 5-59 to figure 5-64 [37].

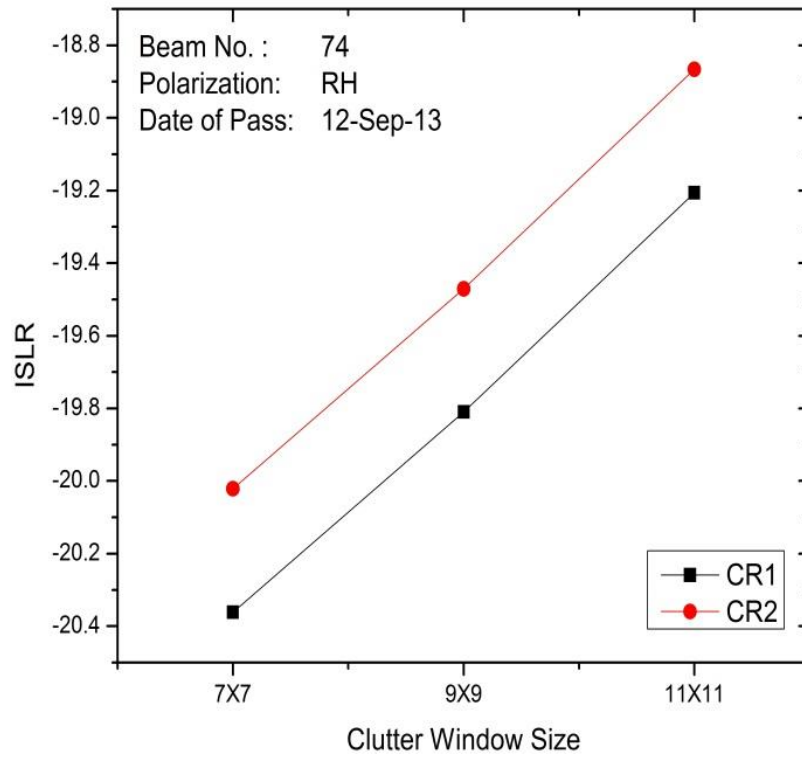


Figure 5-59 ISLR Variation for 12Sep13\_RH\_Beam no.74

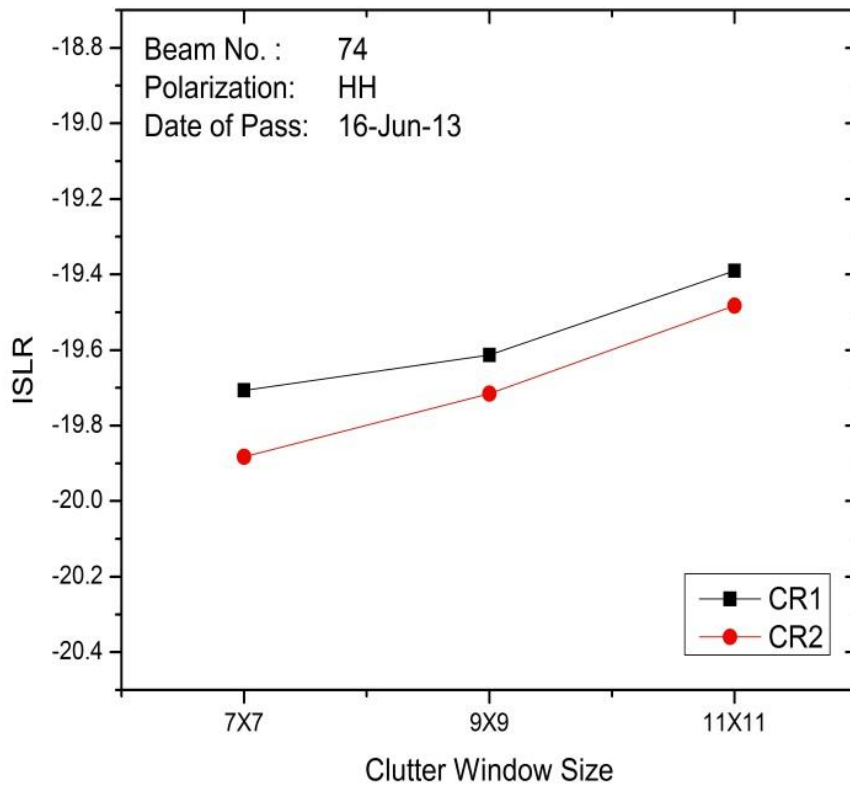


Figure 5-60 ISLR Variation for 16June13\_HH\_Beam no.74

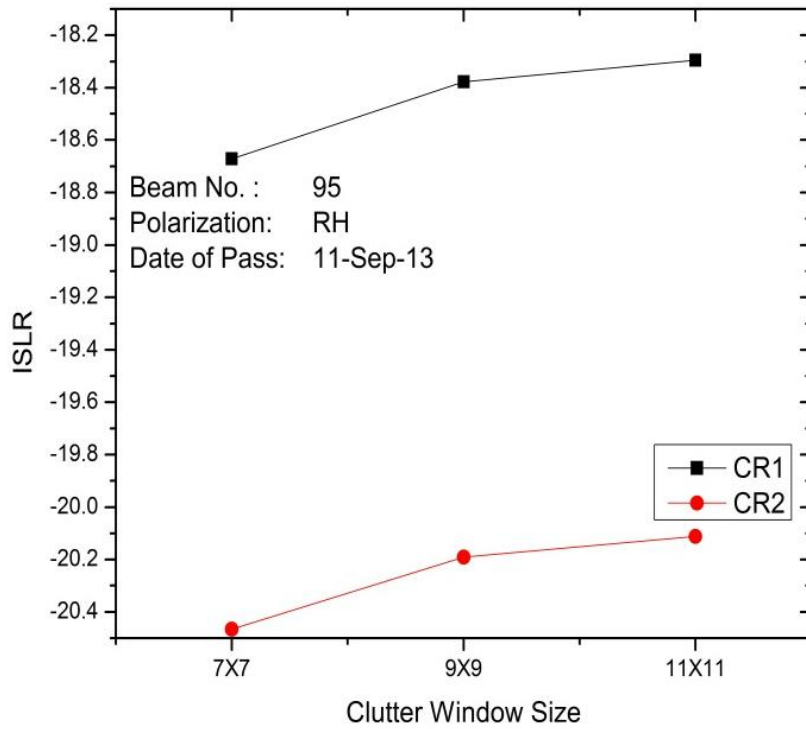


Figure 5-61 ISLR Variation for 11sep13\_RH\_Beam no.95

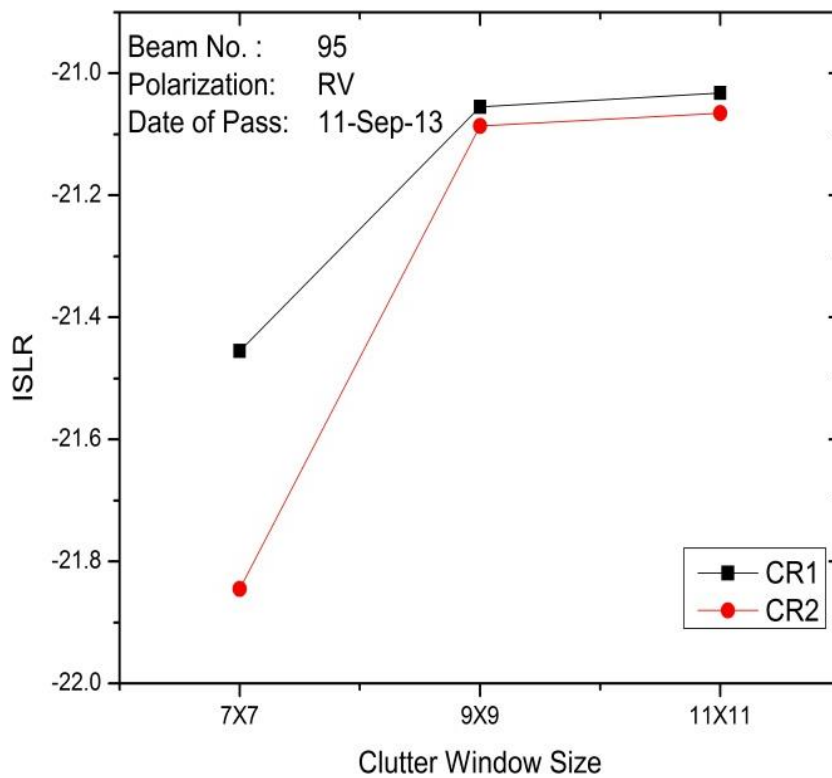


Figure 5-62 ISLR Variation for 11Sep13\_RV\_Beam no.95

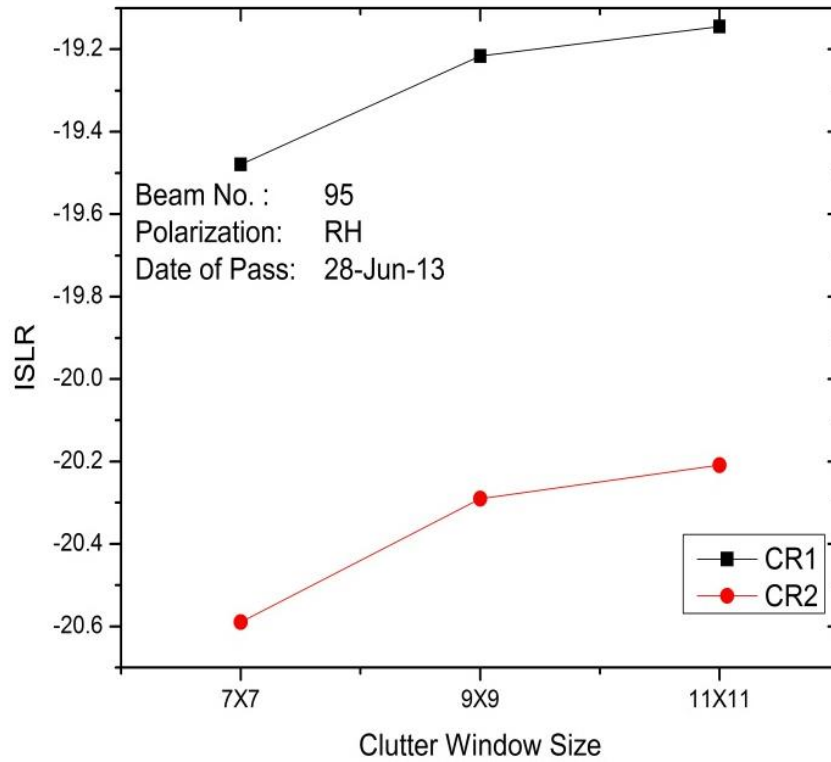


Figure 5-63 ISLR Variation for 28June13\_RH\_Beam no.95

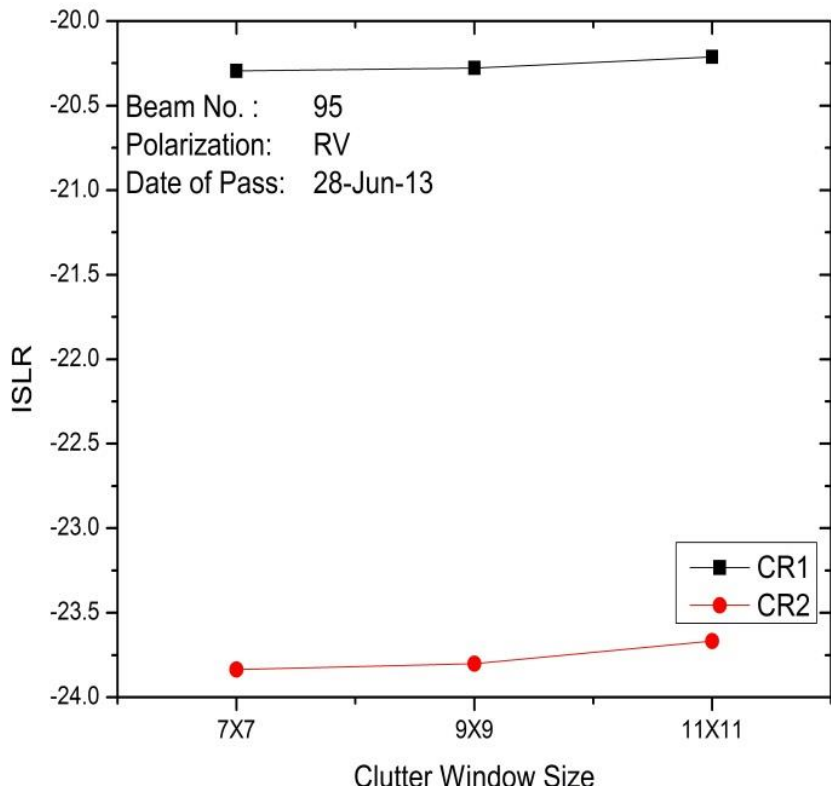
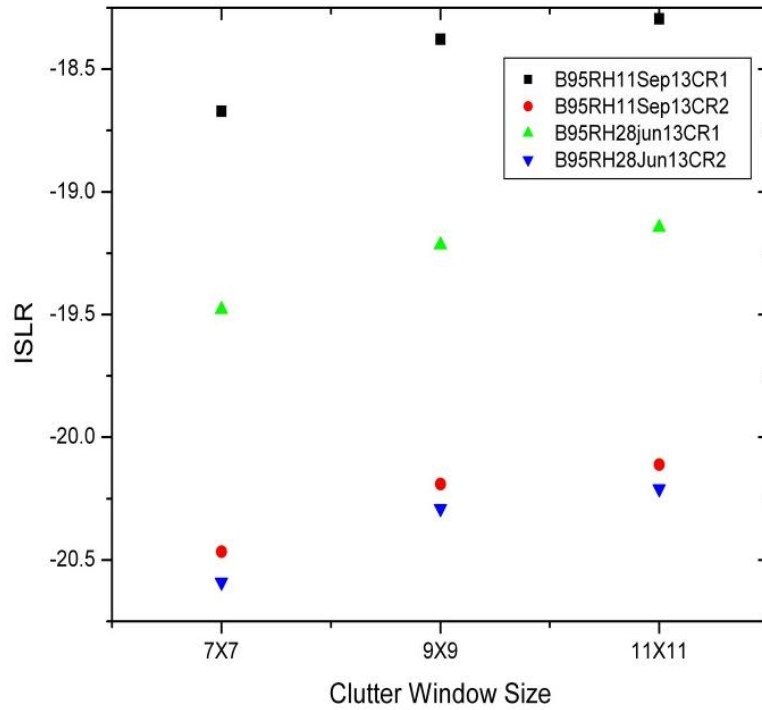


Figure 5-64 ISLR Variation for 28June13\_RV\_Beam no.95

In this study, efforts are made to identify the influence of date of pass on ISLR results. A comparative analysis was carried out to analyse the effect of date of pass on ISLR values. It

was observed that there is not much variation in the ISLR values by date of pass. The plot between ISLR and clutter window size for different date of pass is shown in figure 5-65 and figure 5-66



**Figure 5-65 Variation of ISLR for different date of pass for RH polarization**

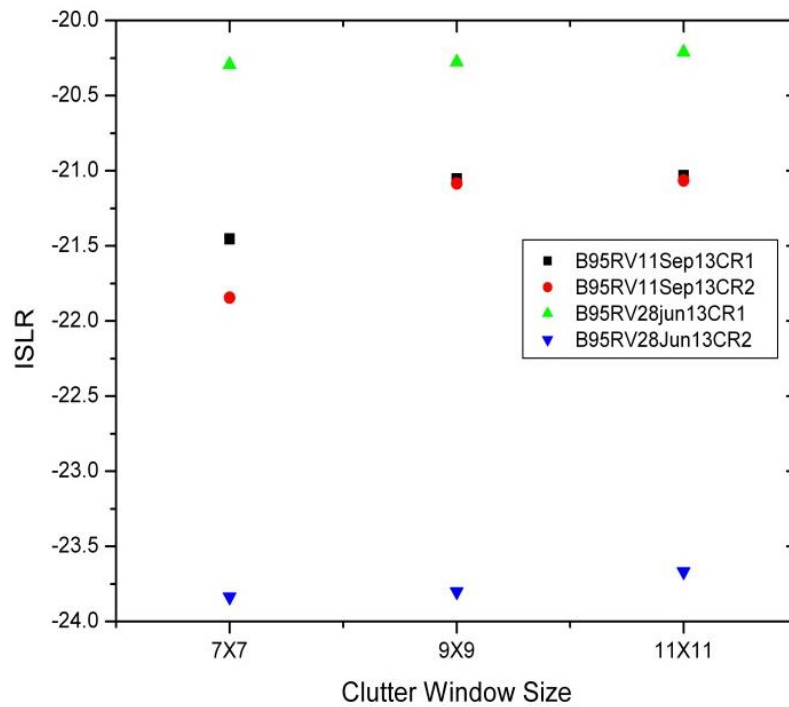


**Figure 5-66 Variation of ISLR for different date of pass for RV polarization**

## 6 CONCLUSIONS

---

---

The present study shows the recent results of the absolute radiometric calibration of RISAT-1 FRS and MRS mode data using point targets and distributed target (Amazon rainforest). In total, 12 dates data (4 dates FRS-1 and 8 dates MRS) spanning from 21<sup>st</sup> April 2015 to 15<sup>th</sup> February 2016 was analysed. It was found that for Ahmedabad site the Signal to clutter ratio was much greater than the required value of 20dB for FRS-1 mode data whereas, for MRS mode data, the value of SCR was found to be less than 20dB. For the precisely calibrated results, SCR value should be greater than 20dB, hence, it is concluded that SAC-Bopal site is suitable only for the calibration of FRS mode data. Desalpar, Rann of Kutch site was selected as the alternate site for MRS calibration and this site proved its potential for the calibration of both MRS and FRS data. It is concluded from this study that the Desalpar site in Rann of Kutch can be used as an operational SAR calibration site for C-band, whereas, for other frequencies, the suitability of this site needs to be checked.

The results obtained show that the difference between the estimated average calibration constants for FRS-1 data with the provided value was found to be within 1dB for all the beams except for beam 66 for which, the difference was within 2dB. For MRS mode data, the difference was found to be within 1dB where the SCR value approaches 20dB, whereas for the SCR values between 15 to 20 dB, the difference was within 2 dB. The results for which the signal to clutter ratio was found to be nearly equal to 20dB are considered to be precise. Radiometric calibration using distributed target yielded the average difference of -0.33dB and 0.87 dB for HH and HV respectively, which is lesser than the 1dB specifications of the satellite. Further validation of the calibration constant can be performed by performing similar exercise over other dates of data and also for different distributed target sites like Congo forest and Valdivian Rainforest.

Preliminary geometric calibration exercise was also done in order to find out the geo-location error in Geo-Tiff data of FRS-1 and MRS mode. For MRS the RMSE was found to be ~43 m in latitude and ~15m for longitude. Although the results showed the geo-location error to be within the specified value, a more precise results can be obtained using DGPS measurements as the accuracy of handheld GPS is only 3m.

Background plays an important role in the calibration and as it was seen that SCR plays important role for checking the quality of the results, an experiment was conducted to study the effect of artificial background on the results. Black cloth of size 5\*5 m was used as a

background for CR deployment and it was found that in FRS data the signal to clutter ratio was increased.

## **7 FUTURE SCOPE**

---

---

Following work has been planned in the near future:

- Rann of Kutch site suitability test for L-band, which will be useful for NISAR SAR Calibration and validation activities.
- Geometric calibration using DGPS measurements.
- To explore the methodology for characterizing The RCS of CR that are presently being used.
- To explore the sites for the calibration activities of other frequencies (L-band, S-band) apart from C-band.
- Validation of the calibration constant estimated from the study using the RCS calculation approach.
- Analysis of same beam FRS mode data for soil moisture study.
- Phase calibration using Active Radar Calibrator (ARC)\*.

\*provided ARC is available

## **Acknowledgements**

Authors gratefully acknowledge the encouragement and guidance received from Shri AS Kiran Kumar, ISRO. Authors express their sincere gratitude to Shri Tapan Misra, Director, Space Applications Centre, Ahmedabad and Dr B S Gohil, Deputy Director, EPSA for their guidance and support to carry out this activity. Authors are grateful to Director, Institute of Technology, Nirma University, HOD, Civil Engineering Department, Nirma University and Principal, M.G. Science Institute, Ahmedabad for their institutional support for carrying out this activity. Authors also thankfully acknowledge the cooperation and technical help received from Shri D. B. Dave, Shri Ramanujam, Shri Amit Shukla and Shri Raghav Mehra for this activity. The help and support rendered by Shri Ganuba, Shri Digvijay and Shri Parvat during the deployment of Corner reflectors at Desalpar and their geographical guidance of the local area was of utmost importance for the successful calibration campaigns.

## **Important Web resources and Reference**

- [1]. Paul J. Gibson and Clare H. Power, 'Introductory Remote Sensing: Digital Image Processing and Applications' George Joseph, 'Fundamentals of remote sensing', Second edition
- [2]. Yongsheng Zhou<sup>1</sup>, Chuanrong Li, Lingling Ma<sup>1</sup>, Michael Ying Yang, Qi Liu, "Improved Trihedral Corner Reflector For High-Precision SAR Calibration And Validation" IGARSS 2014
- [3]. Fawwaz T. Ulaby, Richard K. Moore, Adrian K. Fung, 'Microwave Remote Sensing Active and Passive Vol. II
- [4]. Masanobu Shimada, Hiromi Oaku, and Masao Nakai, "SAR calibration using Frequency Tunable Active Radar Calibrators", *IEEE Trans. Geosci. Remote Sensing*, vol. 37, No. 1, pp. 564 – 573, Jan 1999
- [5]. Ian G. Cumming, and Frank H. Wong, 'Digital Processing of Synthetic Aperture RADAR Data', Artech House, Boston, London
- [6]. 'Documentation on Hardware Specifications of RISAT', Space Applications Centre (ISRO), Ahmedabad
- [7]. John C. Curlander, Robert N. McDonough, 'SYNTHETIC APERTURE RADAR Systems and Signal Processing', Wiley Series in Remote Sensing
- [8]. D. R. Brunfeld and F. T. Ulaby, "Active reflector for radar calibration", *IEEE Trans. Geosci. Remote Sensing*, vol. GE - 22, pp. 165 – 169, March 1984
- [9]. M. Dobson, F. Ulaby, D. Brunfeld, and D. Held, "External calibration of SIR – B imagery with area extended point targets", *IEEE Trans. Geosci. Remote Sensing*, vol. GE 24, pp. 453 – 461, July 1986
- [10]. 'RADAR CALIBRATION', Proceedings of EARSeL Workshop, Alpbach, Austria, 6 – 10 december 1982, jointly organized by ESA, ASSA, DFVLR
- [11]. L. M. H. Ulander, "Accuracy using point targets for SAR calibration", *IEEE Trans. Aerosp. Electron. Syst.* vol. 27, pp. 139 – 148, Jan 1991
- [12]. P. J. Bird, G. E. Keyte, and D. R. D. Kenward, "An Experiment for the Radiometric Calibration of the ERS – 1 SAR", *Canadian journal of Remote Sensing*, Vol. 19, No. 3, pp 232 – 238, August 1993
- [13]. Laurence Gray, Paris W. Vachon, Charles E. Livingstone, Tom I. Lukowski, "SAR Calibration Using Reference Reflectors", *IEEE Trans. Geosci. Remote Sensing*, vol. 28, No. 3, pp. 374 – 383, May 1990

- [14]. Calibration of the ERS SAR PRI data product, ESA Earthnet Online, European Space Agency ‘Absolute calibration of ASAR level – 1 products generated with PF – ASAR’, ESA, Issue 1 revision 5, pp. 1 -26, October 2004
- [15]. D. R. D. Kenward, “A Precision Corner Reflector For ERS – 1 SAR Calibration”, *Canadian journal of Remote Sensing*, Vol. 19, No. 3, pp 218 – 224, August 1993
- [16]. Zéner, Mirko Panozzo. "SAR Image Quality Assessment." (2012). Accessed from [aulavirtual.ig.conae.gov.ar](http://aulavirtual.ig.conae.gov.ar) on 20 January 2016.
- [17]. Garthwaite, M. C., et al. "Design of radar corner reflectors for the Australian Geophysical Observing System." *Geoscience Australia* 3 (2015).
- [18]. Masanobu Shimada, Hiromi Oaku, and Masao Nakai, “SAR calibration using Frequency Tunable Active Radar Calibrators”, *IEEE Trans. Geosci. Remote Sensing*, vol. 37, No. 1, pp. 564 – 573, Jan 1999
- [19]. John C. Curlander, Robert N. McDonough, ‘Synthetic Aperture Radar Systems and Signal Processing’, Wiley Series in Remote Sensing
- [20]. Freeman, “SAR calibration: An overview,” *IEEE Transactions on Geoscience and Remote Sensing*, vol. 30, no. 6, pp. 1107–1121, Nov. 1992.
- [21]. M. Schwerdt, B. Bräutigam, M. Bachmann, B. Döring, D. Schrank, and J. Hueso Gonzalez, “Final TerraSARX calibration results based on novel efficient methods,” *IEEE Transactions on Geoscience and Remote Sensing*, vol. 48, no. 2, pp. 677–689, Feb. 2010.
- [22]. S Srivastava, S Cote, S Muir, and R Hawkins, “The RADARSAT-1 imaging performance, 14 years after launch, and independent report on RADARSAT-2 image quality”, 2010, IEEE, Geoscience and Remote Sensing Symposium (IGARSS), pp. 3458 – 3461, doi:10.1109/IGARSS.2010.5650129
- [23]. R Hawkins, E Attema, R Crapolicchio, P Lecomte, J Closa, P J Meadows, “Stability of Amazon Backscatter at C-Band: Space borne Results from ERS-1/2 and RADARSAT-1.”, 2000, SAR Workshop: CEOS Committee on Earth Observation Satellites; Working Group on Calibration and Validation, Proceedings of a Conference held 26-29 October 1999, Toulouse, France. Edited by Robert A. Harris and L. Ouwehand. Publisher: Paris: European Space Agency, ESA-SP vol. 450, ISBN: 9290926414, p.99.
- [24]. Martínez and J. Marchand, “SAR Image Quality Assessment,” *Revista AET (Asociación Española de Teledetección)*, Nov. 1993.

- [25]. ESA, Technical note on the ECISAR test image, ER-TN-EPO-GP-1901, ESATECESA ed., 1990.
- [26]. ESA Ecisar Test Image: quality analysis and calibrations measurements, er-tn-epo-gp-1902, estec-esa ed., 1991.
- [27]. Mishra, Mayank D., et al. "Absolute radiometric calibration of FRS-1 and MRS mode of RISAT-1 Synthetic Aperture Radar (SAR) data using corner reflectors." *International Journal of Advanced Engineering Research and Science* 1.6 (2014): 78-89.
- [28]. Gray, A. L., P. W. Vachon, C. E. Livingstone, and T. I. Lukowski (1990), Synthetic Aperture Radar Calibration Using Reference Reflectors, *IEEE Transactions on Geoscience and Remote Sensing*, 28(3), 374-283.
- [29]. Tapan Misra, S. S. Rana, N. M. Desai, D. B. Dave, Rajeevjyoti, R. K. Arora, C. V. N. Rao, B. V. Bakori, R. Neelakantan and J. G. Vachchani, "Synthetic Aperture Radar payload on-board RISAT-1: configuration, technology and Performance", *CURRENT SCIENCE*, VOL. 104, NO. 4, 25 FEBRUARY 2013.
- [30]. Rosich B., Meadows P., "Absolute Calibration of ASAR Level 1 Products Generated with PF – ASAR" 2004, Technical Note, ESA, ESRIN.
- [31]. Mohan S., Basu S. K., Jha A. M., Mishra Tapan, Kewalia R. K., (1995), Calibration of ERS-1 SAR Data', Scientific report, SAC/RSA/RSAG/ERS-1/SN/07/95.
- [32]. FENG Zongmin, HUANG Lei, TANG Zhihua, LIU Jiuli, ZHAO Liangbo "Airborne SAR radiometric calibration using point targets" 35th International Symposium on Remote Sensing of Environment (ISRSE35), Earth and Environmental Science 17 (2014)
- [33]. Maneesha Gupta, Anuja Sharma and B. Kartikeyan, "Image quality assessment of RISAT-1 SAR using trihedral corner reflectors in different beams", *Journal of Geomatics*, Vol.8, No.2, pp:130-139, October 2014.
- [34]. Norris J., P.W. Vachon, D. Schlingmeier, R. English and L. Gallop (2004). Expendable trihedral corner reflectors for target enhancement and position control in RADARSAT-1 fine beam mode SAR imagery: Results from an exercise Narwhal Pre-Trial Deployment defence R&D Canada-Ottawa TECHNICAL MEMORANDUM DRDC Ottawa TM 2004-197 September 2004.
- [35]. Donald, M. Ugsang, K. Honda and G. Saito (2001). Assessment of small passive corner reflectors for geometric correction of RADARSAT fine beam mode SAR data. 22nd Asian conference on Remote Sensing, 5-9 November 2001, Singapore.

- [36]. Gupta M., B. Kartikeyan and S. Chowdhury, (2014), An approach to evaluate and monitor RISAT-1 SAR from level-0 raw data. International Journal of Remote Sensing, <http://dx.doi.org/10.1080/01431161.2014.943323>.
- [37]. Gautam Dadhich, Shweta Sharma, Parul R. Patel and A.K. Mathur, “Effect of clutter window size on ISLR for SAR (RISAT-1) Image evaluation”, National symposium on Geomatics for digital India and Annual Conventions of ISG & ISRS, Poster, December 2015.
- [38]. ‘RISAT-1 Data Products formats (September, 2015)’, SIPA, Space Applications Centre (ISRO), Ahmedabad

## **Visual Walkthrough of Deployed Corner reflector**

### **Corner reflector deployment on 30<sup>th</sup> July 2015**



Grass and shrubs are observed on Bopal Cal Val site due to Rainey season.



Building construction near Cal Val Site



CR Deployment at SAC-Bopal



CR Deployment was not possible at Nirma University due to heavy rainfall on 29/7/15

CR Deployment at Nirma University

